Mechanisms of methane bubble formation, storage and release in freshwater sediments

by
Liu Liu
Born in Hubei, China

Accepted Dissertation thesis for the partial fulfillment of the requirements for a
Doctor of Natural Sciences
Fachbereich 7: Natur- und Umweltwissenschaften
Universität Koblenz-Landau

Thesis examiners:
Prof. Dr. Andreas Lorke, Landau
Prof. Dr. Daniel F. McGinnis, Geneva
Prof. Dr. Sebastian Sobek, Uppsala

Date of the oral examination: 25 January 2019

This dissertation is based on the following manuscripts and publications (ordered by date):

Liu, L., J. Wilkinson, K. Koca, C. Buchmann, and A. Lorke (2016). The role of sediment structure in gas bubble storage and release. Journal of Geophysical Research: Biogeosciences 121: 1992-2005. doi: 1910.1002/2016JG003456.

Liu, L. T. De Kock, J. Wilkinson, V. Cnudde, S. B. Xiao, C. Buchmann, D. Uteau, S. Peth and A. Lorke (2018). Methane bubble growth and migration in aquatic sediments observed by X-ray μCT. Environmental Science & Technology 52: 2007-2015. doi: 2010.1021/acs.est.2007b06061.

Dück Y., L. Liu, A. Lorke, I. Ostrovsky, R. Katsman and C. Jokiel. A novel freeze corer for characterization of methane bubbles and coring disturbances. Submitted to Limnology and Oceanography: Methods, conditional acceptance, in revision.

Liu L., K. Sotiri, Y. Dück, S. Hilgert, I. Ostrovsky, E. Uzhansky, R. Katsman, B. Katsnelson, R. Bookman, J. Wilkinson and A. Lorke. The control of sediment gas accumulation on spatial distribution of ebullition in Lake Kinneret. To be submitted.

Table of Contents

Abstract 1

1 Introduction 3

1.1 The significance of methane emission from inland waters 3

1.2 The controls of methane flux from freshwaters 3

1.2.1 The biogeochemical controls 3

1.2.2 The importance of ebullition in transporting methane 4

1.3 Processes controlling ebullition: from formation of methane bubbles to their release 6

1.3.1 The formation of methane bubbles in aquatic sediments 6

1.3.2 Release of sediment methane bubbles and their fate in the water column 7

1.4 Current understanding about ebullition and research needs 9

2 Hypotheses and research questions 11

3 Outline 13

4 Discussion 15

4.1 Achievements and limitations in characterizing methane bubbles 16

4.2 Sediment gas storage capacity: characterization and controlling factors 17

4.3 The control of sediment gas storage on temporal dynamics of ebullition 18

4.4 Factors affecting spatial distributions of gas ebullition 20

4.5 Implications to future modelling work 21

5 Conclusions 23

6 References 24

Author contributions 30

Declaration 31

Curriculum Vitae 32

Acknowledgements 33

Appendices 34

Appendix I 35

The role of sediment structure in gas bubble storage and release

Appendix II 36

Methane Bubble Growth and Migration in Aquatic Sediments Observed by X‐ray μCT

Appendix III 37

A novel freeze corer for characterization of methane bubbles and coring disturbances

Appendix IV 64

The control of sediment gas accumulation on spatial distribution of ebullition in Lake Kinneret

Abstract

Lakes and reservoirs are important sources of methane, a potent greenhouse gas. Although freshwaters cover only a small fraction of the global surface, their contribution to global methane emission is significant and this is expected to increase, as a positive feedback to climate warming and exacerbated eutrophication. Yet, global estimates of methane emission from freshwaters are often based on point measurements that are spatio-temporally biased. To better constrain the uncertainties in quantifying methane fluxes from inland waters, a closer examination of the processes transporting methane from sediment to atmosphere is necessary. Among these processes, ebullition (bubbling) is an important transport pathway and is a primary source of uncertainty in quantifying methane emissions from freshwaters. This thesis aims to improve our understanding of ebullition in freshwaters by studying the processes of methane bubble formation, storage and release in aquatic sediments. The laboratory experiments demonstrate that aquatic sediments can store up to ~20% (volumetric content) gas and the storage capacity varies with sediment properties. The methane produced is stored as gas bubbles in sediment with minimal ebullition until the storage capacity is reached. Once the sediment void spaces are created by gas bubble formation, they are stable and available for future bubble storage and transport. Controlled water level drawdown experiments showed that the amounts of gas released from the sediment scaled with the total volume of sediment gas storage and correlated linearly to the drop in hydrostatic pressure. It was hypothesized that not only the timing of ebullition is controlled by sediment gas storage, but also the spatial distribution of ebullition. A newly developed freeze corer, capable of characterizing sediment gas content under in situ environments, enabled the possibility to test the hypothesis in a large subtropical lake (Lake Kinneret, Israel). The results showed that gas content was variable both vertically and horizontally in the lake sediment. Sediment methane production rate and sediment characteristics could explain these variabilities. The spatial distribution of ebullition generally

was in a good agreement with the horizontal distribution of depth-averaged (surface 1 m) sediment gas content. While discrepancies were found between sediment depth-integrated methane production and the snapshot ebullition rate, they were consistent in a long term (multi-year average). These findings provide a solid basis for the future development of a process-based ebullition model. By coupling a sediment transport model with a sediment diagenetic model, general patterns of ebullition hotspots can be predicted at a system level and the uncertainties in ebullition flux measurements can be better constrained both on long-term (months to years) and short-term (minutes to hours) scales.

1 Introduction

1.1 The significance of methane emission from inland waters

Counter-intuitive to the fact that inland waters cover only < 1% of earth's surface (Downing et al. 2006), their contribution to global carbon (carbon dioxide (CO_2) and methane) emissions is disproportionally high (Bastviken et al. 2004; Borges et al. 2015; Cole et al. 2007; Deemer et al. 2016; Holgerson and Raymond 2016; Li and Bush 2015; Li et al. 2015; Tranvik et al. 2009). While methane emission contributes only ~12% to the total (CO_2 and methane) in terms of mass, as a conservative estimate it corresponds to 25% of the terrestrial carbon sink (Bastviken et al. 2011). This is because methane is 28-34 times CO_2 equivalent in terms of global warming potential (Myhre et al 2013). Furthermore, enhanced methane emissions are expected in response to the exacerbated global eutrophication and climate warming (DelSontro et al. 2018; Sepulveda-Jauregui et al. 2018). In addition to methane's significance in global carbon cycling, in freshwaters methane also serves as a food and energy source in freshwater food webs (Bastviken et al. 2003; Jones and Grey 2011; Mbaka et al. 2014). It is therefore important to improve our understanding of methane cycling and quantify the magnitude of methane fluxes from global inland waters.

1.2 The controls of methane flux from freshwaters

In typical freshwater systems, many processes (both biogeochemical and physical) should be considered to make an accurate budget of methane cycling (see Figure 1 for a schematic description of these processes).

1.2.1 The biogeochemical controls

Methane emitted from inland waters is typically of biogenic origin, i.e., by anaerobic decomposition of organic matter in aquatic sediments as a result of microbial activities (Whiticar et al. 1986; Yvon-Durocher et al. 2014), or by methane production under aerobic

environments as a byproduct of complex biochemical processes (Donis et al. 2017; Grossart et al. 2011; Tang et al. 2016). Anaerobic methanogenesis in sediments has been identified as a significant source of methane in many freshwater systems (Bastviken et al. 2004; Bastviken et al. 2008), particularly in impounded rivers and reservoirs where sediment deposition rates are high (Deemer et al. 2016; DelSontro et al. 2011; DelSontro et al. 2010; Maeck et al. 2013; Sobek et al. 2012). Before methane reaches the atmosphere, a portion can be eliminated by oxidation in anoxic sediments by a number of potential oxidizers/reducers such as iron/manganese (Beal et al. 2009; Sivan et al. 2011), sulfate (Kuivila et al. 1989; Lovley and Klug 1983) and nitrate (Deutzmann et al. 2014). Methane can be also oxidized by oxygen in the water column (Oswald et al. 2015; Rahalkar and Schink 2007). These methane production and consumption processes determine the amounts of methane emitted from freshwaters.

1.2.2 The importance of ebullition in transporting methane

In spite of the fact that methane budgets in aquatic systems are primarily determined by biogeochemical processes (Bastviken et al. 2008), accurate estimation of methane fluxes requires a close examination on internal methane transport pathways. Methane can be transported by diffusion, ebullition (bubbling), released by overturn mixing from hypolimnion storage or by plants (Bastviken et al. 2004). Diffusive methane transport is limited by vertical mixing in the water column and gas exchange at the air-water interface. In deep lakes, that experience seasonal density stratification, dissolved methane can accumulate in the hypolimnion and be emitted during lake overturn (Schubert et al. 2012). Compared to the slow diffusive transport, ebullition has been considered much more efficient in transporting methane because bubbles can rise fast in water and bypass oxidation (McGinnis et al. 2006). In many systems, bubble-mediated flux is a large component of the total and even often dominates over other pathways (Bednařík et al. 2017; DelSontro et al. 2010; Maeck et al. 2013; Sobek et al. 2012; Xiao et al. 2014).

Similar to the well-accepted temperature dependence of methanogenesis (Yvon-Durocher et al. 2014), methane ebullition has been found also highly temperature-sensitive. Temperate mesotrophic mesocosms experiments suggested that ebullition can increase exponentially with temperatures above 10 °C and begin to dominate diffusion, which is much less temperature dependent (Aben et al. 2017). A positive feedback on ebullition is expected (Aben et al. 2017) due to the fact that global lake water is displaying a warming trend over the last decades (O'Reilly et al. 2015). However, ebullition from northern lakes and ponds cannot be simply explained by this temperature dependence and the trophic states of ecosystems also play an important role (DelSontro et al. 2016). Given the important role of ebullition yet poorly understood governing processes, quantifying ebullition flux is crucial for better understanding and more effectively constraining methane emissions from inland waters.

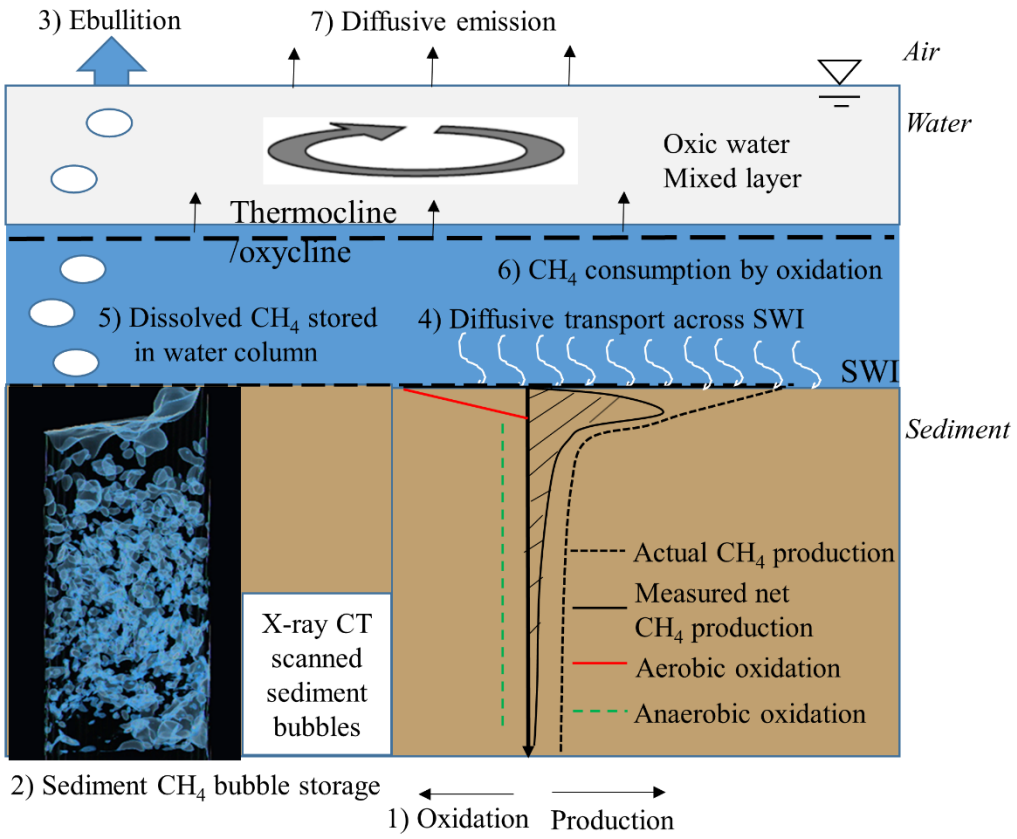

Figure 1. Schematic of production and consumption processes that affect methane emission in a typical freshwater system (plant-mediated transport is not included here).

1.3 Processes controlling ebullition: from formation of methane bubbles to their release

1.3.1 The formation of methane bubbles in aquatic sediments

Methane bubble formation in sediment is primarily governed by gas production rate and diffusion (Boudreau et al. 2001; Li and Yortsos 1995; Van Kessel and Van Kesteren 2002). Without a sufficient methane production to overcome diffusive limitations, porewater oversaturation and bubble formation will never occur. This had been studied in artificial sediments (van Kesteren and van Kessel 2002), showing that not only is the growth rate of methane bubbles controlled by gas production rate, but also the distance between bubbles and the size of bubbles.

Sediment characteristics and mechanical properties also play a role in sediment bubble growth. Many mechanisms had been proposed. Firstly, methane bubbles can grow and migrate in extremely weak sediment in analogy to bubbles in geo-fluids such as water (e.g., (Chanson et al. 2006)) that was termed fluidization. As illustrated in Figure 2, the second mechanism contends that in coarse-grained sediments, micro-bubbles (sub millimeter) form by pushing porewater out of capillary pores which was termed capillary invasion (Choi et al. 2011; Jain and Juanes 2009). The gas pressure allowing gas to enter a sediment pore is inversely related to the sediment grain size (Jain and Juanes 2009). A third mechanism (Figure 2) asserts that in cohesive fine sediments, capillary entry pressure is greater than the strength of sediment, large bubbles (mm to cm, at least 10 times greater than sediment grain size) can grow by elastic/plastic deforming surrounding sediment matrix (Wheeler 1988). In this case, the mixture of porewater and sediment grains can be treated as one phase instead of two (Boudreau 2012). Lastly, based on the phase approximation made in the third mechanism, linear elastic fracture mechanics had been proposed to explain bubble growth as a result of tensile fracture. This theory considers the combined strength of all the bonds, i.e., electrostatic, organic, water-based, etc. (Barry et al. 2010; Johnson et al. 2002). Unlike the third theory, this one had been proven

capable of predicting the shape and size of methane bubbles in aquatic sediments (Boudreau et al. 2005; Gardiner et al. 2003). However, these studies (Algar and Boudreau 2009; Algar and Boudreau 2010; Katsman 2015) were limited to an ideal case, i.e., a single bubble in homogenized fine-grained marine sediments, which may not be applicable to multiple bubble growth in freshwater sediments.

Apart from these fundamental studies, research on gas bubble growth and migration in sediments has been scarce and limited to the effect of gas formation on storage capacity in artificial sludge containers (Gauglitz and Terrones 2002; Van Kessel and Van Kesteren 2002; Gauglitz et al. 2012; Johnson et al. 2017).

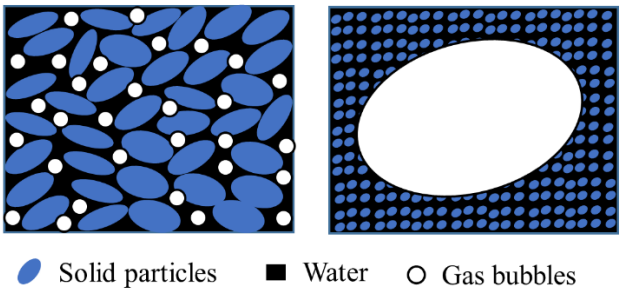

Figure 2. Bubble formation in aquatic sediments by capillary invasion (left) and elastic/plastic deformation (right).

1.3.2 Release of sediment methane bubbles and their fate in the water column

Methane bubbles leave the sediment as they grow sufficiently large, many mechanisms of have been proposed for bubble rise in aquatic sediments (Figure 3). In weak slurries, bubbles can rise by fluidization (Sherwood and Sáez. 2014). It has been first suggested by Wheeler (1990) to calculate this critical size by assuming spherical bubbles rise in plastic sediment driven by buoyancy. However, in aquatic sediments bubbles were predicted to be unrealistically large (1 m diameter) in order to rise, which could not be supported by any experiments (Boudreau 2012). It had been observed in later experiments that bubbles came out through established channels/conduits (Van Kessel and Van Kesteren 2002) though the

prediction of the maximum depth of the conduits did not succeed (Powell et al. 2014). Further studies (Boudreau 2005; Algar et al. 2011a) demonstrated that bubbles rise could be initiated by fracturing and these fractures could facilitate subsequent bubble rise. The release of methane bubble from sediment could be triggered by pressure drop-induced pre-existing conduit re-open (Algar et al. 2011b; Scandella et al. 2011).

After release from sediment, the rising methane bubbles exchanges with gases dissolved in the water column. The fraction of methane eventually reaching the atmosphere depends primarily on many factors affecting the gas exchange efficiency and is most sensitive to the initial size of bubbles and water depth (Leifer and Patro 2002; McGinnis et al. 2006). This partly explains the more frequently observed higher ebullition flux in the shallow zones of lakes. A field study also suggested that large bubbles (initial diameter) are capable of transporting more methane to the atmosphere than small ones though they are less frequent (Delsontro et al. 2015), which could partly explain the spatio-temporal variabilities of ebullition flux. A more recent study (Delwiche and Hemond 2017) demonstrated that bubble size distributions were highly variable in space even at small spatial scales, suggesting a control of sediment conditions on bubble size which is currently poorly understood.

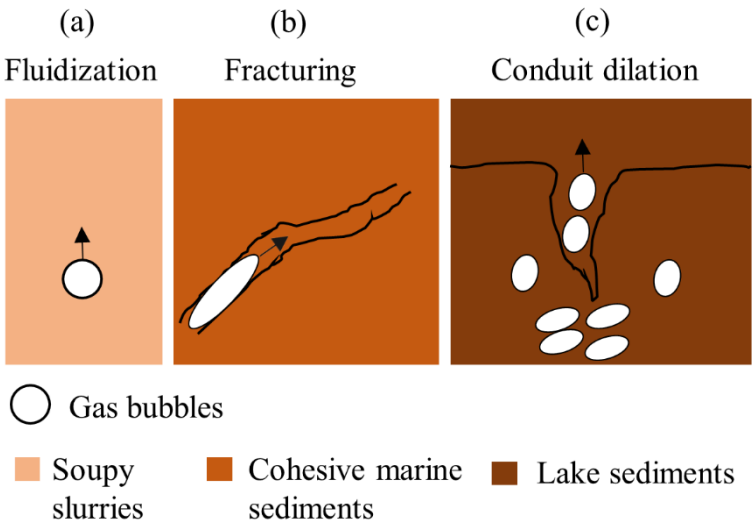

Figure 3. Schematic illustration of bubble release mechanisms: (a) fluidization in weak sediments (Sherwood and Sáez. 2014), (a) bubble rise by fracturing (Algar et al. 2011a) and (c) bubble release by conduit dilation (Van Kessel and Van Kesteren 2002; Scandella et al. 2011).

1.4 Current understanding about ebullition and research needs

Although ebullition is important for methane transport, it is extraordinarily difficult to quantify accurately as it has been often described as sporadic and unpredictable both in time and space (Scandella et al. 2016; Wik et al. 2013). Continuous one-year ebullition flux measurements in River Saar captured an extreme ebullition event in a week that accounted for ~13% of the yearly total (Wilkinson et al. 2015). This suggests that flux estimates based on short-term observations may have underestimated the emission potential from freshwaters (Maeck et al. 2014; Wik et al. 2016). On the other hand, ebullition is also spatially heterogeneous (Bastviken et al. 2008; Beaulieu et al. 2016; Tušer et al. 2017) which has often been explained by sediment accumulation patterns (DelSontro et al. 2011; Maeck et al. 2013; Wilkinson et al. 2015) and water depth (de Mello et al. 2018; Tušer et al. 2017), adding another complexity to measurements. The difficulty in quantifying/predicting ebullition flux from freshwaters is currently one of the major constraints in estimating methane emissions from inland waters.

While as mentioned above ebullition is primarily driven by gas production in the long term (Wilkinson et al. 2015; Aben et al. 2017), its short-term dynamics has often been found closely related to hydrostatic/atmospheric pressure changes (Chanton et al. 1989; Maeck et al. 2014; Scandella et al. 2016; Varadharajan and Hemond 2012). Forcing mechanisms of ebullition have been explored and simulated with a simple mechanistic model by linking ebullition flux to methane bubbles stored in sediment (Scandella et al. 2011), in which sediment bubbles dilate as total hydrostatic pressure drops. However, pressure drops did not always trigger ebullition and sometimes delays in response were observed (Maeck et al. 2014; Varadharajan and

Hemond 2012). This suggested a potential role of sediment gas storage in regulating ebullition dynamics. Field measurements demonstrated that lake sediments can store large amounts of methane gas (Anderson and Martinez 2015), though the control of sediment gas content on ebullition remained unclear (Martinez and Anderson 2013).

Regardless of our knowledge advancements in both fundamental and applied studies of gas bubble formation mechanics in marine and artificial sediments, the controls on the dynamics of methane bubble growth in freshwater sediments remain poorly understood. While convincing observations in laboratory experiments (Scandella et al. 2017) supported the conduit opening mechanism for bubble release from the sediment, to date direct observations of bubbles movement in sediments have been scarce (Boudreau 2012) and little is known about the link between sediment gas storage and bubble release. These small-scale single bubble-based theories have difficulties predicting the large-scale dynamics of ebullition in freshwaters.

To improve our ability to understand/predict temporal dynamics and spatial distributions of ebullition flux, all abovementioned empirical findings need to be refined. Examining further to establish a linkage between sediment methane bubble storage and ebullition seems a promising approach. To achieve this goal, detailed studies on the processes controlling methane bubble formation and release in freshwater sediments are required.

2 Hypotheses and research questions

This thesis aims to advance our mechanistic understanding about the dynamics of methane bubble formation, storage and migration in freshwater sediments in lakes. The link between sediment bubble storage behavior and gas ebullition has been explored both in the laboratory and field. Four research questions are answered in present thesis corresponding to four hypotheses.

Hypothesis 1: Aquatic sediments can store large amounts of free gas, which explains the temporal dynamics of gas ebullition.

Question 1: How does sediment gas content evolve over time? How does gas ebullition respond to sediment gas content development and hydrostatic pressure drops?

Hypothesis 2: Depending on hydrological and hydrodynamic settings, natural freshwater sediments are characterized by a wide range of grain size from coarse sand (even gravel) to fine-grained clay. Sediment gas content and gas ebullition vary with sediment texture.

Question 2: What controls gas storage capacity in freshwater sediments, grain size distribution or sediment mechanical properties, or both?

Hypothesis 3: Previous studies suggested that bubbles either need to reach a critical size in order to migrate, or they migrate through the pre-existing conduits. However, there are no direct observations to support these theories. We hypothesize that once the gas storage capacity of a sediment is reached, the established pore network structure can be used for future bubble storage and migration. This would allow the formulation of a numerical model based on volumetric gas content.

Question 3: How do methane bubbles grow and migrate in aquatic sediments?

Hypothesis 4: Since sediment gas production and grain size distribution can potentially control methane bubble formation and storage in sediment, we hypothesize that the spatial distribution of gas ebullition can be linked to the pattern of in situ free gas content in surface sediment.

Question 4: What gas content is expected in a natural lake sediment, where are the free methane bubbles located and do the spatial distributions of gas and ebullition correlate?

3 Outline

The experiments used to answer the research questions are divided into four parts and the findings are presented in four articles. The articles, attached as Appendices, either have been published/accepted or are under review by peer-reviewed journals. The research questions addressed in each part are outlined below.

Part 1

A lab experiment was performed to investigate the development of gas content in different types of sediment (*Question 1*). Gas storage capacity of freshwater sediments was quantified (*Question 2*). The role of sediment grain size in bubble formation and storage was explored and the response of ebullition to hydrostatic pressure drops was studied (*Question 1 and 2*).

Appendix I -

Liu, L., J. Wilkinson, K. Koca, C. Buchmann, and A. Lorke (2016). The role of sediment structure in gas bubble storage and release. Journal of Geophysical Research: Biogeosciences 121: 1992-2005. doi: 1910.1002/2016JG003456.

Part 2

Another lab experiment was conducted to study detailed bubble formation and migration in different types of sediment (*Question 3*). The role of sediment characteristics and mechanical properties in collective bubble formation was investigated (*Question 2 and 3*).

Appendix II -

Liu, L. T. De Kock, J. Wilkinson, V. Cnudde, S. B. Xiao, C. Buchmann, D. Uteau, S. Peth and A. Lorke (2018). Methane bubble growth and migration in aquatic sediments observed by X-ray μCT. Environmental Science & Technology 52: 2007-2015. doi: 2010.1021/acs.est.2007b06061.

Part 3

In order to characterize sediment gas content, a novel freeze corer has been developed and applied to Lake Kinneret, Israel (*Question 4*).

Appendix III -

Dück Y., L. Liu, A. Lorke, I. Ostrovsky, R. Katsman and C. Jokiel. A novel freeze corer for characterization of methane bubbles and coring disturbances. Submitted to Limnology and Oceanography: Methods, conditional acceptance, in revision.

Part 4

Two joint field campaigns were conducted in Lake Kinneret, Israel to measure sediment gas content and characterize its relationship with gas ebullition. Hydroacoustic measurements were used to determine the spatial distributions of both sediment gas bubbles and ebullition and freeze coring was used to determine sediment gas content. In combination, the techniques were used to profile sediment methane production, determine the spatial distribution of sediment gas and investigate its relationship with gas ebullition (*Question 4*).

Appendix IV -

Liu L., K. Sotiri, Y. Dück, S. Hilgert, I. Ostrovsky, E. Uzhansky, R. Katsman, B. Katsnelson, R. Bookman, J. Wilkinson and A. Lorke. The control of sediment gas accumulation on spatial distribution of ebullition in Lake Kinneret. Submitted to Limnology and Oceanography, under review.

4 Discussion

The present work advances our understanding of sediment methane bubble growth and release in aquatic sediments with a series of laboratory experiments and field measurements (Figure 4). The laboratory experiments focus on detailed sediment bubble growth behaviors in homogenized natural sediments. Field measurements were conducted in Lake Kinneret to validate the findings in the laboratory by taking the advantage of newly developed method to characterize in situ sediment gas content.

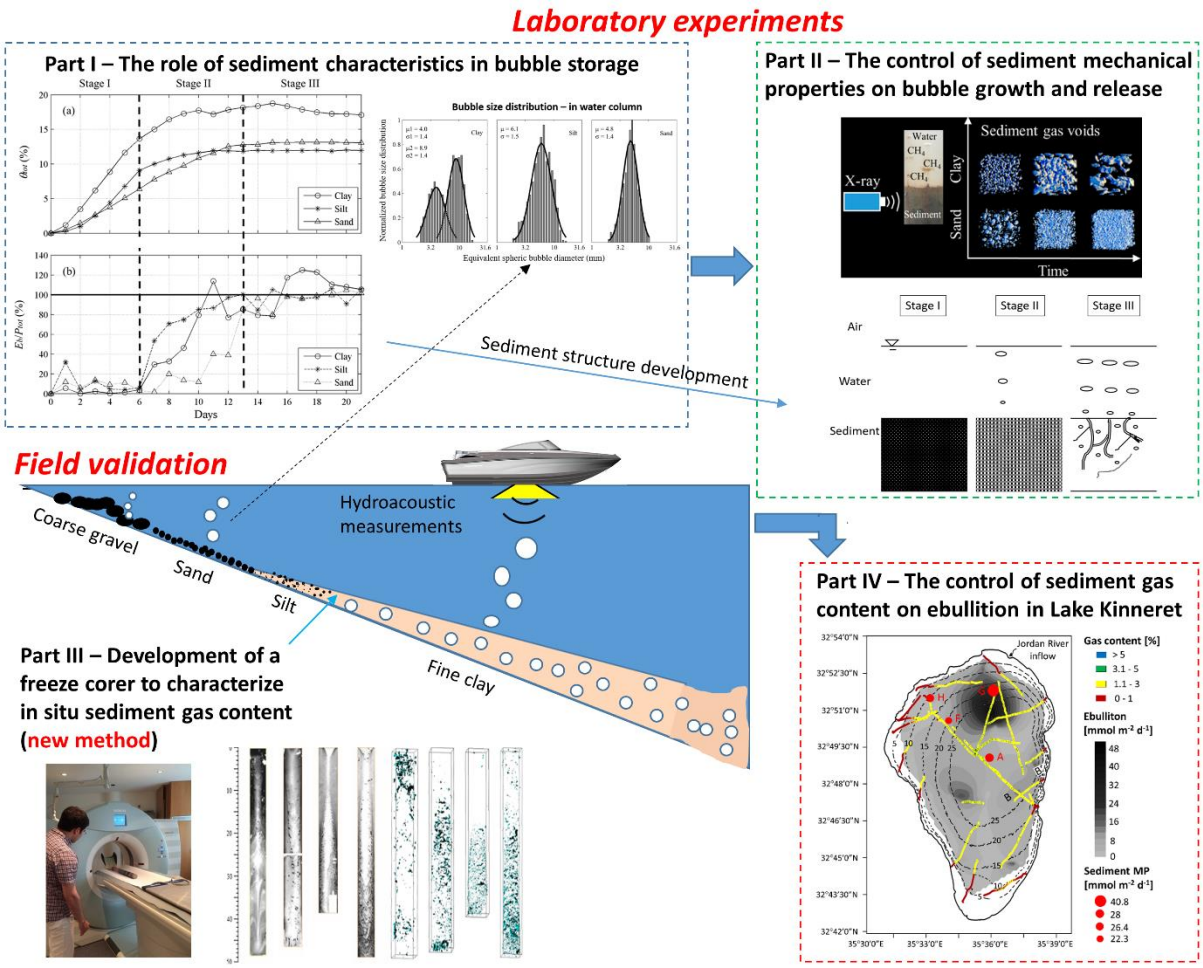

Figure 4. Summary of the achievements in understanding bubble growth and release in aquatic sediments and their link to ebullition in this thesis.

4.1 Achievements and limitations in characterizing methane bubbles

Observing methane bubbles in aquatic sediments is challenging due to the opacity of aquatic sediments. In this thesis, advanced methods were adapted/developed to overcome this difficulty.

μCT enables direct detailed observation of methane bubble formation in aquatic sediments. High spatial resolution allows visualization of methane bubble growth at the pore scale (Appendix II). A novel freeze corer was developed that preserves the sediment gas composition (Appendix III). To characterize gas content in lake sediments, traditional corers cannot be used because they are not able to maintain hydrostatic pressure and gas content is altered. While a pressurized corer (Anderson et al. 1998) would work, the new freeze corer provides a more cost-effective alternative for obtaining detailed depth profiles of sediment gas content. To complement the sediment gas profiles, hydroacoustic measurements were performed in Lake Kinneret (Appendix IV) to allow for characterizing the horizontal distribution of sediment gas content and ebullition flux (Ostrovsky et al. 2008).

Methods of characterizing methane bubbles at different scales (pore to core scale and system) each has strengths and limitations. For example, the high spatial resolution of μCT is achieved at the cost of temporal resolution; scanning at a resolution of ~64 μm requires ~20 min, but achieving a spatial resolution of ~20 μm doubles the scan time (refer to Appendix II for details). This causes difficulties in characterizing initial bubble growth in sediments because, at pore scale, bubble growth rate is a function of the square root of time (Brennen 2013) and only a few minutes are required for a micro-bubble to occupy a ~10 μm capillary pore at an average gas supply rate (Boudreau 2012). The limitation in temporal resolution also applies to hydroacoustic methods for characterizing bubbles, particularly when measuring ebullition, which is extremely variable in time. Thus, the spatial distribution of ebullition flux measured hydroacoustically can potentially be masked by temporal dynamics and should be interpreted

with caution. Future developments that address these technical difficulties are needed for a more complete understanding of the processes controlling sediment methane bubble formation and release.

4.2 Sediment gas storage capacity: characterization and controlling factors

Sediment gas content has been measured in the lab experiments as high as ~20% in a homogenized clayey sediment (Appendix I). This high sediment gas content has never been observed in natural systems though field measurements were few. In shallow gassy marine sediments, e.g., Eckernförde Bay and Baltic Sea, gas content can vary in a wide range (~0.1-3.4%) (Anderson et al. 1998; Best et al. 2004; Tóth et al. 2014). An average of 6.17±2.19 L m^{-2} (corresponding to 0.62±0.22% volumetric content) sediment gas content was estimated in Lake Elsinore (Anderson and Martinez 2015). Relatively high sediment gas content (> 1%) in the profundal zone of Lake Kinneret was estimated in this study (Appendix IV), which is one order of magnitude higher than previous estimate of < 0.2% using an acoustic method (Katsnelson et al. 2017). This difference can be explained by the fact that the acoustic method used by Katsnelson et al. (2017) could only provide a depth-integrated estimate, in contrast to the present study that defines the first meter of sediment. In addition to the horizontal distribution of sediment gas content, this work demonstrated a variability of the vertical distribution of sediment gas, which has never been studied in freshwater systems. While an improved understanding of sediment gas content distribution has been achieved, more field measurements should be done to have a better knowledge of sediment gas storage capacity in other freshwater systems, particularly in reservoirs that are characterized by high spatial heterogeneities in sediment deposition and sediment characteristics.

In addition, the control of sediment grain size and mechanical properties on sediment gas storage capacity has been revealed by the laboratory experiments (Appendix I and II). In general, the storage capacity seems to increase with the increasing fraction of fine particles in

the sediments. This has been validated in the study conducted in Lake Kinneret (Appendix IV). Little/no sediment gas content was detected in the littoral zone of the lake where sediments were dominated by coarse sand (Ostrovsky and Tęgowski 2010). The role of sediment properties has been also demonstrated (Appendix II) as a higher gas content was observed in clay that was chracterized with low sediment shear strengths (< 15 Pa) than in stiffer sand (shear yield strength > 100 Pa). This is consistent to previous findings that the increase in sediment shear yield strength allows bubbles to grow by internal fracturing, resulting in a reduction in sediment gas storage (Gauglitz et al. 2012; Johnson et al. 2017). It is, however, contrary to a former study (Sherwood and Sáez 2014) showing that in weak sediments (shear yield strength < 10 Pa), bubbles were unable to grow larger before leaving the sediment.

4.3 The control of sediment gas storage on temporal dynamics of ebullition

While field-based ebullition data suggested a possible link to the sediment gas reservoirs (Chanton et al. 1989; Maeck et al. 2014; Varadharajan and Hemond 2012), the experiments explicitly demonstrated this control (Appendix I and II). Sediment gas storage capacity must be reached before intense bubble release is observed. During gas accumulation, the intensity of ebullition is minimal. Simply stated, the sediment storage capacity defines the potential for gas ebullition. This was demonstrated (Appendix I) with a controlled water level drop experiment; the amount of ebullition scaled with the total volume of gas stored in the sediment.

Sediment gas storage capacity can be used to explain the temporal dynamics of ebullition. In lakes and riverine impoundments, forcing of ebullition by hydrostatic/atmospheric pressure reductions was seemingly well established. However, rather than a linear response of ebullition decreasing pressure, no significant correlation was found between them (Maeck et al. 2014; Varadharajan and Hemond 2012). This lack of correlation can be explained by sediment gas

content, i.e., little or no ebullition is triggered while the sediment gas content is below the storage capacity.

The gas storage-ebullition mechanism has important implications. It had been thought that long-term ebullition flux depended on sediment temperature change (Aben et al. 2017; Wilkinson et al. 2015) and that short-term variability of ebullition did not alter total average methane emission from freshwaters. This might be true for water bodies that experience minimal water level fluctuations as in many freshwater lakes, but can lead to substantial differences in reservoirs/impoundments with frequent water level fluctuations. Recent studies (Beaulieu et al. 2018; Harrison et al. 2017) suggest that water level drawdowns could decrease or increase methane emissions from reservoirs depending on the water level management strategy of the reservoir.

In fact, both sediment gas storage capacity and water level management strategy can affect methane emission from reservoirs by altering the fraction of methane transported by bubbles. While the sediment gas storage capacity in aquatic sediments has been poorly characterized, it was estimated for Lake Lacamas, that sediments can hold 50-700% of the annual ebullition flux during periods with no drawdown (Harrison et al. 2017). With storage capacities that are large relative to the average ebullition flux in natural systems, water level drawdowns can create short periods of intense ebullition and increase the fraction of methane transported by bubbles. This bypasses diffusive transport, decreasing the proportion of methane oxidized compared to water bodies with more stable water levels. Reservoirs with large storage capacities, such as Three Gorges Reservoir (Liu et al. 2012), have annual drawdown up to 30 m and remain at a low level for an extended period. These systems are especially prone to sediment methane bubble formation and ebullition. Given the global boom in large dam constructions for hydropower and flood control (Zarfl et al. 2015), understanding the temporal dynamics of ebullition flux

from reservoirs is increasingly important for supporting development of management practices that mitigate methane emission.

4.4 Factors affecting spatial distributions of gas ebullition

The experiment included in Appendix I show how sediment structure controls sediment gas content. The follow-up field study (Appendix IV) in Lake Kinneret confirmed this finding.

The finding that gas ebullition is inactive in the littoral zone of Lake Kinneret is contrary to what others reported from many other lakes. In typical freshwater lakes, the shallow littoral zones have been recognized as hot spots for ebullition (Bastviken et al. 2004; Walter et al. 2006; Wang et al. 2006; Wik et al. 2013). The shallower water depths favor methane bubble formation because of the resultant lower gas saturation limits and the exposure to solar radiation. In Lake Kinneret, the change in sediment grain size from coarse sand in the littoral zone to fine clay towards the profundal zone of the lake (Ostrovsky and Tęgowski 2010) provides a plausible explanation for this unusual spatial variability of ebullition in a natural lake. The low sediment gas content in the littoral zone suggests a control of sediment structure on gas storage in sediment. The similar has been found in Lake Elsinore, CA, a small eutrophic temperate lake, where sediment texture showed a strong influence on sediment gas content, i.e., sediment gas content increases with the increasing fraction of fine-grained sediments (Martinez and Anderson 2013).

While it has been demonstrated by the present work that sediment ebullition can be linked to sediment gas content, more field measurements are required to validate these findings. So far direct measurements of sediment gas content in freshwater lakes are limited in number. The only quantitative study was performed in Lake Elsinore (Martinez and Anderson 2013) and suggested a strong correlation between gas ebullition and sediment gas content at individual sites, while no simple correlation occurred across the entire lake. Surprisingly, they also found that ebullition rates were positively correlated to sand content in sediment (Martinez and

Anderson 2013). This suggests a potential role of sediment gas storage capacity in regulating gas release regime: the highest sediment volumetric gas content was ~1% in the central part of this lake where clay content was high in the sediment (Anderson and Martinez 2015) though the actual sediment storage capacity in this lake was unknown. The higher ebullition rates from the sandy sediment could be the result of a lower sediment gas storage capacity that can be easier to reach compared to the clay-bearing sediment in this lake.

It should also be noted that sediment structure can affect size distribution of bubbles (Appendix I). The predominance of small bubbles was observed from the coarse-grained sediment, in contrast to the transition to increasing fraction of large bubbles from the fine-grained sediment. This small-scale variability of bubble size distribution has been also observed in lake sediments (Delwiche and Hemonde 2017). The size of methane bubbles eventually contributes to the spatial heterogeneity of ebullition flux in natural freshwaters: small-diameter bubbles can hardly reach the water surface due to the re-dissolution of rising methane bubbles (McGinnis et al. 2006) and large methane bubbles thus make a more significant contribution to the total flux though they are less frequent in occurrence (DelSontro et al. 2015).

4.5 Implications to future modelling work

The present work provides a basis for a process-based ebullition model. The sediment storage capacity can be set to an upper limit for sediment volumetric gas content and the temporal dynamics of ebullition can be explained by the interplay between the three factors: gas supply rate (bubble formation), pressure reductions (bubble expansion) and historic storage (sediment gas content). This model is, if historical sediment gas content data is available, unlike previous models that considered only gas volume/mass change in response to pressure reductions (Scandella et al. 2011; Tang et al. 2010).

The control of sediment properties (and associated sediment gas storage capacity) on ebullition (Appendix I and IV) suggests another possibility for model development. The

methods used in this thesis (coupling hydroacoustic measurements with sediment freeze coring, Appendix IV) should be applied in different freshwater systems, so that general patterns can be discerned for sediment gas content and its relation to gas ebullition. More information on sediment characteristics (e.g. grain size distribution and organic matter content) can and should be extracted from the hydroacoustic measurements (Hilgert 2015) to provide additional evidence for explaining the spatial variabilities of sediment gas content and ebullition. By coupling a sediment transport model with a sediment methane production model, the spatial distribution of ebullition could be predicted at a system level.

Estimates on global methane fluxes can benefit from the development of such process-based models. Methane emissions can be better constrained by using a "bottom-up" approach that integrates the key methane production (from sediment), consumption (due to oxidation) and transport processes (Figure 1). Instead of measuring highly variable fluxes that limits the ability to do measurements at a large scale with a sufficient temporal resolution, the rates of methane production, consumption and transport can be integrated into a 1D process-based model. This enables the possibility of (1) an improved process-based understanding of controls on methane emissions across systems, (2) a more accurate upscaling (compared to empirical models), (3) a better prediction of methane emissions from inland waters under a changing climate (e.g. extended ice-off time periods in northern lakes; longer and stronger stratification in temperate deep lakes and direct warming of sediments in well-mixed shallow waters) and (4) a better understanding of the effects of human perturbations (e.g. sediment and water level management in reservoirs; eutrophication) on methane emissions and seeking for possible mitigation strategies.

5 Conclusions

This thesis project advances our understanding of formation, storage and migration of methane bubbles in freshwater sediments. It revealed the role of sediment structure in methane bubble formation. Micro-bubbles form in coarse-grained sediments by capillary invasion and larger bubbles form in fine-grained sediments by elastic/plastic deformation of the sediment-water mixture. Consequently, cohesive fine-grained sediments can store more gas than sandy sediments. Furthermore, the role of sediment mechanical properties in the formation of large bubbles was characterized. In sediments characterized by a relatively low shear yield strength (< 100 Pa), large bubbles can form and even dominate. Gas ebullition was found to be closely related to methane bubble formation and storage. Followed by initial growth by capillary invasion, bubbles continue to grow by deforming the surrounding sediment matrix. This is associated with the development of interconnected methane bubble networks and minimal ebullition was observed during this phase. Once the sediment gas storage capacity was reached, intense ebullition was observed. The bubble networks then serve as void spaces for bubble formation and provide preferential paths for bubble movement. Field measurements of the spatial distribution of gas ebullition and sediment gas content in Lake Kinneret validated laboratory findings, i.e., gas ebullition was only detected in areas where free gas had accumulated in surface sediment.

The research revealed the importance of sediment gas storage in explaining ebullition dynamics in freshwaters. Sediment gas storage capacity can be used to predict the timing of gas ebullition. A quiescent period occurs when sediment gas content is lower than the storage capacity. This concept also applies to the interpretation of spatial distributions of ebullition. Future work is needed to (1) test this theory by setting up an extended laboratory incubation experiment in which sediment gas content and ebullition flux are continuously tracked and (2) development of a process-based ebullition model that includes the role of sediment gas storage.

6 References

Aben, R. C. and others 2017. Cross continental increase in methane ebullition under climate change. Nature communications **8:** 1682. doi: 1610.1038/s41467-41017-01535-y

Algar, C., and B. Boudreau. 2009. Transient growth of an isolated bubble in muddy, fine-grained sediments. Geochimica et Cosmochimica Acta **73:** 2581-2591. doi: 2510.1016/j.gca.2009.2502.2008.

---. 2010. Stability of bubbles in a linear elastic medium: Implications for bubble growth in marine sediments. Journal of Geophysical Research: Earth Surface **115:** F03012. doi:03010.01029/02009JF001312.

Algar, C. K., B. P. Boudreau, and M. A. Barry. 2011a. Initial rise of bubbles in cohesive sediments by a process of viscoelastic fracture. Journal of Geophysical Research: Solid Earth **116**: B04207. doi: 04210.01029/02010JB008133.

---. 2011b. Release of multiple bubbles from cohesive sediments. Geophysical Research Letters **38**: L08606. doi: 08610.01029/02011GL046870.

Anderson, A., F. Abegg, J. Hawkins, M. Duncan, and A. Lyons. 1998. Bubble populations and acoustic interaction with the gassy floor of Eckernförde Bay. Continental Shelf Research **18:** 1807-1838. doi: 1810.1016/S0278-4343(1898)00059-00054.

Anderson, M. A., and D. Martinez. 2015. Methane gas in lake bottom sediments quantified using acoustic backscatter strength. Journal of Soils and Sediments **15:** 1246-1255. doi: 1210.1007/s11368-11015-11099-11361.

Barry, M., B. Boudreau, B. Johnson, and A. Reed. 2010. First - order description of the mechanical fracture behavior of fine - grained surficial marine sediments during gas bubble growth. Journal of Geophysical Research: Earth Surface **115:** F04029. doi: 04010.01029/02010JF001833.

Bastviken, D., J. Cole, M. Pace, and L. Tranvik. 2004. Methane emissions from lakes: Dependence of lake characteristics, two regional assessments, and a global estimate. Global biogeochemical cycles **18:** GB4009. doi: 4010.1029/2004GB002238.

Bastviken, D., J. J. Cole, M. L. Pace, and M. C. Van de Bogert. 2008. Fates of methane from different lake habitats: Connecting whole - lake budgets and CH4 emissions. Journal of Geophysical Research: Biogeosciences **113:** G02024. doi: 02010.01029/02007JG000608.

Bastviken, D., J. Ejlertsson, I. Sundh, and L. Tranvik. 2003. Methane as a source of carbon and energy for lake pelagic food webs. Ecology **84:** 969-981. doi: 910.1890/0012-9658(2003)1084[0969:MAASOC]1892.1890.CO;1892.

Bastviken, D., L. J. Tranvik, J. A. Downing, P. M. Crill, and A. Enrich-Prast. 2011. Freshwater methane emissions offset the continental carbon sink. Science **331:** 50-50. doi: 10.1126/science.1196808.

Beal, E. J., C. H. House, and V. J. Orphan. 2009. Manganese-and iron-dependent marine methane oxidation. Science **325:** 184-187. doi: 110.1126/science.1169984.

Beaulieu, J. J. and others 2018. Effects of an Experimental Water-level Drawdown on Methane Emissions from a Eutrophic Reservoir. Ecosystems **21:** 657-674. doi: 610.1007/s10021-10017-10176-10022.

Beaulieu, J. J., M. G. McManus, and C. T. Nietch. 2016. Estimates of reservoir methane emissions based on a spatially balanced probabilistic - survey. Limnology and Oceanography **61:** S27-S40. doi: 10.1002/lno.10284.

Bednařík, A., M. Blaser, A. Matoušů, P. Hekera, and M. Rulik. 2017. Effect of weir impoundments on methane dynamics in a river. Science of the Total Environment **584:** 164-174. doi: 110.1016/j.scitotenv.2017.1001.1163.

Best, A. I., M. D. Tuffin, J. K. Dix, and J. M. Bull. 2004. Tidal height and frequency dependence of acoustic velocity and attenuation in shallow gassy marine sediments. Journal of Geophysical Research: Solid Earth **109**: B08101. doi: 08110.01029/02003JB002

Borges, A. V. and others 2015. Globally significant greenhouse-gas emissions from African inland waters. Nature Geoscience **8:** 637-642. doi:610.1038/ngeo2486.

Boudreau, B. P. 2012. The physics of bubbles in surficial, soft, cohesive sediments. Marine and Petroleum Geology **38:** 1-18. doi: 10.1016/j.marpetgeo.2012.1007.1002.

Boudreau, B. P. and others 2005. Bubble growth and rise in soft sediments. Geology **33:** 517-520. doi: 510.1130/G21259.21251.

Boudreau, B. P., B. S. Gardiner, and B. D. Johnson. 2001. Rate of growth of isolated bubbles in sediments with a diagenetic source of methane. Limnology and Oceanography **46:** 616-622. doi: 610.4319/lo.2001.4346.4313.0616.

Brennen, C. E. 2013. Cavitation and bubble dynamics. Cambridge University Press.

Chanson, H., S. Aoki, and A. Hoque. 2006. Bubble entrainment and dispersion in plunging jet flows: freshwater vs. seawater. Journal of Coastal Research **3:** 664-677. doi: 610.2112/2103-0112.2111.

Chanton, J. P., C. S. Martens, and C. A. Kelley. 1989. Gas transport from methane - saturated, tidal freshwater and wetland sediments. Limnology and Oceanography **34:** 807-819. doi: 810.4319/lo.1989.4334.4315.0807.

Choi, J. H., Y. Seol, R. Boswell, and R. Juanes. 2011. X - ray computed - tomography imaging of gas migration in water - saturated sediments: From capillary invasion to conduit opening. Geophysical Research Letters **38:** L17310. doi: 17310.11029/12011GL048513.

Cole, J. J. and others 2007. Plumbing the global carbon cycle: integrating inland waters into the terrestrial carbon budget. Ecosystems **10:** 172-185. doi: 110.1007/s10021-10006-19013-10028.

de Mello, N. A. S. T., L. S. Brighenti, F. A. R. Barbosa, P. A. Staehr, and J. F. Bezerra Neto. 2018. Spatial variability of methane (CH4) ebullition in a tropical hypereutrophic reservoir: Silted areas as a bubble hot spot. Lake and Reservoir Management **34:** 105-114. doi: 110.1080/10402381.10402017.11390018.

Deemer, B. R. and others 2016. Greenhouse Gas Emissions from Reservoir Water Surfaces: A New Global Synthesis. BioScience **66:** 949-964. doi.org/910.1093/biosci/biw1117.

DelSontro, T., J. J. Beaulieu, and J. A. Downing. 2018. Greenhouse gas emissions from lakes and impoundments: Upscaling in the face of global change. Limnology and Oceanography Letters **3:** 64-75. doi: 10.1002/lol1002.10073.

DelSontro, T., L. Boutet, A. St - Pierre, P. A. del Giorgio, and Y. T. Prairie. 2016. Methane ebullition and diffusion from northern ponds and lakes regulated by the interaction between temperature and system productivity. Limnology and Oceanography **61**: S62-S77. doi: 10.1002/lno.10335.

DelSontro, T., M. J. Kunz, T. Kempter, A. Wüest, B. Wehrli, and D. B. Senn. 2011. Spatial heterogeneity of methane ebullition in a large tropical reservoir. Environmental Science & Technology **45:** 9866-9873. doi: 9810.1021/es2005545.

DelSontro, T., D. F. McGinnis, S. Sobek, I. Ostrovsky, and B. Wehrli. 2010. Extreme methane emissions from a Swiss hydropower reservoir: contribution from bubbling sediments. Environmental Science & Technology **44:** 2419-2425. doi: 2410.1021/es9031369.

DelSontro, T., D. F. McGinnis, B. Wehrli, and I. Ostrovsky. 2015. Size does matter: Importance of large bubbles and small-scale hot spots for methane transport. Environmental Science & Technology **49:** 1268-1276. doi: 1210.1021/es5054286.

Delwiche, K. B., and H. F. Hemond. 2017. Methane Bubble Size Distributions, Flux, and Dissolution in a Freshwater Lake. Environmental Science & Technology **51**: 13733-13739. doi: 13710.11021/acs.est.13737b04243.

Deutzmann, J. S., P. Stief, J. Brandes, and B. Schink. 2014. Anaerobic methane oxidation coupled to denitrification is the dominant methane sink in a deep lake. Proceedings of the National Academy of Sciences **111:** 18273-18278. doi: 18210.11073/pnas.1411617111.

Donis, D., S. Flury, A. Stöckli, J. E. Spangenberg, D. Vachon, and D. F. McGinnis. 2017. Full-scale evaluation of methane production under oxic conditions in a mesotrophic lake. Nature communications **8:** 1661. doi: 1610.1038/s41467-41017-01648-41464.

Downing, J. and others 2006. The global abundance and size distribution of lakes, ponds, and impoundments. Limnology and Oceanography **51:** 2388-2397. doi: 2310.4319/lo.2006.2351.2385.2388.

Gardiner, B., B. Boudreau, and B. Johnson. 2003. Growth of disk-shaped bubbles in sediments. Geochimica et Cosmochimica Acta **67:** 1485-1494. doi: 1410.1016/S0016-7037(1402)01072-01074.

Gauglitz, P. A., W. C. Buchmiller, S. G. Probert, A. T. Owen, and F. J. Brockman. 2012. Strong-Sludge Gas Retention and Release Mechanisms in Clay Simulants. Pacific Northwest National Lab.(PNNL), Richland, WA (United States).

Gauglitz, P. A., and G. Terrones. 2002. Estimated Maximum Gas Retention from Uniformly Dispersed Bubbles in K Basin Sludge Stored in Large Diameter Containers. PNNL-13893 Pacific Northwest National Laboratory, Richland, WA.

Grossart, H.-P., K. Frindte, C. Dziallas, W. Eckert, and K. W. Tang. 2011. Microbial methane production in oxygenated water column of an oligotrophic lake. Proceedings of the National Academy of Sciences **108:** 19657-19661. doi: 19610.11073/pnas.1110716108.

Harrison, J. A., B. R. Deemer, M. K. Birchfield, and M. T. O'Malley. 2017. Reservoir water-level drawdowns accelerate and amplify methane emission. Environmental Science & Technology **51:** 1267-1277. doi: 1210.1021/acs.est.1266b03185.

Hilgert, S. 2015. Analysis of spatial and temporal heterogeneities of methane emissions of reservoirs by correlating hydro-acoustic with sediment parameters. Karlsruhe Institute of Technology.

Holgerson, M. A., and P. A. Raymond. 2016. Large contribution to inland water CO2 and CH4 emissions from very small ponds. Nature Geoscience **9:** 222-226. doi: 210.1038/ngeo2654.

Jain, A., and R. Juanes. 2009. Preferential mode of gas invasion in sediments: Grain - scale mechanistic model of coupled multiphase fluid flow and sediment mechanics. Journal of Geophysical Research: Solid Earth **114:** B08101. doi: 08110.01029/02008JB006002

Johnson, B. D., B. P. Boudreau, B. S. Gardiner, and R. Maass. 2002. Mechanical response of sediments to bubble growth. Marine Geology **187:** 347-363. doi: 310.1016/S0025-3227(1002)00383-00383.

Johnson, M., M. Fairweather, D. Harbottle, T. N. Hunter, J. Peakall, and S. Biggs. 2017. Yield stress dependency on the evolution of bubble populations generated in consolidated soft sediments. AIChE Journal **63:** 3728-3742. doi: 3710.1002/aic.15731.

Jones, R. I., and J. Grey. 2011. Biogenic methane in freshwater food webs. Freshwater Biology **56:** 213-229. doi: 210.1111/j.1365-2427.2010.02494.x.

Katsman, R. 2015. Correlation of shape and size of methane bubbles in fine-grained muddy aquatic sediments with sediment fracture toughness. Journal of Structural Geology **70**: 56-64. doi: 10.1016/j.jsg.2014.1011.1002.

Katsnelson, B., R. Katsman, A. Lunkov, and I. Ostrovsky. 2017. Acoustical methodology for determination of gas content in aquatic sediments, with application to Lake Kinneret, Israel, as a case study. Limnology and Oceanography: Methods **15:** 531-541. doi: 510.1002/lom1003.10178.

Kuivila, K., J. Murray, A. Devol, and P. Novelli. 1989. Methane production, sulfate reduction and competition for substrates in the sediments of Lake Washington. Geochimica et Cosmochimica Acta **53:** 409-416. doi: 410.1016/0016-7037(1089)90392-X.

Leifer, I., and R. K. Patro. 2002. The bubble mechanism for methane transport from the shallow sea bed to the surface: A review and sensitivity study. Continental Shelf Research **22**: 2409-2428. doi: 2410.1016/S0278-4343(2402)00065-00061.

Li, S., and R. T. Bush. 2015. Revision of methane and carbon dioxide emissions from inland waters in India. Global change biology **21:** 6-8. doi: 10.1111/gcb.12705

Li, S., Q. Zhang, R. T. Bush, and L. A. Sullivan. 2015. Methane and CO2 emissions from China's hydroelectric reservoirs: a new quantitative synthesis. Environmental Science and Pollution Research **22:** 5325-5339. doi: 5310.1007/s11356-11015-14083-11359.

Li, X., and Y. Yortsos. 1995. Theory of multiple bubble growth in porous media by solute diffusion. Chemical Engineering Science **50:** 1247-1271. doi: 1210.1016/0009-2509(1295)98839-98837.

Liu, L., D. Liu, D. M. Johnson, Z. Yi, and Y. Huang. 2012. Effects of vertical mixing on phytoplankton blooms in Xiangxi Bay of Three Gorges Reservoir: Implications for management. Water research **46:** 2121-2130. doi: 2110.1016/j.watres.2012.2101.2029.

Lovley, D. R., and M. J. Klug. 1983. Sulfate reducers can outcompete methanogens at freshwater sulfate concentrations. Applied and Environmental Microbiology **45:** 187-192. doi: 0099-2240/0083/010187-010106$010102.010100/010180.

Maeck, A. and others 2013. Sediment trapping by dams creates methane emission hot spots. Environmental Science & Technology **47:** 8130-8137. doi: 8110.1021/es4003907.

Maeck, A., H. Hofmann, and A. Lorke. 2014. Pumping methane out of aquatic sediments: Ebullition forcing mechanisms in an impounded river. Biogeosciences **11:** 2925-2938. doi: 2910.5194/bg-2911-2925-2014.

Martinez, D., and M. A. Anderson. 2013. Methane production and ebullition in a shallow, artificially aerated, eutrophic temperate lake (Lake Elsinore, CA). Science of the total environment **454:** 457-465. doi: 410.1016/j.scitotenv.2013.1003.1040.

Mbaka, J. G., C. Somlai, D. Köpfer, A. Maeck, A. Lorke, and R. B. Schäfer. 2014. Methane-derived carbon in the benthic food web in stream impoundments. PloS one **9:** e111392. doi: 111310.111371/journal.pone.0111392.

McGinnis, D. F., J. Greinert, Y. Artemov, S. Beaubien, and A. Wüest. 2006. Fate of rising methane bubbles in stratified waters: How much methane reaches the atmosphere? Journal of Geophysical Research: Oceans **111:** C09007. doi: 09010.01029/02005JC003183.

Myhre, G. and others 2013. Anthropogenic and natural radiative forcing. Climate change **423**: 658-740.

O'Reilly, C. M. and others 2015. Rapid and highly variable warming of lake surface waters around the globe. Geophysical Research Letters **42:** 10773-10781. doi: 10710.11002/12015GL066235.

Ostrovsky, I., D. F. McGinnis, L. Lapidus, and W. Eckert. 2008. Quantifying gas ebullition with echosounder: The role of methane transport by bubbles in a medium - sized lake. Limnology and Oceanography: Methods **6:** 105-118. doi: 110.4319/lom.2008.4316.4105.

Ostrovsky, I., and J. Tęgowski. 2010. Hydroacoustic analysis of spatial and temporal variability of bottom sediment characteristics in Lake Kinneret in relation to water level fluctuation. Geo-Marine Letters **30:** 261-269. doi: 210.1007/s00367-00009-00180-00364.

Oswald, K. and others 2015. Light-dependent aerobic methane oxidation reduces methane emissions from seasonally stratified lakes. PLoS One **10:** e0132574. doi: 0132510.0131371/journal.pone.0132574.

Rahalkar, M., and B. Schink. 2007. Comparison of aerobic methanotrophic communities in littoral and profundal sediments of Lake Constance by a molecular approach. Applied and environmental microbiology **73:** 4389-4394. doi: 4310.1128/AEM.02602-02606.

Powell, M. R. and others 2014. Evaluation of Gas Retention in Waste Simulants: Intermediate-Scale Column and Open-Channel-Depth Tests. Pacific Northwest National Lab.(PNNL), Richland, WA (United States).

Scandella, B. P., K. Delwiche, H. Hemond, and R. Juanes. 2017. Persistence of bubble outlets in soft, methane - generating sediments. Journal of Geophysical Research: Biogeosciences **122:** doi:10.1002/2016JG003717.

Scandella, B. P., L. Pillsbury, T. Weber, C. Ruppel, H. F. Hemond, and R. Juanes. 2016. Ephemerality of discrete methane vents in lake sediments. Geophysical Research Letters **43:** 4374-4381. doi: 4310.1002/2016GL068668.

Scandella, B. P., C. Varadharajan, H. F. Hemond, C. Ruppel, and R. Juanes. 2011. A conduit dilation model of methane venting from lake sediments. Geophysical Research Letters **38:** L06408. doi: 06410.01029/02011GL046768.

Schubert, C. J., T. Diem, and W. Eugster. 2012. Methane emissions from a small wind shielded lake determined by eddy covariance, flux chambers, anchored funnels, and boundary model calculations: a comparison. Environmental Science & Technology **46**: 4515-4522. doi: 4510.1021/es203465x.

Sepulveda-Jauregui, A. and others 2018. Eutrophication exacerbates the impact of climate warming on lake methane emission. Science of The Total Environment **636:** 411-419. doi: 410.1016/j.scitotenv.2018.1004.1283.

Sherwood, D. J., and A. E. Sáez. 2014. The start of ebullition in quiescent, yield-stress fluids. Nuclear Engineering and Design **270**: 101-108. doi: 110.1016/j.nucengdes.2013.1012.1050.

Sivan, O. and others 2011. Geochemical evidence for iron - mediated anaerobic oxidation of methane. Limnology and Oceanography **56:** 1536-1544. doi: 1510.4319/lo.2011.1556.1534.1536

Sobek, S., T. DelSontro, N. Wongfun, and B. Wehrli. 2012. Extreme organic carbon burial fuels intense methane bubbling in a temperate reservoir. Geophysical Research Letters **39:** L01401. doi: 01410.01029/02011GL050144.

Tang, J., Q. Zhuang, R. Shannon, and J. White. 2010. Quantifying wetland methane emissions with process-based models of different complexities. Biogeosciences **7:** 3817-3837. doi: 3810.5194/bg-3817-3817-2010.

Tang, K. W., D. F. McGinnis, D. Ionescu, and H.-P. Grossart. 2016. Methane production in oxic lake waters potentially increases aquatic methane flux to air. Environmental Science & Technology Letters **3:** 227-233. doi: 210.1021/acs.estlett.1026b00150.

Tranvik, L. J. and others 2009. Lakes and reservoirs as regulators of carbon cycling and climate. Limnology and Oceanography **54:** 2298-2314. doi: 2210.4319/lo.2009.2254.2296_part_2292.2298.

Tóth, Z., V. Spiess, J. M. Mogollón, and J. B. Jensen. 2014. Estimating the free gas content in Baltic Sea sediments using compressional wave velocity from marine seismic data. Journal of Geophysical Research: Solid Earth **119**: 8577-8593. doi: 8510.1002/20

Tušer, M., T. Picek, Z. Sajdlová, T. Jůza, M. Muška, and J. Frouzová. 2017. Seasonal and Spatial Dynamics of Gas Ebullition in a Temperate Water - Storage Reservoir. Water Resources Research **53:** 8266-8276. doi: 8210.1002/2017WR020694.

Van Kessel, T., and W. Van Kesteren. 2002. Gas production and transport in artificial sludge depots. Waste Management **22:** 19-28. doi: 10.1016/S0956-1053X(1001)00021-00026.

van Kesteren, W., and T. van Kessel. 2002. Gas bubble nucleation and growth in cohesive sediments. Proceedings in Marine Science **5:** 329-341. doi: 310.1016/S1568-2692(1002)80025-80020.

Varadharajan, C., and H. F. Hemond. 2012. Time - series analysis of high - resolution ebullition fluxes from a stratified, freshwater lake. Journal of Geophysical Research: Biogeosciences **117:** G02004, doi: 02010.01029/02011JG001866.

Walter, K. M., S. Zimov, J. Chanton, D. Verbyla, and F. Chapin Iii. 2006. Methane bubbling from Siberian thaw lakes as a positive feedback to climate warming. Nature **443:** 71-75. doi: 10.1038/nature05040.

Wang, H., J. Lu, W. Wang, L. Yang, and C. Yin. 2006. Methane fluxes from the littoral zone of hypereutrophic Taihu Lake, China. Journal of Geophysical Research: Atmospheres **111:** D17109. doi: 17110.11029/12005JD006864.

Wheeler, S. 1988. A conceptual model for soils containing large gas bubbles. Geotechnique **38:** 389-397. doi: 310.1680/geot.1988.1638.1683.1389.

---. 1990. Movement of large gas bubbles in unsaturated fine - grained sediments. Marine Georesources & Geotechnology **9:** 113-129. doi: 110.1080/10641199009388234.

Whiticar, M. J., E. Faber, and M. Schoell. 1986. Biogenic methane formation in marine and freshwater environments: CO2 reduction vs. acetate fermentation—isotope evidence. Geochimica et Cosmochimica Acta **50:** 693-709. doi: 610.1016/0016-7037(1086)90346-90347.

Wik, M., P. M. Crill, R. K. Varner, and D. Bastviken. 2013. Multiyear measurements of ebullitive methane flux from three subarctic lakes. Journal of Geophysical Research: Biogeosciences **118:** 1307-1321. doi.org/1310.1002/jgrg.20103.

Wik, M., B. F. Thornton, D. Bastviken, J. Uhlbäck, and P. M. Crill. 2016. Biased sampling of methane release from northern lakes: A problem for extrapolation. Geophysical Research Letters **43:** 1256-1262. doi: 1210.1002/2015GL066501.

Wilkinson, J., A. Maeck, Z. Alshboul, and A. Lorke. 2015. Continuous seasonal river ebullition measurements linked to sediment methane formation. Environmental Science & Technology **49:** 13121-13129. doi: 13110.11021/acs.est.13125b01525.

Xiao, S. and others 2014. Gas transfer velocities of methane and carbon dioxide in a subtropical shallow pond. Tellus B **66:** 23795. doi: 23710.23402/tellusb.v23766.23795.

Yvon-Durocher, G. and others 2014. Methane fluxes show consistent temperature dependence across microbial to ecosystem scales. Nature **507:** 488-491. doi: 410.1038/nature13164.

Zarfl, C., A. E. Lumsdon, J. Berlekamp, L. Tydecks, and K. Tockner. 2015. A global boom in hydropower dam construction. Aquatic Sciences **77:** 161-170. doi: 110.1007/s00027-00014-00377-00020.

Author contributions

This thesis is based on four original research articles provided in Appendix I-IV which were conceived by all of the authors. I am the lead author of three of the articles (Part 1, 2, and 4 of the thesis). The contributions of all authors are explained in the following:

Part 1: Liu, L., J. Wilkinson, K. Koca, C. Buchmann, and A. Lorke (2016). The role of sediment structure in gas bubble storage and release. Journal of Geophysical Research: Biogeosciences 121: 1992-2005. doi: 1910.1002/2016JG003456. (Appendix I)

Conception and design: LL, AL
Data acquisition: LL, KK, CB
Data analysis: LL, KK, CB
Interpretation of results: LL, AL, JW
Writing the manuscript: LL
Revising the manuscript: AL, JW

Part 2: Liu, L. T. De Kock, J. Wilkinson, V. Cnudde, S. B. Xiao, C. Buchmann, D. Uteau, S. Peth and A. Lorke (2018). Methane bubble growth and migration in aquatic sediments observed by X-ray μCT. Environmental Science & Technology 52: 2007-2015. doi: 2010.1021/acs.est.2007b06061. (Appendix II)

Conception and design: LL, TDK, AL
Data acquisition: LL, TDK, CB, DU
Data analysis: LL
Interpretation of results: LL, AL
Writing the manuscript: LL
Revising the manuscript: AL, JW, VC, SBX, DU, SP

Part 3: Dück Y., L. Liu, A. Lorke, I. Ostrovsky, R. Katsman and C. Jokiel. A novel freeze corer for characterization of methane bubbles and coring disturbances. Submitted to Limnology and Oceanography: Methods, under review. (Appendix III)

Conception and design: YD, LL, AL, CJ
Data acquisition: YD, LL, RK
Data analysis: YD, LL (lab experiments; CT image analysis for sediment gas content)
Interpretation of results: YD, LL
Writing the manuscript: YD, LL
Revising the manuscript: AL, LL, CJ, IO, RK

Part 4: Liu L., K. Sotiri, Y. Dück, S. Hilgert, I. Ostrovsky, E. Uzhansky, R. Katsman, B. Katsnelson, R. Bookman, J. Wilkinson and A. Lorke. The control of sediment gas accumulation on spatial distribution of ebullition in Lake Kinneret. Submitted to Limnology and Oceanography, under review. (Appendix IV)

Conception and design: LL, AL, IO, MK, MH
Data acquisition: LL, KS, SH, IO, YD, EU
Data analysis: LL, KS, IO
Interpretation of results: LL, KS, SH, AL
Writing the manuscript: LL
Revising the manuscript: AL, IO, KS, SH, YD, EU, RK, BK, RB, JW

Declaration

I hereby declare that the thesis entitled "*Mechanisms of methane bubble formation, storage and release in freshwater sediments*" is the result of my own work except where otherwise indicated. It has not been submitted for any other degree at another university or scientific institution.

Landau, 29 October 2018 …….

Liu Liu

Curriculum Vitae

Liu Liu (刘流)	
Date of birth	25 June 1987
Place of birth	Hubei, China
Nationality	China
Current address	Bornheimer Str. 15
	76829 Landau, Germany
Email	liu@uni-landau.de

Since March 2015	PhD candidate, Institute for Environmental Sciences, University of Koblenz-Landau, Germany
September 2009 - July 2012	MSc, College of Hydraulic & Environmental Engineering, China Three Gorges University, China
September 2005 - July 2009	BSc, College of Hydraulic & Environmental Engineering, China Three Gorges University, China
September 2001 - July 2005	Senior High School of Baokang No. 1, Hubei, China

Acknowledgements

To close, I would like to take this opportunity to thank all of you who helped me to accomplish this thesis. This would not have been possible without any of you.

First and foremost, thanks to my family for their love and support, particularly to my wife Wang Si who has been accompanying me all the time since I started being obsessed to science. Thanks also to my parents in China who always unconditionally back me up.

I thank my supervisor, Andreas Lorke, for his guidance, patience and encouragement throughout my time studying at University of Koblenz-Landau (Uni Landau). I appreciate the maximum freedom he provided in proposing research questions, and enjoyed very much the long discussions during our meetings. Working with him was such a pleasure. I will benefit for my whole lifetime from him, not only because of the excellent research skills I learned from him, but also his enthusiasm for research.

I am deeply grateful to my collaborators who have made this research ever possible. They are Yannick Dück at Cologne University of Applied Science, Laura Bolsenkötter and Eric Zimmermann at DB Sediments, Klajdi Sotiri and Stephan Hilgert at KIT, Christian Buchmann, David Jan and Eva Kröner at Uni Landau, Tim De Kock and Veerle Cnudde at Ghent University, Daniel Uteau and Stephan Peth at University of Kassel, Regina Katsman, Ernst Uzhansky, Boris Katsnelson and Revital Bookman at University of Haifa, Shangbin Xiao at China Three Gorges University, Kyle Delwiche at MIT and Jorge Ramirez at University of Bern.

I felt lucky to be a member of Environmental Physics group at Uni Landau. Thanks to the good atmosphere developed by my colleagues, I enjoyed so much staying in Landau. Angelika Holderle, the secretary of our group, saved me from filling forms and solving daily-life issues. Without her kind assistance, starting at Uni Landau would not have been so smooth and easy and I would not have been able to 100% devote myself into research. Christoph Bors, the technician in our group, supported me from the lab to the field. Without his help, all the plans would only have been plans. Jeremy Wilkinson, helped me improve my research skills with his valuable experience, and others like Christian Noss, Kaan Koca, Florian Burgis and Pascal Bodmer helped in many ways including but not limited to inspiring discussions during lunch breaks and sharing resources inside the group.

Many thanks to Ilia Ostrovsky at Kinneret Limnological Laboratory. Studying Lake Kinneret would not have been possible without his generous support. Thanks to Daniel McGinnis, Sabine Flury, Daphné Donis, Dominic Vachon, Timon Langenegger and Cesar Fernando Ordonez Valdebenito at University of Geneva, and Andreas Mäck, Mike Fuchs and Christof Hübner who supported me in the lab and field. Thanks also to David Johnson and Jorge Ramirez for critically proofreading the first draft of the thesis.

Acknowledgements to those whose names are not listed here: the doctors and nurses who gave me access to the medical X-ray CT scanners in clinic center of Landau, Germany and in the hospital of Tiberias, Israel, and technicians at Kinneret Limnological Laboratory, Israel.

This work was financially supported by the German Research Foundation (grant LO 1150/5) and the short-term completion scholarship provided by the German Academic Exchange Service (DAAD).

Appendices

Appendix I

The role of sediment structure in gas bubble storage and release

L. Liu[1], J. Wilkinson[1], K. Koca[1], C. Buchmann[1], and A. Lorke[1]

[1] Institute for Environmental Sciences, University of Koblenz-Landau, Landau, Germany

Please click the following link to read the publication

https://agupubs.onlinelibrary.wiley.com/doi/full/10.1002/2016JG003456

Appendix II

Methane Bubble Growth and Migration in Aquatic Sediments Observed by X-ray μCT

Liu Liu[1], Tim De Kock[2], Jeremy Wilkinson[1], Veerle Cnudde[2], Shangbin Xiao[3], Christian Buchmann[1], Daniel Uteau[4], Stephan Peth[4], and Andreas Lorke[1]

[1] Institute for Environmental Sciences, University of Koblenz-Landau, 76829 Landau, Germany

[2] PProGRess-UGCT, Department of Geology, Ghent University, Krijgslaan 281/S8, 9000 Ghent, Belgium

[3] College of Hydraulic & Environmental Engineering, China Three Gorges University, 443002 Yichang, China

[4] Department of Soil Science, University of Kassel, 37213 Witzenhausen, Germany

Please click the following link to read the publication

https://pubs.acs.org/doi/abs/10.1021/acs.est.7b06061

Appendix III

A novel freeze corer for characterization of methane bubbles and coring disturbances

Yannick Dück,[*1] Liu Liu,[2] Andreas Lorke,[2] Ilia Ostrovsky,[3] Regina Katsman[4] and Christian Jokiel[1]

[1] Cologne University of Applied Science, Institute of Hydraulic Engineering and Water Resources Management, Betzdorfer Str. 2, 50679 Cologne, Germany

[2] University of Koblenz-Landau, Institute for Environmental Sciences, Fort Str. 7, 76829 Landau, Germany

[3] Yigal Allon Kinneret Limnological Laboratory, Israel Oceanographic and Limnological Research, Migdal, Israel

[4] The Dr. Moses Strauss Department of Marine Geosciences, Faculty of Natural Sciences, University of Haifa, Mount Carmel, Haifa, 3498838, Israel

A novel freeze corer for characterization of methane bubbles and coring disturbances

Yannick Dück,[*1] Liu Liu,[2] Andreas Lorke,[2] Ilia Ostrovsky,[3] Regina Katsman[4] and Christian Jokiel[1]

[1] Cologne University of Applied Science, Institute of Hydraulic Engineering and Water Resources Management, Betzdorfer Str. 2, 50679 Cologne, Germany

[2] University of Koblenz-Landau, Institute for Environmental Sciences, Fort Str. 7, 76829 Landau, Germany

[3] Yigal Allon Kinneret Limnological Laboratory, Israel Oceanographic and Limnological Research, Migdal, Israel

[4] The Dr. Moses Strauss Department of Marine Geosciences, Faculty of Natural Sciences, University of Haifa, Mount Carmel, Haifa, 3498838, Israel

[*] Correspondence: yannick.dueck@th-koeln.de

I. Abstract

Aquatic ecosystems with organic-rich sediments are a globally significant source of methane to the atmosphere. Particularly in shallow waters, ebullition is often a dominant emission pathway, although current knowledge on the processes controlling gas bubble formation, persistence and release in aquatic sediments is limited. A prerequisite for accurate quantification of the structure and quantity of methane bubbles in aquatic sediments is to preserve the ambient in situ conditions during recovery and analysis. A novel freeze corer has been developed, which is facilities sampling of gas-bearing and water saturated sediments for laboratory analysis of gas bubble characterization using X-ray computer tomography. The corer freezes the sediment inside of a double-walled corer by a mixture of dry-ice and ethanol, added into the space between the corer walls. This corer offers several advantages: moderate costs, simple and robust design that allows the deployment from small boats and the ability to preserve the *in situ* features of the sediment. To validate application of the freeze coring technique for gas bubble observations, laboratory experiments were conducted to investigate the effect of freezing on sediment gas content, bubble size and geometry by comparing computer tomography scans of frozen and unfrozen cores. The performance of the sediment freeze corer was evaluated under field conditions in Lake Kinneret (the Sea of Galilee, Israel). The results demonstrate the capability of the freeze-coring method for the sampling of gas-bearing sediments, but also suggest the need for further investigations on physical disturbances of the sediment column during corer penetration.

II. INTRODUCTION

In recent years, aquatic ecosystems (e.g. lakes, reservoirs, rivers and coastal waters) have been recognized as an important source of methane (Bastviken et al. 2011). Methane is formed in aquatic sediment through anaerobic decomposition of organic matter (Martens and Berner 1974), and can be stored and released as bubbles. In shallow waters, ebullition (bubbling) can be a dominant pathway for methane emissions (Martens and Berner 1974; Martens and Albert 1995; DelSontro et al. 2010; Maeck et al. 2013; Xiao et al. 2014). Ebullition-mediated flux is often highly variable in space and time (Maeck et al. 2014; Varadharajan and Hemond 2012; Wilkinson et al. 2015), with sediment gas storage being an important parameter for explaining this dynamics (Liu et al. 2016). In addition, experiments demonstrated that gas formation and transport in sediments can be described as a function of gas bubble shape, orientation and size distributions (Algar et al. 2011; Boudreau et al. 2005; Liu et al. 2016). To apply these experimental and theoretical findings to natural lakes, *in situ* sediment gas content and bubble size distribution in aquatic sediments need to be characterized.

To preserve gas bubbles in sediment samples, an appropriate coring technique with minimal disturbance is required. Wever et al. (1998) demonstrated that sediment gas content can increase up to six fold in half an hour in response to a pressure reduction of 0.5 bar, corresponding to recovery of a sediment core from relatively shallow waters. The gas bubble expansion resulting from the decreased hydrostatic pressure during core recovery can change the size and position of bubbles (Scandella et al. 2011), while destroying sediment structure and layering. In addition, new bubbles may form from dissolved gas in the porewater due to the rise in temperature (lake bed is usually colder than the temperature at the surface of the aquatic system), causing reduction in methane solubility (Lane and Taffs 2002) and increased gas production. Therefore none of traditional coring techniques (e.g., gravity corers, percussion corers, vibra-corers and drill corers) is capable of taking intact cores without causing significant disturbances in gas-bearing sediment. Moreover, common tube samplers are not suitable for taking undisturbed cores of water-saturated sediments, if cohesion is low (Strasser et al. 2015), where the sample liquefies and can be lost during core recovery. For this purpose, regular (non-pressurized) cores are not desirable.

These drawbacks can be avoided by preserving *in situ* hydrostatic pressure in closed coring devices. Pressure corer have been developed for characterizing gas-bearing sediments in the Baltic Sea (Abegg and Anderson 1997). The *in situ* hydrostatic pressure was preserved by capping a pressure tight aluminum transfer chamber at the seabed floor with the help of divers. However, the application of pressure cores obtained by divers are limited to shallow depths

(Abegg and Anderson 1997). Various pressure corers have been developed and deployed in marine environments, such as the Pressure Coring Barrel developed by the Deep Sea Drilling Project and the Pressure Coring Sampler developed by the Ocean Drilling Program (Li et al. 2016). Such pressure corer requires expertise and a dedicated working platform, which makes it expensive, though the average core recovery ratio for these pressure corer is less than 60% (e.g. Yamamoto et al. 2012; Riedel et al. 2006).

As an alternative technique, freeze corer have been introduced for detailed stratigraphic analysis of lake sediments (Lisle 1989) and for sampling of fluffy sediment. When taking freeze cores, sediment is frozen to the surface of the sampler, which is filled with a coolant such as liquid nitrogen (Pachur et al. 1984) or dry ice, preferably mixed with ethanol. Freezing the sediment preserves gas bubbles under *in situ* hydrostatic pressure and thus provides information on bubble population in sediment samples.

Freeze coring potentially has additional advantages in comparison to other coring techniques. The vertical sediment structure is not disturbed by gas bubble expansion and release upon lifting the corer through the water column (Wright 1993). Freeze coring can facilitate sampling of undisturbed sediment cores, which are unaffected by the fast degassing that occur after a drop in hyrostatic pressure (Verschuren 2000), particularly in lakes and reservoirs with organic-rich sediments (which favors methane production under anaerobic conditions). Compared to pressure corers, freeze coring has lower costs, requires less equipment (a small fishing boat is sufficient), is easier to handle (2-3 people without requiring much expertise) and can be applied over a wide range of water depths.

Although extensive research has been carried out on freeze core sampling, little is known about how freezing affects the amount and size distribution of free gas in sediments. Here we present a new freeze corer, which allows sampling of gas-bearing lake sediment. With laboratory experiments, we evaluated the cooling effect (approx. from +14°C to -78°C) on gas bubble volume, shape, size distribution and on the total gas content in sediment cores. The freeze corer was tested in Lake Kinneret, Israel, to characterize methane bubbles in lake sediment.

III. MATERIALS AND PROCEDURES

A. Freeze Corer: Design and Components

The novel freeze coring technique is a further development of the remote-controlled freeze corer described by Lotter et al. (1997). The corer consists of four main components (Fig. 1):

(A) tripod as a supporting frame; (B) freeze corer, (C) pulley system and (D) underwater video camera.

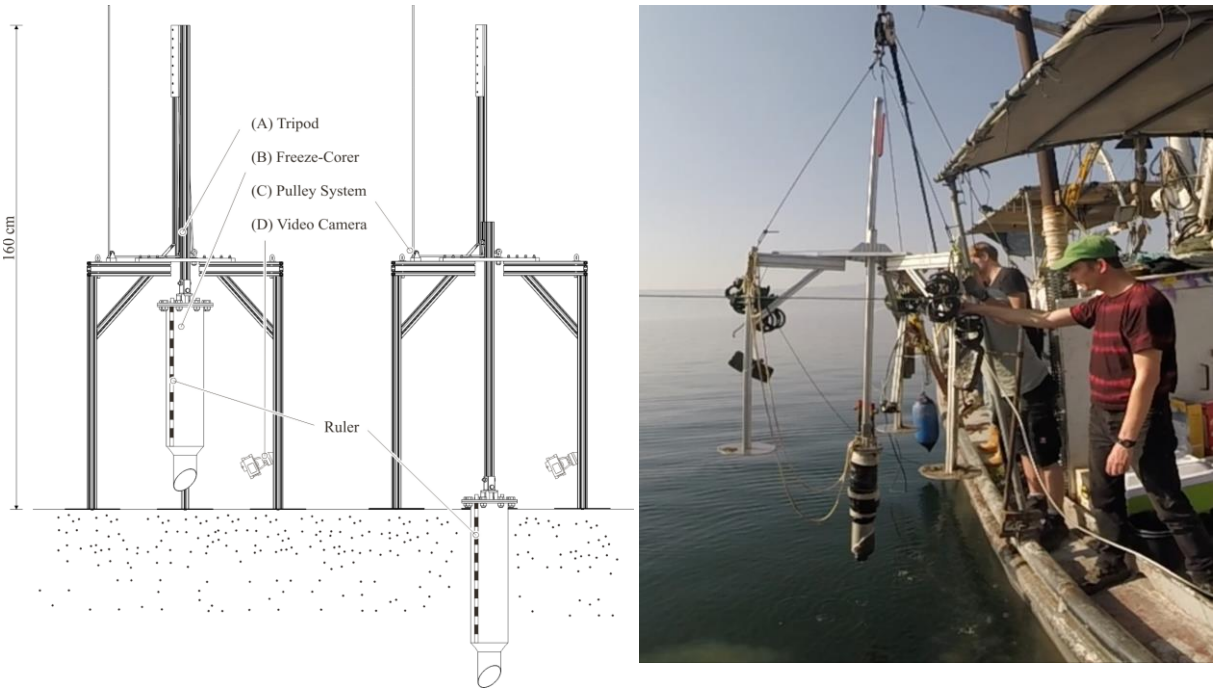

Figure 1. Left: Sketch of the tripod and corer with position before and after penetration; Right: Photo of sediment sampling at Lake Kinneret, Israel, showing the recovery of a core.

Tripod

The tripod (height 160 cm) is made of low-weight modular aluminum profiles, which can easily be assembled and extended. The three bars, with stabilizing crossbars, have a length of 50 cm. All components can be fitted in two aluminum cases with a total weight of 40 kg. Round plates with a diameter of 30 cm are mounted below the legs to prevent the tripod from sinking into the sediment, which is important for representative sampling (Blomqvist 1991; Flannagan 1970). After deployment at the lake bottom, the tripod remains loosely tethered to an anchored boat. This prevents that rolling and pitching of the vessel cause coring disturbances, although care must be taken that the sampler does not hit the lake bed and causes disturbance before the corer actually enters the sediment (Hessler and Jumars 1974; Snider et al. 1984). Depending on the consolidation status of the sediment, additional weights can be attached to improve stability.

A high penetration velocity increases the risk of washing away the surficial sediment layer before impact due to a hydraulic shock wave (McIntyre 1971; Glew et al. 2002). To reduce this effect, corer penetration is controlled manually by a static rope. With a 4-way pulley system, a transmission of 1:4 is achieved and a precise penetration with constant force is facilitated. With

this, the hydraulic impulse induced by penetration can be minimized and the corer is driven at a constant velocity of approx. 7 cm/s into the sediment to reduce the risk of core shortening (Blomqvist 1991).

Corer

The corer is made of 2 mm thick stainless steel to ensure sufficient penetration strength. It mainly consists of a (1) cutting edge, (2) a double-walled tube and a (3) corer head. Contrary to common freeze corer designs, where a lance or wedge type corer freezes the sediment at the outside of the wall, the sediment is frozen within the corer walls in the present design. This ensures a defined sample volume, reduces the freezing time, because the sediment freezes radially to the center of the core, while a sharp cutting edge reduces disturbances to sediment structure.

(1) Cutting edge: To reduce penetration resistance, the lower end of the corer was beveled to a 45° angle edge (inner diameter 72 mm, length 75 mm). Above the cutting edge, the tube outer diameter increases gradually from 76 to 100 mm to reduce friction.

(2) Double-walled tube: The double-walled tube is a container for the cooling agent, which starts 75 mm above the cutting edge. The length of the tube is 70 cm, but can be adjusted to collect longer sediment cores. The 72 mm inner diameter was chosen to allow for a relatively low wall friction and a reduced freezing time (< 30 min).

(3) Corer head: The corer head is a massive (10 mm) stainless-steel flange. It is equipped with two overpressure valves and a junction to connect the corer to the tripod. Two overpressure valves mounted on the lid of the corer head allow the release of CO_2 as a result of sublimation of dry ice at excess pressure.

Video camera

An underwater video camera is used to obtain an optimum position for tripod deployment, to avoid disturbance of the sediment structure before penetration and to support the penetration procedure. A low-cost underwater video camera (GoPro 4 Black: up to 4K/30 fps; waterproofed up to 40 m water depth) and illumination system is mounted on the tripod (Fig. 1). For real-time video transmission, a coaxial cable is mounted at the backside of the camera to transmit the WiFi signal under water. The signal can be received at the other end of the cable using a common smartphone or tablet. This supports the optimum placement of the tripod on the sediment surface and the control of penetration speed as well as measurement of corer penetration depth to determine the extent of core shortening. Penetration depth can be measured

with the camera using a ruler, which is attached to the corer. Furthermore, the degree of disturbance caused by corer penetration can be evaluated by observing the amount of released gas bubbles during penetration.

B. **Lab Experiment: Setup**

A lab experiment was conducted to evaluate quantitatively the effects of freezing on the number and size distribution of sediment gas bubbles. Three types of homogenized natural sediments were used, which differed in predominant grain size (clay: D_{50} = 20 μm, silt: D_{50} = 200 μm and sand: D_{50} = 400 μm, where D_{50} denotes the median grain diameter). To fuel biogenic gas production and bubble formation, the sediments were amended with air-dried leaf litter (10 g L^{-1} of wet sediment) (Liu et al. 2016).

Triplicates of each sediment were prepared in identical Plexiglas tubes (6 cm diameter; 25 cm long). The tubes were filled with a 10 cm (0.3 L) wet sediment and a 5 cm (0.15 L) layer of tap water. An initial 10 cm high headspace was left to allow the water level to rise due to gas bubble formation in sediment. The tubes were kept upright and capped at both ends to create an anaerobic environment for methane production. A 1 L inflatable gas bag was connected to the top cap to collect gas and to avoid gas pressure build-up. The sediment cores were stored in darkness at a constant temperature of 19°C for one week to allow for gas bubble formation.

Lab Experiment: X-ray CT scan

After an incubation period of one week, the cores were carefully transported to a local clinic for X-ray computed tomography (CT) scanning. The cores were fitted into a plastic frame and scanned simultaneously with a medical CT scanner (Simons AS, 120 kV, exposure time 1 s, slice thickness 0.6 mm). The spatial resolution (voxel size) of the CT image was 0.04 mm^3 ($0.273^2 \times 0.6$ mm^3). After the initial scan, the cores were placed into a plastic box containing dry ice mixed with ethanol (temperature ~ -78°C). After 45 min, the cores were completely frozen and a second CT scan was performed.

Lab Experiment: Data analysis

Bubble size (D_{eq}: equivalent sphere diameter) distribution in the sediments before and after freezing were analyzed using Blob 3D (Ketcham 2005). Raw CT images were converted to gray-scale images (gray-scale value 0 - 255) and then imported to Blob 3D software. By selecting areas on CT images representing gas bubbles, an averaged gray-scale value for gas phase was determined. Binary images were then created by applying a global threshold to the

gray-scale images, resulting in black-white images that separate gas bubbles from sediment matrix. Bubble volume distributions were calculated using three-dimensional object identification and classification features of the Blob 3D software. Depth profiles of volumetric gas content (θ) in sediment cores were calculated from the fraction of black area on each vertical slice. A global threshold (image intensity < 5) was chosen for all cores for meaningful comparison according to the histogram of all intensity distributions. 3D visualizations of sediment gas bubbles were created using the ImageJ 3D volume viewer (Schmid et al. 2010).

Lake Kinneret: Study Site

Lake Kinneret is a large meso-eutrophic and moderately deep (maximum depth ~ 42 m) freshwater lake, located in the northern part of the Afro-Syrian Rift Valley (Figure 2). The lake is thermally stratified during April - December, resulting in anoxic conditions in the hypolimnion during May - June. Lake Kinneret sediments are rich in authochthonous organic material (Sobek et al. 2011) and contain large amount of gaseous methane (Ostrovsky and Tegowski 2010; Katsnelson et al. 2017). Sediments are usually sandy in the shallower zone, and silty-muddy in the pelagic zone (Ostrovsky and Yacobi 1999). The mineralogical compositions of sediments differs between shallow sites (especially those close to the Jordan River inlet, Figure 2), and the lake center. The sediments in the shallow northern part contain a high proportion of heavy iron-rich silicates and rutile, both of terrestrial origin. At the central site of the lake, the sediment is richer in light silicates (containing sodium and potassium) and calcite, typical of autochthonous plankton debris, massively precipitating in spring (Koren and Ostrovsky 2002). Other shallow sites (away from the Jordan inlet) contain a mixture of these groups of minerals (Sobek et al. 2011).

Close to the Jordan inflow, mineral surface area (36.6 $m^2\ g^{-1}$) is about two-fold larger than that at other sites in the lake. Sedimentation rates are highest at locations close to the River inlet (6.3 mm yr^{-1}), lower at other shallow sites of the lake (2.0 - 2.8 mm yr^{-1}), and intermediate at the lake center (4.5 mm yr^{-1}) (Sobek et al. 2011).

Lake Kinneret: Field Masurements

In December 2016, the freeze corer was tested during a field campaign at Lake Kinneret, Israel. Four freeze cores were taken along a North-Western (Figure 2) radial offshore transect from shallow to deep at 11.5, 19, 35.8 and 35.9 m water depth, respectively, to cover the variability in sediment type. An additional freeze core (using a hollow lance filled with coolant) was taken close to the Jordan River inflow, for visual inspection of sediment bubble distribution.

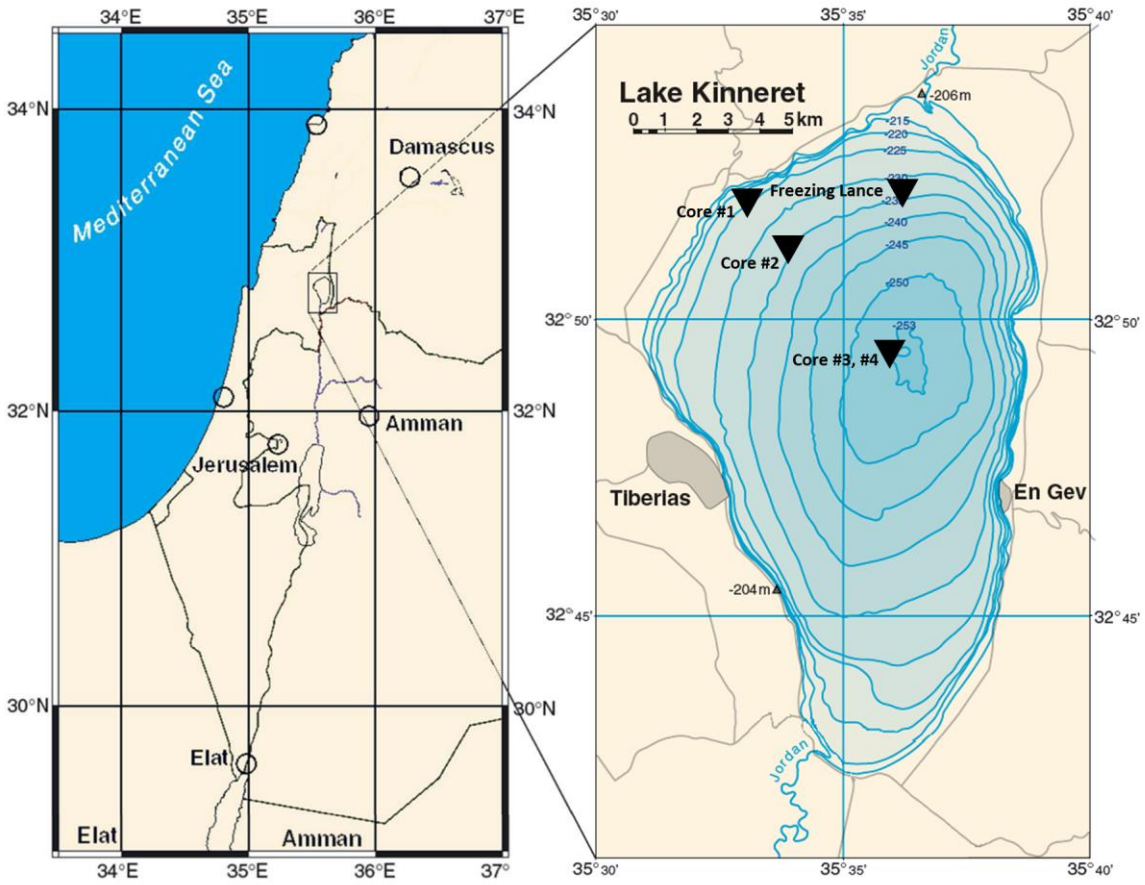

Figure 2. Map of Israel and neighboring countries with the location of Lake Kinneret. The map on the right hand side shows depth contours and the location of the sampling sites for freeze cores Adapted from (Ron et al. 2007).

The corer was operated on an 18 m long fishing boat equipped with a crane, which was used to deploy and to recover the tripod. 60 kg weights were attached to the tripod for stabilization. The boat was anchored at two sides (front and back) before coring.

The double-walled tube of the corer was filled with dry ice, while ethanol was slowly added (mixing ratio ~ 5:1 resulting in a temperature of approx. -78°C). The mixture of dry-ice and ethanol was stirred continuously until a homogenous viscous fluid was observed. After filling, the corer was attached to the tripod, lowered to the lakebed and then pushed into sediment. Figure 3 shows an image sequence of corer penetration. No gas bubbles were observed during the descending of tripod and corer penetration.

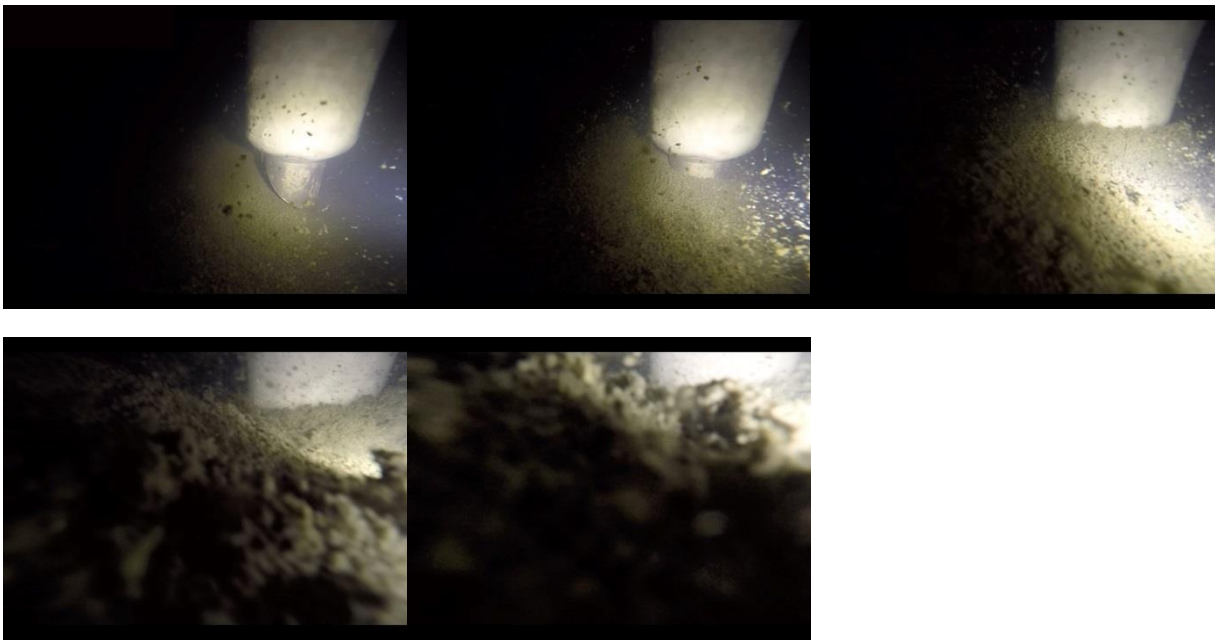

Figure 3. Image sequence showing the corer penetration process, recorded with an underwater camera.

The time for freezing was estimated based on preliminary experiments that showed that 30 minutes are sufficient to completely freeze the sediment within the corer. After freezing, the corer was recovered onto the boat and detached from tripod. Warm water was filled into the double-walled tube of the corer to melt the core skin and retrieve it from the corer. The cores were then wrapped in aluminum foil and stored in a cooling box filled with dry ice. The frozen cores were transported to the nearest hospital for CT scans (Simons AS, 120 kV) to visualize the sediment structure and characterize sediment methane bubbles. Methane bubbles can be clearly visible by using X-ray CT, because the large density difference between gas and solid sediment matrix causes a large difference in X-ray attenuation (Liu et al. 2018).

IV. Assessment

A. Laboratory Investigations

The effects of freezing on gas bubbles (void structures in the sediment core) were assessed under laboratory conditions by comparing CT scans of mechanically undisturbed sediment columns before and after freezing. The highest depth-averaged gas content (θ) was observed in clay (> 15%), compared to much lower in silt (1.3%) and sand (2.3%). A consistent reduction of θ during freezing by 27.1 ± 6.1% (mean and standard deviation of triplicates) occurred at all depths in the clay cores (Figure 4). The effect of freezing on θ was more variable for silt and sand, where the relative change in θ at freezing varied between -37.2 - 14.5% and -9.3 - 42.2%, respectively.

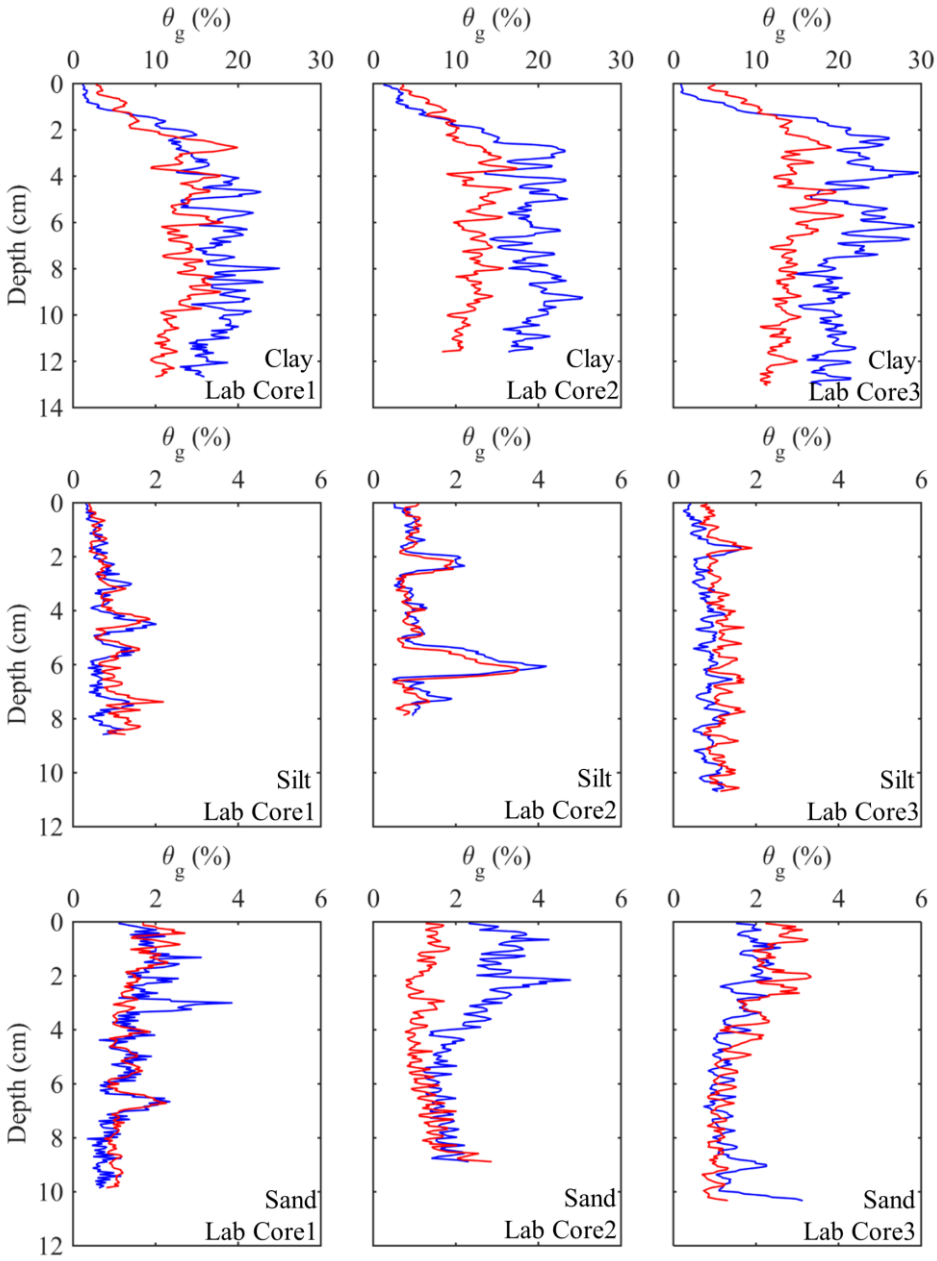

Figure 4. Depth profiles of volume gas content (θ) in the sediment cores (clay, silt and sand) before (blue lines) and after (red lines) freezing.

Most abundant bubbles (in terms of volume) before freezing were constrained to a small size range ($D_{eq} \leq 1$ mm) with very few large bubbles with equivalent diameters up to 15 mm (Fig. 5). The bubbles in clay were significantly larger compared to silt and sand. In clay, the largest bubbles reached 12.7 - 15 mm in diameter, in contrast to 5.1 - 7.4 mm in silt and sand.

Freezing caused changes to the size distribution of gas bubbles by increasing the volume of small bubbles. On average (for all 3 clay cores), the volume of small bubbles ($D_{eq} < 1.3$ mm) increased by 50.5% (from 2220 to 3326 mm^3), compared to the very little volume change (2.2%) in silt and small volume contraction (-21%) in sand. This is in contrast to the volume decrease

for the large bubbles (D_{eq} > 3 mm): -43.2% was observed in clay and -14.5% and -2.8% in silt and sand, respectively.

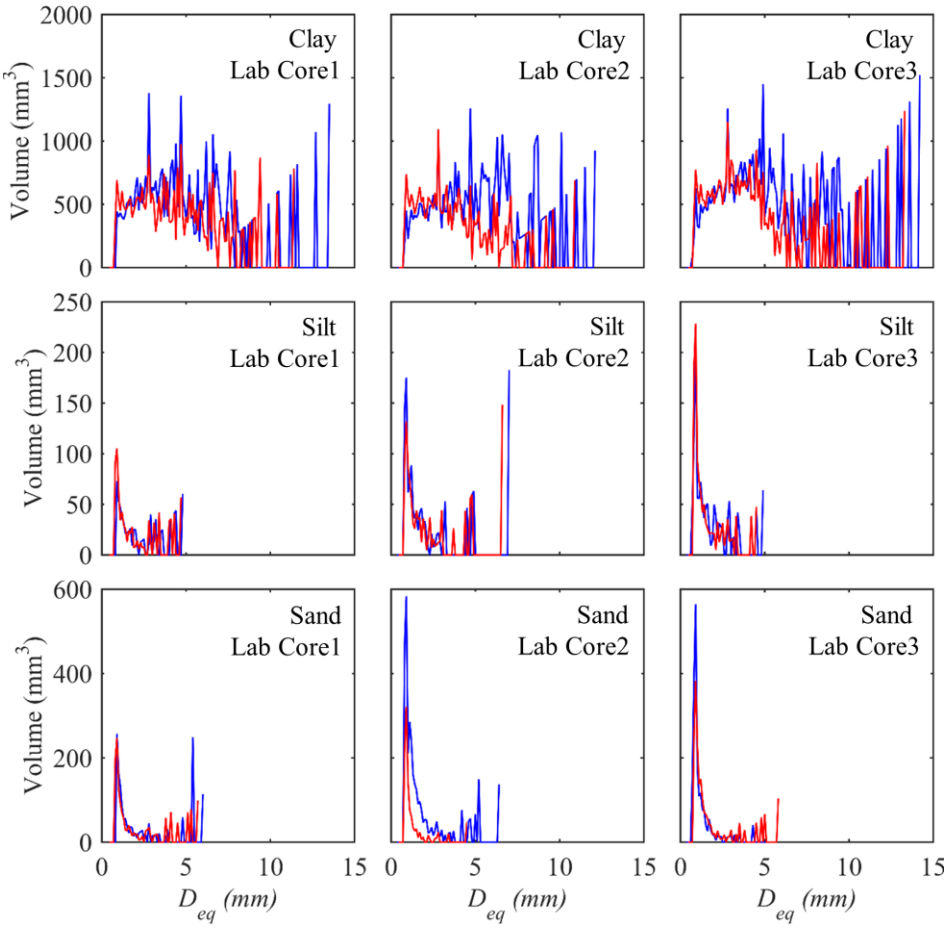

Figure 5. Bubble size (volume) distribution in sediment cores (clay, silt and sand) before (blue lines) and after (red lines) freezing. D_{eq} is the equivalent spherical diameter of bubbles.

There are three possible explanations for the observed change in bubble size distribution:

1. The change in gas volume: The decrease of sediment gas content due to freezing can be estimated from Charles' Law by assuming that the pressure (and mass) in the gas voids did not change: $V_{after} = V_{before} \cdot T_{after}/T_{before}$. As a result of a temperature change from +20 before freezing (T_{before}=293 K) to -78°C after freezing (T_{after}=195 K), the reduction of gas volume from before freezing (V_{before}) to after freezing (V_{after}) is 33 %, which is in the range of the observed changes in clay cores.

2. The expansion of sediment porewater at freezing: Stephanson et al. (1996) stated that ice crystal formation due to freezing may cause a migration of sediment porewater towards the freezing front, whereas solids can be excluded. In addition, the expansion of water occurs mainly during freezing when the density suddenly decreases by 8.3% and is followed by a

steady expansion of the ice volume while the temperature decreases to -78°C. The expansion of ice may result in a relocation of bubbles and solids and/or compression of gas bubbles, due to the large compressibility of gas. The latter also changes bubbles internal pressure and thus increase gas dissolution. Freezing-induced deformations in soils have been found to be affected by different processes, including isotropic expansion (or contraction) of the sediment matrix, continuous phase transition at the ice-water phase boundary, and the temperature-induced deformation of the internal microstructures (Grechichsev 1972, 1973). However, considering that, in clay, water content is highest (65.6%) compared to sand (28.6%) (Liu et al. 2018), the decrease in bubble volume in clay due to freezing can be expected most significant (Figure 5). Alternatively, because expansion within the steel framed corer is limited to the vertical direction (as in a state of uni-axial strain), and the cores were frozen inward, the inner part of the core can be squeezed and pushed either up- or downwards or both.

3. The behavior of dissolved gas in sediment porewater during freezing: Gas solubility in ice is at least two orders of magnitude smaller than in water (Killawee et al. 1998) and freezing can be expected to result in bubble formation. Boereboom et al. (2012) showed that nucleation of methane bubbles can occur in winter lake ice, when the ice-water interface becomes supersaturated. Carte (1961) observed the nucleation and entrapment of gas bubbles at an advancing ice-water interface. Therefore, bubbles may form at the water-ice boundary when the water at the interface becomes supersaturated. The critical oversaturation was determined to be about 30-fold (Lipp et al. 1987). Beside this, bubble concentration and sizes were found to depend on the rate of freezing (Carte 1961). After nucleation, bubble growth is controlled by gas adsorption and thus limited by diffusive transport of dissolved gases towards the bubble surface as well as by bubble migration with the advancing ice front. At higher freezing rates, less time is available for bubble growth and bubbles are “trapped” in the ice. Lipp et al. (1987) found that the bubble sizes were <40 µm for freezing velocities (propagation velocity of the ice-water interface) exceeding 30 µm s^{-1}. Thus, this maximum expected bubble size due to nucleation in our experiments was smaller than the spatial resolution of the CT scanner (voxel size: 0.04 mm^3).

The relative role of the aforementioned processes in the observed changes of bubble size distributions during freezing in our experiments (Figure 5) cannot be precisely evaluated. Nevertheless, our results show, that the reduction in bubble size due to freezing (Charles Law) should be taken into consideration for correcting gas content observed by CT scanning of frozen cores to that *in situ* conditions at the core sampling site.

B. **Field application**

Analyses of CT scans

X-ray CT scanning of free cores sampled in Lake Kinneret revealed the presence of gas bubbles in all cores (Figure 6). 3D visualization of the sediment bubbles in the cores reveals that the depth distribution of bubbles varied from site to site. In Core #1 (11 m water depth, north-west of Lake Kinneret, close to lake shore) significant accumulations of bubbles were observed below ~4 cm depth into the sediment, similar to Core #4 (in the central part of the lake). The depth below which bubbles could be detected increased to ~10 cm in Core #2 and to ~15 cm in Core #3.

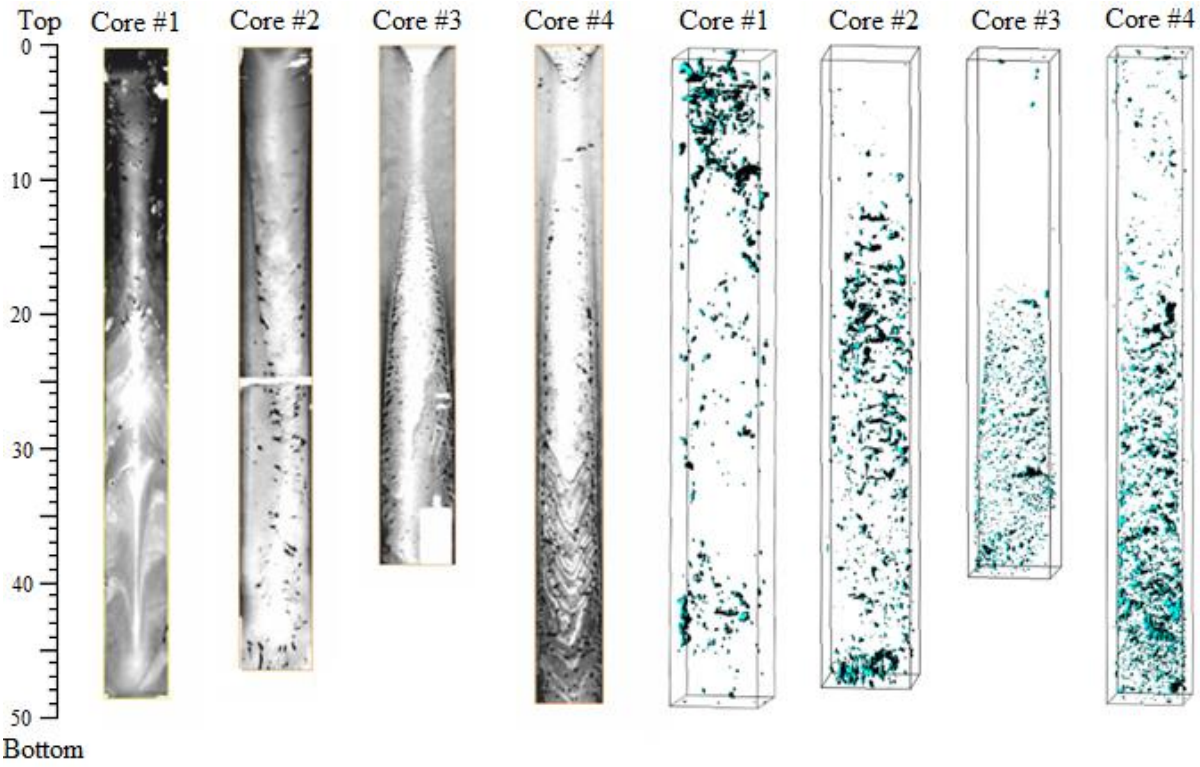

Figure 6. Bubble distribution in four frozen cores sampled in Lake Kinneret (Core #1 to Core #4, see Figure 2 for location of the sampling sites). Left: Cross-sectional view of the X-ray CT images. Gas bubbles are black. Core #1 and #4 show strong coring disturbances, which caused radial up- and downward displacement of sediment layers. Right: 3D visualizations of gas bubbles in the 4 cores.

Low gas content in the top 15 cm of Cores #2 - #4 was observed, whereas the depth where gas content was maximal slightly increased and was at a depth of 40 cm in Core #4 (Figure 8). At the inflow of the Jordan River into the lake (Figure 2), an additional freeze core were taken using a different corer design (freezing lance). Visual observation of the cores confirmed the increasing amount of gas bubbles with increasing depth (Figure 7).

Figure 7. Freeze core obtained with a freezing lance (dimensions in cm).

In general, the shape of bubble size distributions quantified from CT scans in the four cores are quite similar (Figure 9). In all cores, the smallest detectable bubbles were around 0.8 - 0.9 mm in diameter and certainly limited by the spatial resolution of the CT scanning. The largest bubble present in Core #1 - #4 were 7.9, 6.6, 5.6 and 9.5 mm in size, respectively (Figure 9). Bubbles in Core #3 and #4, which were taken in a close proximity to each other, were found mainly below 20 cm depth with D_{eq}~ 2.3 - 2.4 mm and were larger than those in Core #1 and #2 (1.5 mm and 2.0 mm, respectively). This is consistent with smaller bubbles usually found in coarse-grained sands (e.g., Core #1 and #2), vs. larger bubbles in fine-grained cohesive muds (e.g., Core #3 and #4) (Boudreau 2012).

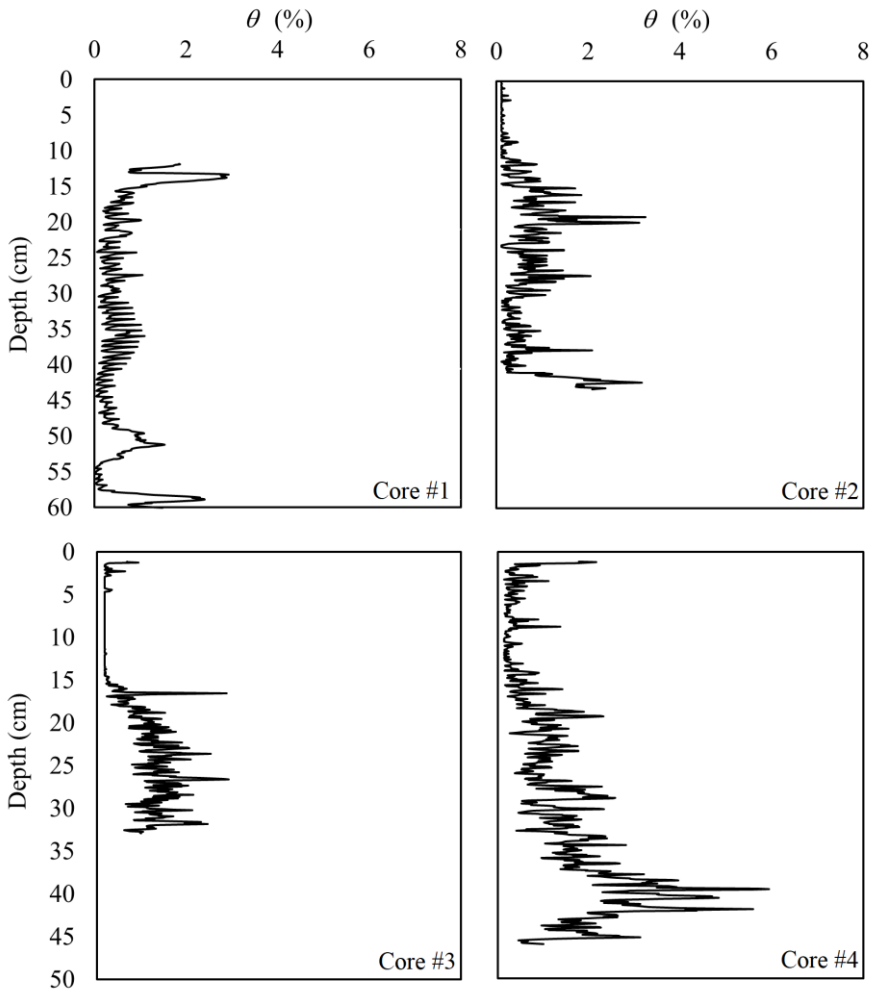

Figure 8. Depth profiles of volumetric gas content (θ) in freeze cores from Lake Kinneret. The depth averaged gas content of Core #1 to #4 were 0.4, 0.5, 0.5 and 1.3 %, respectively. 0 cm indicates the position of sediment-water interface; the upper 12 cm of Core #1 were excluded from analysis because the frozen core broke in this region during core handling.

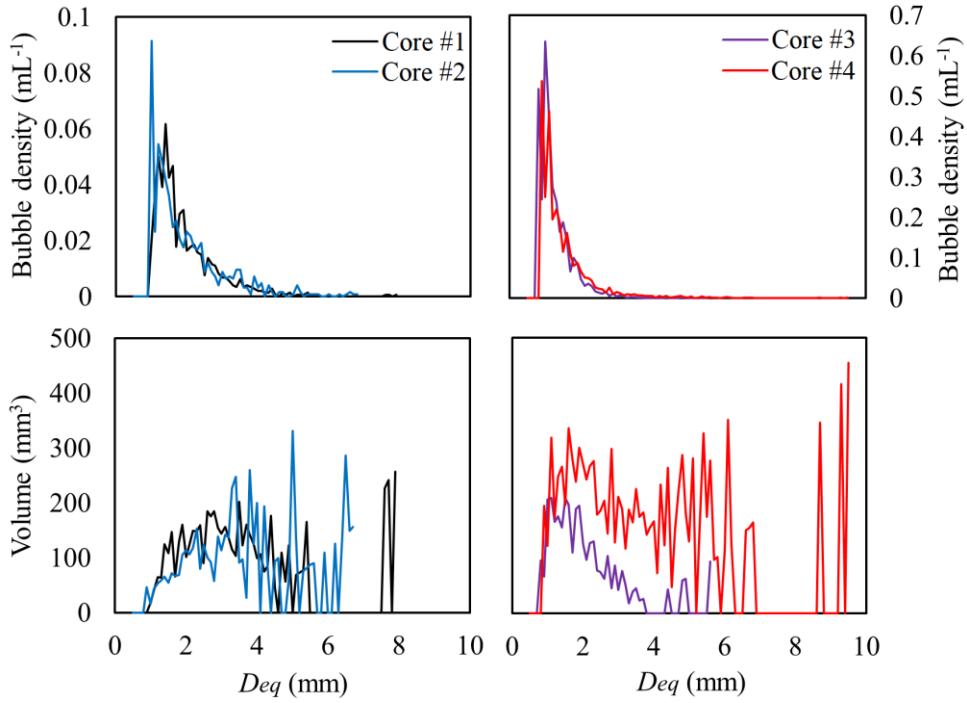

Figure 9. Bubble size - density distribution in the frozen cores collected in Lake Kinneret. Bubble density is defined as total number of bubbles normalized by analyzed sediment volume (mL^{-1}).

Comparison of freeze core data with quantifications of sediment gas content in Lake Kinneret

Gas content and bubble size distributions in Lake Kinneret have been estimated for the first time using a direct (freeze core) method. Their validity is estimated by comparing the results to those obtained in other studies. The variations in gas content revealed in this study (Figure 8) was correlated with the spatial pattern of organic carbon distribution in sediments of the Lake Kinneret, which fuels methane production by anaerobic decomposition. Organic carbon is generated in the lake mostly by primary production (Yacobi et al. 2014). Although the productivity of the lake is considered to be spatially homogeneous except the Jordan River inlet zone, where phytoplankton biomass is higher in spring (Ostrovsky and Yacobi 2010), the organic-rich particulate material is concentrated to the profundal zone due to complex hydrodynamic interactions (Ostrovsky and Yacobi 2010). While the shallow sites (Core #1 and #2) in Lake Kinneret have been found to have similar organic carbon content (mean 1.6 - 1.9 %, Sobek et al. 2011), the deep site (Core #3 and #4) has a higher organic carbon (3.9 %). Similarly, Ostrovsky and Tegowski (2010) found that the organic carbon content of the

uppermost sediment layer increased along the north-west transect sampled in the present study from the shallowest location to a water depth of ~18-22 m to ~12%, and then slightly varied with depth, still showing a maximum organic carbon content at the deepest location.

The spatial differences in gas content between Core #1 - #4 are also in line with acoustic measurements of Katsnelson et al. (2017), who found that sediment gas content decreased from the lake center toward its periphery, and, the maximum gas content was measured in the deepest part of the lake. However, a direct comparison of the gas contents is not appropriate, as the new acoustic method used by Katsnelson et al. (2017) has not yet been validated by direct gas content measurements. In addition, gas content at the same locations can vary over time due to partial sediment degassing at low water levels (Ostrovsky et al. 2013). Apart from the insights discussed above, the knowledge about free gas within the sediment of Lake Kinneret is rather limited. Adler et al. (2011) found bubbles between depths 7-15 cm into the sediment at the deepest part of the lake by visual inspection of sediment cores. Core sampling in that study has been conducted with a rather short non-pressurized corer and, therefore, the bubble distribution within this core might be disturbed due to bubble expansion and/or ebullition caused by drop in hydrostatic pressure during core retrieval.

Coring disturbances

Coring disturbances, which usually occur when using gravity or piston corer, may partially differ from those of the new freeze core method (Jutzeler et al. 2014). A common coring disturbance is core shortening, also termed “core compaction” or “entry deficit”, describing the phenomenon in which the length of the retrieved sediment column is shorter than the corer’s penetration depth. Shortening occurs due to the frictional force, which increases inside of the tube with increasing length of the sediment column in the corer (Glew et al. 2002). The magnitude of core shortening can be up to 50% of the core length (Wright 1993; Skinner and McCave 2003). The length of the recovered cores in Lake Kinneret are 48 cm of Core #1, 46 cm of Core #2, 39 cm of Core #3 and 49 cm of Core #4. As the corer penetrated the lake-bed up to the maximum depth of 60 cm, shortening varied between 18 and 35 % and was small in comparison to Emery and Dietz (1941), who observed that the core-length varied from 40 to 70% of the depth of penetration and Emery and Hulsemann (1964), who found an average shortening factor of 50%.

The cross-sectional view of Core #4 (Figure 6) showed distinct deformations of $CaCO_3$ layers ($CaCO_3$ intensively precipitates in Lake Kinneret in March - April) at the lower third of the core image. The downward bending increased with increasing depth. The vertical displacement of

the outer layer relatively to the inner layer was of approximately 30 – 40 mm. The same effect was observed in the lower half of Core #1. It can be ruled out that the deformation of the layer is the result of friction between the corer and the sediment. Such deformation would appear as downward bends at the outer perimeter of the sediment core, which increases radially from the center of the core (Acton et al. 2002). The reason for the coring artifact observed in Core #1 and #4 is probably the volume expansion of pore water during freezing. As the core freezes from the outside to the inside, the expansion can result in vertical (up- and downward) displacement of the unfrozen sediments in front of the radially propagating freezing front. In the upper few centimeter of the core, freezing advances more slowly because of convective heat transport from the overlaying water. Below this region, water content can be expected to decrease with increasing depth and therefore freezing of the sediment is proceeding more slowly with higher depths.

This assumption is supported by the cross-sectional CT images (Figure 10), which show an accumulation of gas bubbles around a conically shaped surface in all cores. The circular arrangement of gas voids may be an artifact of the freezing because it coincided with a sharp interface of different X-ray absorption (darker shade of gray), which may indicate higher water content, and the inner circle, where the frozen water, sediment and bubbles are located. This finding corroborates to the hypothesis of Stephanson et al. (1996), who stated that ice crystal formation causes a flux of the sediment porewater into the center of the core, excluding some solids. This effect may also result in a lateral displacement of gas bubbles from the outer perimeter into the center of the core.

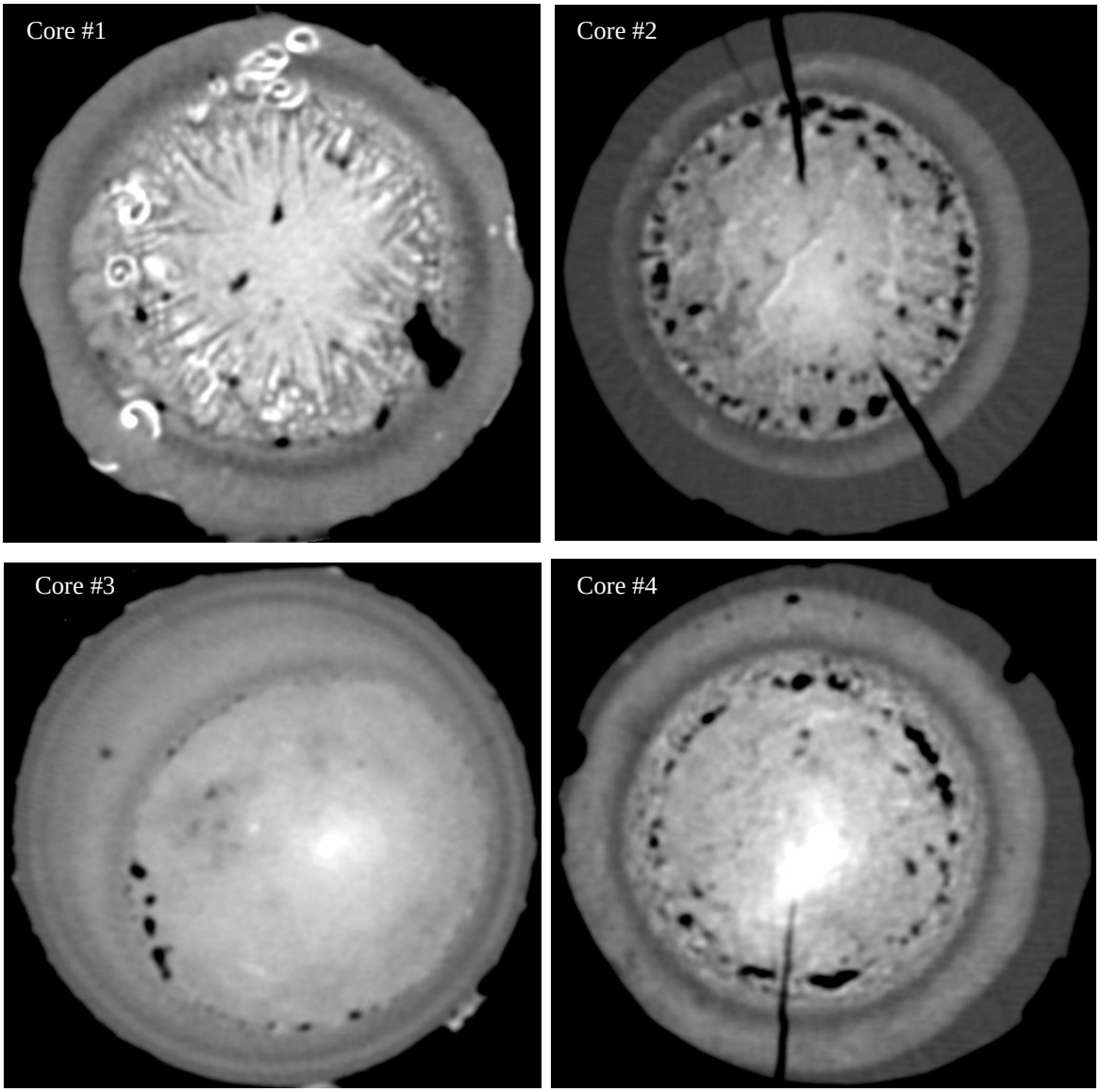

439

Figure 10. Gas voids are arranged along a circle, which is exemplarily shown for cross section at the upper part of Core #1, #2, #3, and lower part of Core #4.

V. CONCLUSIONS AND RECOMMENDATIONS

The novel freeze corer proved its applicability as an inexpensive and easy to use tool for sampling sediment cores for gas bubble characterization using X-ray CT. The sediment gas content generally followed previously described spatial patterns in sediment organic carbon content and hydro-acoustic gas content estimates in Lake Kinneret. Therefore, this corer and its further improvement, can open a new field for studies aiming at a quantitative understanding of the structure and quantity of methane bubbles in aquatic sediments under *in situ* conditions.

The cost of this freeze corer including the tripod was approximately 1400 €, which is comparable or even less expensive than a commercial gravity or piston corer. Compared to pressurized corers, the price is orders of magnitude lower and its application requires less technical effort and operational costs (e.g., expenses for a boat or working platform). As the

corer is light-weighted, easy to disassemble and transport, only few additional facilities are needed, including a winch or an A-frame and sufficient working space, which are commonly available on fishing boats or working platforms.

Laboratory tests confirmed the capability of the new freeze corer in characterizing sediment gas bubbles. The effects of freezing on sediment gas content, bubble size and geometry, were investigated by comparing CT scans of frozen and unfrozen cores under laboratory conditions. The results showed that freezing caused a volume contraction of gas bubbles and an increase in number of small bubbles, but the general shape of the bubble size distribution remained almost unchanged.

Freezing of gas-bearing sediment may potentially result in the formation of methane hydrate, which requires appropriate pressure-temperature conditions, as well as sufficient water and the presence of methane in excess of its solubility in surrounding pore water (Ruppel and Kessel 2017; Zatsepina and Buffett 1998). According to the phase equilibrium P-T curve of methane hydrate stability, gas hydrate can form where local thermal conditions are colder than the gas hydrate stability curve at any given pressure (see Siažik et al. 2017). These are not attained under the operating conditions at the Lake Kinneret.

In the present study, the corer has only been tested in one lake with soft and gassy sediment. The corer described here can easily be adapted or modified for other study sites and other research questions. The corer inner diameter can be increased up to 100 mm, as a maximum possible core diameter, because it can be frozen with a mixture of dry ice and ethanol within reasonable time (< 80 min) (Renberg and Hansson 1993). An increasing diameter improves coring quality considerably, as large-diameter coring tubes minimizes wall friction, down-bowing of sediments along the tube walls and core shortening (Baxter et al. 1981; Pedersen 1985; Blomqvist 1991; Chaney and Almagor 2015). The amplitude of structural disturbances can therefore be reduced in comparison to common used lance freeze corer, where Liernur et al. (2017) found a high variability of the vertical displacement of the sediment layer with an average of 3.7 (± 1.2 cm).

The length of the corer can be increased up to 2 m. Compared to a gravity corer, the resistance of the double-walled freeze corer increases more rapidly with increasing depth due to the increasing diameter of the corer above the cutting edge. The core depth is limited by the type of sediment, as the resistance to penetration can increase with depth as well as sediment grain size distribution (and sediment compactness).

Two effects were observed which need further investigation: Firstly, the X-ray CT revealed that the sediment layers within the sediment column were bended up- and downward, which

indicates disturbances of the sediment structure caused by the freezing processes. These disturbances may affect the vertical distribution of the gas bubbles within the sediment column. However, the core integrity is not affected by freezing and X-ray CT scanning allows a reconstruction of the initial sediment structure. Such a reconstruction is not possible for sediment cores sampled with common tube samplers, where the sediment structure has been disturbed by gas bubble expansion during core recovery. Secondly, the size and shape of the bubbles changed during the freezing process and may not correspond to the *in situ* size distributions of methane bubbles. However, X-ray CT scanning facilitated the identification of disturbances in the sediment structure and bubble distribution.

The results of the laboratory experiments suggest that the cooling effect on sediment bubble size follows Charles Law and thus can be mathematically corrected (approx. 33% contraction of gas volume). Additional corrections could be applied to remove vertical displacement of bubbles caused by coring disturbances, as it is related to sediment water content.

For all coring methods based on tube samplers, further research is needed to quantify and to minimize coring disturbances. The extent of sampling bias that occurs when obtaining cores will largely be the result of the choice of corer design, water depth and mechanical properties of the sediment. Many authors have questioned the validity of results obtained from sediment core analysis because of the potential sampling bias associated with the coring device (Baxter et al. 1981; Blomqvist 1985; Buckley et al. 1994; Ostrovsky 2000). This study has identified questions for further investigations. The coring disturbances of this freeze corer and the freezing effect on sediment should be analyzed by further laboratory experiments and in-situ sampling for a broader range of sedimentary conditions.

ACKNOWLEDGEMENTS

The authors would like to thank Timo Fahlenbock, Eric Zimmermann and Michael Schaub for their help throughout the design and construction of the corer. We would also like to thank Jeremy Wilkinson, Stephan Hilgert and Klajdi Sotiri for their help during field work. Finally, we would also thank Mr. Shimon Mendel in the Baruch Padeh Medical Center, Poriya,, Israel, and clinic in Landau, Germany for their great assistance in CT scans of sediment cores.

FUNDING

This study was conducted in the framework of a project of the European Regional Development Fund / Investment for Growth and Employment, project number EFRE-0800107, project number 214-17-007 funded by Ministry of Natural Infrastructures, Energy and Water Resources of Israel, and project number 1441-14 funded by the Israel Science Foundation.

REFERENCES

Abegg, F., and A. L. Anderson. 1997. The acoustic turbid layer in muddy sediments of Eckernfoerde Bay, Western Baltic: methane concentration, saturation and bubble characteristics. Marine Geology 137: 137-147, doi:10.1016/S0025-3227(96)00084-9

Acton, G. D., M. Okada, B. M. Clement, S. P. Lund, and T. Williams. 2002. Paleomagnetic overprints in ocean sediment cores and their relationship to shear deformation caused by piston coring, J. Geophys. Res., 107(B4), doi:10.1029/2001JB000518

Adler, M., Eckert, W. and O. Sivana. 2011. Quantifying rates of methanogenesis and methanotrophy in Lake Kinneret sediments (Israel) using pore-water profiles. Limnology and Oceanography. 56, doi: 10.4319/lo.2011.56.4.1525

Algar, C. K., B. P. Boudreau, and M. A. Barry. 2011. Initial rise of bubbles in cohesive sediments by a process of viscoelastic fracture. Journal of Geophysical Research: Solid Earth 116: B04207, doi:10.1029/2010JB008133

Bastviken, D., L. J. Tranvik, J. A. Downing, P. M. Crill, and A. Enrich-Prast. 2011. Freshwater methane emissions offset the continental carbon sink. Science 331: 50-50, doi: 10.1126/science.1196808

Baxter, M. S., Farmer, J. G., McKinley, I. G., Swan, David S. and W. Jack. 1981. Evidence of the unsuitability of gravity coring for collecting sediment in pollution and sedimentation rate studies. Environ. Sci. Technol. 15: 843–846, doi: 10.1021/es00089a014

Blomqvist, S. 1985. Reliability of core sampling of soft bottom sediment - an in situ study. Sedimentology. 32: 605–612, doi:10.1111/j.1365-3091.1985.tb00474.x

Blomqvist, S. 1991. Quantitative sampling of soft-bottom sediments: Problems and solutions. Mar. Ecol. Prog. Ser. 72: 295–304, doi:10.3354/meps072295

Boereboom, T., Depoorter, M., Coppens, S., and Tison, J.-L. 2012. Gas properties of winter lake ice in Northern Sweden: implication for carbon gas release. Biogeosciences. 9. 827-838, https://doi.org/10.5194/bg-9-827-2012

Boudreau, B. P. et al. 2005. Bubble growth and rise in soft sediments. Geology 33(6): 517-520, doi:10.1130/G21259.1

Buckley, D. E., MacKinnon, W. G., Cranston, R. E. and H. A. Christian. 1994. Problems with piston core sampling: Mechanical and geochemical diagnosis. Marine Geology. 117: 95-106.

Carte, A. E. 1961. Air bubbles in Ice. Proceedings of the Physical Society. 77.

Chaney, R. C., and G. Almagor. 2015. Seafloor professes and geotechnology. CRC Press.

DelSontro, T., D. F. McGinnis, S. Sobek, I. Ostrovsky, and B. Wehrli. 2010. Extreme methane emissions from a Swiss hydropower reservoir: contribution from bubbling sediments. Environmental science & technology 44(7): 2419-2425, doi:10.1021/es9031369

Emery, K.O. and R.S. Dietz. 1941. Gravity coring instrument and mechanics of sediment coring. Geological Society of America Bulletin. 53:1685-1714

Emery, K. O. and J. Hulsemann. 1964. Shortening of sediment cores collected in open-barrel gravity corers. Sedimentology. 3:144-154

Flannagan, J. F. 1970. Efficiencies of various grabs and corers in sampling freshwater benthos. J. Fish. Bd. Canada 27(10): 1691–1700, doi:10.1139/f70-191

Glew J. R., Smol J. P., Last W. M. 2002. Sediment Core Collection and Extrusion. In: Last W.M., Smol J.P. (eds) Tracking Environmental Change Using Lake Sediments. Developments in Paleoenvironmental Research, vol 1. Springer, Dordrecht.

Grechishchev, S. E., The basic regularities of thermogeology and temperature cracking of frozen soils, in Mater. Vtoroi Mezhd. konf. po merzlotovedeniyu. Vyp. 4 (Proc. 2nd Int. Conf. on Geocryology), Yakutsk: Yakutsk. Kn. Izd., 1973, pp. 26–34.

Grechishchev, S. E., Study results of thermal deformations and prediction of frost cracking of soils, in Mater. vsesoyuz. nauchn. sov. po merzlotovedeniyu (Proc. All-Union Sci. Conf. on Geocryology), Moscow: Mosk. Gos. Univ., 1972, pp. 167–186.

Hessler, R. R and P. A. Jumars. 1974. (Table 3) Macro- and meiofaunal species abundance in box core samples from the North Pacific Ocean. PANGAEA, doi:10.1594/PANGAEA.692262

Jutzeler, M., White, J. D. L., Talling, P. J., McCanta, M., Morgan, S., Le Friant, A. and O. Ishizuka 2014. Coring disturbances in IODP piston cores with implications for offshore record of volcanic events and the Missoula megafloods. Geochem. Geophys. Geosyst. 15:3572–3590, doi:10.1002/2014GC005447

Koren, N. and I. Ostrovsky. 2002. Sedimentation in a stratified subtropical lake. Verh Int Ver Theor Angew Limnol. 27:2636–2639

Katsnelson, B., Katsman, R., Lunkov, A. and I. Ostrovsky. 2017, Acoustical methodology for determination of gas content in aquatic sediments, with application to Lake Kinneret, Israel, as a case study. Limnol. Oceanogr. Methods. 15: 531–541, doi:10.1002/lom3.10178

Ketcham, R. A. 2005. Computational methods for quantitative analysis of three-dimensional features in geological specimens. Geosphere 1: 32-41, doi:10.1130/GES00001.1

Killawee, J. A., I. J. Fairchild, J.-L. Tison, L. Janssens and R. R. Lorrain. 1998. Segregation of solutes and gases in experimental freezing of dilute solutions: Implications for natural glacial systems. Geochim. Cosmochim. Acta. 62: 3637–3655.

Lane, C. M. and K. H. Taffs. 2002. The LOG corer – a new device for obtaining short cores in soft lacustrine sediments. Journal of Paleolimnology. 27:145-150, doi:10.1023/A:1013547028068

Liernur, A., Schomburg, A., Turberg, P,. Guenat, C,. Le Bayon, R.-C. and P. Brunner. 2017. Coupling X-ray computed tomography and freeze-coring for the analysis of fine-grained low-cohesive soils. Geoderma. 308: 171-186, doi:10.1016/j.geoderma.2017.08.010

Liu, L., De Kock, T., Wilkinson, J., Cnudde, V., Xiao, S., Buchmann, C., Uteau, D., Peth, S. and A. Lorke. 2018. Methane Bubble Growth and Migration in Aquatic Sediments Observed by X-ray μCT. Environmental Science & Technology. 52(4). DOI: 10.1021/acs.est.7b06061

Lipp, G., Körber, C., Englich, S., Hartmann, U. and G. Rau. 1987. Investigation of the behavior of dissolved gases during freezing. Journal of Cryobiology. 24:489-503, doi.org/10.1016/0011-2240(87)90053-8

Lisle, T. E. 1989. Sediment transport and resulting deposition in spawning gravels, north coastal California, Water Resour. Res., 25: 1303–1319, doi:10.1029/WR025i006p01303

Lotter, A. F., J. Merkt and M. Sturm. 1997. Differential sedimentation versus coring artefacts: a comparison of two widely used piston-coring methods. Journal of Paleolimnology. 18: 75–85, doi:10.1023/A:1007929422169

Maeck, A. et al. 2013. Sediment trapping by dams creates methane emission hot spots. Environmental science & technology 47: 8130-8137, doi: 10.1021/es4003907

Martens C. S. and D. B. Albert. 1995. Biogeochemical processes controlling concentrations and transport of biogenic methane in organic rich coastal sediments. In Proceedings of the Workshop on
Modelling Methane-Rich Sediments of Eckernförde Bay, Eckernförde, 26–30 June, 1995 (ed. T. F. Wever), pp. 10–17. Forschungs Bundeswehr Wasserschall Geophysik.

Martens, C. S. and R. A. Berner. 1974. Methane production in the interstitial waters of sulfate-depleted marine sediments. Science 185: 1167-1169

Li, L., Peng,J., Gao, Q., Sun, M., Liu, Y., Li, M., Chen, B. and B. Kun. 2016. Pressure retaining method based on phase change for coring of gas hydrate-bearing sediments in offshore drilling. Applied Thermal Engineering. 107: 633-641. doi.org/10.1016/j.applthermaleng.2016.06.174.

Liu, L., J. Wilkinson, K. Koca, C. Buchmann, and A. Lorke. 2016. The role of sediment structure in gas bubble storage and release. Journal of Geophysical Research: Biogeosciences 121: 1992-2005, doi:10.1002/2016JG003456

Maeck, A., H. Hofmann, and A. Lorke. 2014. Pumping methane out of aquatic sediments: Ebullition forcing mechanisms in an impounded river. Biogeosciences 11: 2925-2938, doi.org/10.5194/bg-11-2925-2014

McIntyre, A. D. 1971. Deficiency of gravity corers for sampling meiobenthos and sediments. Nature 231: 260, doi: 10.1038/231260a0

Pachur, H.-J., H.-D. Denner, and H. Walter. 1984. A freezing device for sampling the sediment-water interface of lakes. Catena 11:65-70, doi:10.1016/S0341-8162(84)80006-5

Renberg, I. and H. Hansson. 1993. A pump freeze corer for recent sediments. Limnology and Oceanography. 38:1317-1321

Pedersen, T. F. 1985. A lightweight gravity corer for undisturbed sampling of soft sediments. Can. J. Earth Sci. 22: 133-135. Doi;10.1139/e85-011

Ostrovsky, I. 2000. The upper-most layer of bottom sediments: sampling and artifacts. Arch Hydrobiol Spec Issues Advanc Limnol 55: 243-255.

Ostrovsky, I. and J. Tegowski. 2010. Hydroacoustic analysis of spatial and temporal variability of bottom sediment characteristics in Lake Kinneret in relation to water level fluctuation. Geo-Marine Letters, 30: 261–269, doi: 10.1007/s00367-009-0180-4

Ostrovsky, I. and Y. Yacobi. 1999. Organic matter and pigments in surface sediments: possible mechanisms of their horizontal distributions in a stratified lake. Can. J. Fish. Aquat. Sci. 56:1001-1010, doi.org/10.1139/f99-032

Ostrovsky, I. and Y. Z. Yacobi. 2010. Sedimentation flux in a large subtropical lake: Spatiotemporal variations and relation to primary productivity. Limnology and Oceanography. 55. doi: 10.4319/lo.2010.55.5.1918.

Ostrovsky, I., A. Rimmer, Y.Z. Yacobi, A. Nishri, A. Sukenik, O. Hadas, and T. Zohary. 2013. Long-term changes in the Lake Kinneret ecosystem: the effects of climate change and anthropogenic factors. In Climatic Change and Global Warming of Inland Waters: Impacts and Mitigation for Ecosystems and Societies (Eds C.R. Goldman, M. Kumagai, R. D. Robarts). pp. 271-293. John Wiley & Sons, Ltd. Online ISBN: 9781118470596, DOI:10.1002/9781118470596.ch16

M. Riedel, T.S. Collett and M.J. Malone. 2006. The Expedition 311 Scientists. Expedition 311Summary. Proceedings of the Integrated Ocean Drilling Program. Vol. 311.

Ron, H., Nowaczyk, N. R., Frank, U., Schwab, M. J., Naumann, R., Striewski, B. and A. Agnon. 2007. Greigite detected as dominating remanence carrier in Late Pleistocene sediments, Lisan Formation, from Lake Kinneret (Sea of Gelilee), Israel. Geophys. J. Int. 170:117-131.

Ruppel, C. D., and J. D. Kessler. 2017. The interaction of climate change and methane hydrates. Rev. Geophys. 55: 126-168, doi:10.1002/2016RG000534

Scandella, B. P., C. Varadharajan, H. F. Hemond, C. Ruppel, and R. Juanes. 2011. A conduit dilation model of methane venting from lake sediments. Geophys. Res. Lett. 38, doi:10.1029/2011GL046768

Schmid, B., J. Schindelin, A. Cardona, M. Longair, and M. Heisenberg. 2010. A high-level 3D visualization API for Java and ImageJ. BMC bioinformatics 11: 274, doi:10.1186/1471-2105-11-274

Siažik, J., Malcho, M. and Lenhard R. 2017. Proposal of experimental device for the continuous accumulation of primary energy in natural gas hydrates. Experimental Fluid Mechanics. 143. 10.1051/epjconf/201714302106

Skinner, L. C. and I. N. McCave. 2003. Analysis and modelling of gravity- and piston coring based on soil mechanics. 199:181-204, doi:10.1016/S0025-3227(03)00127-0

Snider, L. J., Burnett, B.R. and R. R. Hessler. 1984. The composition and distribution of meiofauna and nanobiota in a central North Pacific deep-sea area. Deep Sea Res. 31:1225-1249, doi:10.1016/0198-0149(84)90059-1

Sobek, S. Zurbrügg, R. and I. Ostrovsky. 2011. The burial efficiency of organic carbon in the sediments of Lake Kinneret. Aquatic Sciences 73:355-364, DOI 10.1007/s00027-011-0183-x

Stephenson, M., Klaverkamp, J. Motycka, M. et al. 1996. Coring artifacts and contaminant inventories in lake sediment. Journal of Paleolimnology. 15:99-106, doi.org/10.1007/BF00176992

Strasser, D., Lensing, H.-J., Nuber, T., Richter, D., Frank, S., Goeppert, N. and N. Goldscheider. 2015. Improved geohydraulic characterization of river bed sediments based on freeze-core sampling – development and evaluation of a new measurement approach. J. Hydrol. 527:133–141, doi:10.1016/j.jhydrol.2015.04.074

Varadharajan, C., and H. F. Hemond. 2012. Time-series analysis of high-resolution ebullition fluxes from a stratified, freshwater lake. Journal of Geophysical Research: Biogeosciences 117. G02004, doi:10.1029/2011JG001866.

Verschuren, D., Tibby, J., Sabbe, K. and Roberts, N. 2000. Effects of depth, salinity, and substrate on the invertebrate community of a fluctuating tropical lake. Ecology. 81:164–182, doi:10.1890/0012-9658(2000)081[0164:EODSAS]2.0.CO;2

Wever, T. F., Abegg, F., Fiedler, H. M., Fechner, G. and I. H. Stender. 1998. Shallow gas in the muddy sediments of Eckernförde Bay, Germany. Continental Shelf Research. 18: 1715-1739.

Wilkinson, J., A. Maeck, Z. Alshboul, and A. Lorke. 2015. Continuous seasonal river ebullition measurements linked to sediment methane formation. Environmental science & technology 49:13121-13129. doi: 10.1021/acs.est.5b01525

Wright Jr. H. E. 1993. Core compression. Limnology and Oceanography. 38, doi: 10.4319/lo.1993.38.3.0699

Xiao, S. et al. 2014. Gas transfer velocities of methane and carbon dioxide in a subtropical shallow pond. Tellus B 66, doi:10.3402/tellusb.v66.23795

Yacobi Y., Erez J. and O. Hadas. 2014. Primary Production. In: Zohary T., Sukenik A., Berman T., Nishri A. (eds) Lake Kinneret. Aquatic Ecology Series. vol 6. Springer, Dordrecht.

K. Yamamoto, N. Inada, S. Kubo, T. Fujii, K. Suzuki and Y. Konno. 2012. Pressure Core Sampling in the Eastern Nankai Trough. Fire in the Ice-Methane Hydrate Newsletter. 12(2): 1–6.

Zatsepina, O. Y., and B. A. Buffett. 1998. Thermodynamic conditions for the stability of gas hydrate in the seafloor. J. Geophys. Res. 103:127–24. doi:10.1029/98JB02137

Appendix IV

The control of sediment gas accumulation on spatial distribution of ebullition in Lake Kinneret

Liu Liu,[1*] Klajdi Sotiri,[2] Yannick Dück,[3] Stephan Hilgert,[2] Ilia Ostrovsky,[4] Ernst Uzhansky,[5] Regina Katsman,[5] Boris Katsnelson,[5] Revital Bookman,[5] Jeremy Wilkinson,[1] Andreas Lorke[1]

[1] Institute for Environmental Sciences, University of Koblenz-Landau, Landau, Germany

[2] Institute for Water and River Basin Management, Karlsruhe Institute of Technology, Karlsruhe, Germany

[3] Institute of Hydraulic Engineering and Water Resources Management, Cologne University of Applied Science, Cologne, Germany

[4] Yigal Allon Kinneret Limnological Laboratory, Israel Oceanographic and Limnological Research, Migdal, Israel

[5] Dr. Moses Strauss Department of Marine Geosciences, Leon H. Charney School of Marine Sciences, University of Haifa, Mount Carmel, Haifa, Israel

The control of sediment gas accumulation on spatial distribution of ebullition in Lake Kinneret

Liu Liu,[1*] Klajdi Sotiri,[2] Yannick Dück,[3] Stephan Hilgert,[2] Ilia Ostrovsky,[4] Ernst Uzhansky,[5] Regina Katsman,[5] Boris Katsnelson,[5] Revital Bookman,[5] Jeremy Wilkinson,[1] Andreas Lorke[1]

[1] Institute for Environmental Sciences, University of Koblenz-Landau, Landau, Germany

[2] Institute for Water and River Basin Management, Karlsruhe Institute of Technology, Karlsruhe, Germany

[3] Institute of Hydraulic Engineering and Water Resources Management, Cologne University of Applied Science, Cologne, Germany

[4] Yigal Allon Kinneret Limnological Laboratory, Israel Oceanographic and Limnological Research, Migdal, Israel

[5] Dr. Moses Strauss Department of Marine Geosciences, Leon H. Charney School of Marine Sciences, University of Haifa, Mount Carmel, Haifa, Israel

*Correspondence: liu@uni-landau.de

Keywords: anaerobic methane production, sulfate, methane bubbles, hydroacoustic measurements, sediment cores, anthropogenic perturbations

Abstract

In freshwater lakes, ebullition is an important pathway for biogenic methane (CH_4) from sediment to reach the atmosphere. However, its high spatial and temporal variability limits our ability to accurately measure or to predict CH_4 fluxes from lakes. To explore the factors controlling the spatial distribution of ebullition, we investigated free gas accumulation in the bottom sediment of Lake Kinneret, Israel. Sediment cores were collected along an offshore transect. Sediment porewater was analyzed for dissolved CH_4 concentration and porewater chemistry. Anaerobic CH_4 production (MP) rates in sediment were determined by incubating sediment sub samples in the laboratory. Hydroacoustic measurements at various frequencies were conducted at the coring sites and along multiple transects over the entire lake for characterizing in situ sediment volumetric gas content. A minimum in MP depth profiles was observed that coincided with enriched porewater sulfate in the upper 30 cm of sediment. The depth-integrated sediment MP provided a robust estimate for the long-term ebullition flux from sediment, while short-term variability is associated with seasonal lake level change. Acoustic measurements revealed the absence of free gas accumulation in sediments of the littoral zone and low ebullition rates in the shallow water zones. For the first time, this study reports the role of MP in determining the spatial variability of free gas content in freshwater sediments. The results further demonstrate the importance of sediment gas content in explaining spatial variability of gas ebullition in lakes.

Introduction

Methanogenesis in anoxic sediments is a major source of methane (CH_4) in lakes and other freshwater systems (Bastviken et al. 2008; Maeck et al. 2013). CH_4 provides an alternative carbon and energy source in aquatic food webs (Jones et al. 2008; Mbaka et al. 2014). Freshwater CH_4 emissions constitute the most important source of uncertainty on the global CH_4 budget (Saunois et al. 2016), with lakes making up the largest contribution (~70%) of freshwater CH_4 emissions (Bastviken et al. 2011). Accurate CH_4 budgets (production, storage and release) are, therefore, required to better constrain the contribution of lakes to global CH_4 emissions and their sensitivity to climate change, eutrophication and other human influences (DelSontro et al. 2018; Sepulveda-Jauregui et al. 2018).

Direct measurements of CH_4 fluxes across the air-water interface are associated with high uncertainties due to the complexities of fluxes mediated by different pathways and their spatial and temporal variability (Bastviken et al. 2004; Natchimuthu et al. 2016; Tušer et al. 2017). This is particularly true for bubble-mediated flux. Compared to diffusive transport, ebullition is much more variable in time and space (DelSontro et al. 2011; Maeck et al. 2014; Varadharajan and Hemond 2012). Recent continuous long-term ebullition measurements demonstrated a close agreement between the average ebullitive flux and the rate of anaerobic CH_4 production in sediment, which is largely controlled by sediment temperature seasonality (Wilkinson et al. 2015). Instantaneous ebullition rates can substantially deviate from the production potential, indicating the importance of sediment gas storage (Varadharajan and Hemond 2012; Wilkinson et al. 2015), which had been confirmed by laboratory experiments (Liu et al. 2018; Liu et al. 2016). The spatial heterogeneity of ebullitive flux has been related to sedimentation pattern in lakes and reservoirs (de Mello et al. 2018; Maeck et al. 2013). Based on the observation that ebullition is controlled by the pressure-driven release of free gas accumulating in sediment until a sediment-specific gas storage capacity is reached (Liu et al. 2016), we hypothesize that the spatial distribution of ebullition is linked to sediment volumetric gas content and hydrostatic/atmospheric pressure changes act as a driver.

Anaerobic CH_4 production in aquatic sediments can play an important role in free gas accumulation in sediment, which has been well documented in marine sediments (Abegg and Anderson 1997; Anderson et al. 1998; Flury et al. 2016) where gas fronts were often observed below the sulfate-reduction (SR) zone. In contrast to the apparent SR zone in marine sediments, where anaerobic CH_4 oxidation (AMO) acts as a major sink for CH_4 (Barnes and Goldberg 1976;

Conrad 2009), low sulfate concentration is an important reason for the higher CH_4 production rates in freshwater sediments. In lakes, the missing SR zone can result in the accumulation of free gas in the surficial sediments (Anderson and Martinez 2015). Yet, slight enrichment of sulfate in sediment porewater has been reported in many freshwater lakes, though the concentrations are low (Adler et al. 2011; Kuivila et al. 1989; Schubert et al. 2011) and it is confined to the uppermost surface layer (< 20 cm) (Whiticar and Faber 1986). At these low sulfate concentrations (< 1 mM), sulfate-reducing bacteria can outcompete methanogens (Lovley and Klug 1983). It is still unclear, to what extent SR affects the CH_4 budget in freshwater sediments and whether this process affects the vertical distribution of sediment gas content.

Ebullition in Lake Kinneret (LK) has been intensively studied by hydroacoustic measurements (Ostrovsky 2003; Ostrovsky et al. 2008). The seasonal and inter-annual variability of ebullition has been found to be correlated to lake level (Eckert and Conrad 2007; Ostrovsky et al. 2013), suggesting a potential control of ebullition dynamics by sediment gas storage (Ostrovsky and Tęgowski 2010). In addition, recent process-based modelling demonstrated a significant contribution of ebullition to total CH_4 emissions from the lake, regardless of its relatively large depth (Schmid et al. 2017), which makes this lake an ideal site for testing our hypothesis. With two field campaigns, we mapped the spatial variability of free gas accumulation in lake sediment, quantified the vertical distribution of sediment CH_4 production rates and examined the linkage between ebullition and the spatial variability of free gas in sediment.

Materials and Methods

Study site

Affected by subtropical Mediterranean climate, LK is a meso-eutrophic lake located in Israel (32°50′N, 35°35′E, Fig. 1). The lake level varies seasonally and inter-annually between -209 m amsl (above mean sea level) and -213 m amsl due to water abstraction for irrigation and drinking water (Berman et al. 2014) and severe reginal droughts persisting in recent years. It is a deep (maximum water depth is 41.7 m at water level of -209 m amsl) monomictic lake featuring strong thermal stratification from March-April to December and full mixing from January to February-March (Rimmer et al. 2011). Water temperature is 14-16 ºC in the hypolimnion throughout the year and 24-30 ºC in the epilimnion during the period of stratification (Imberger and Marti 2014).

Sediment sampling

During December 1-8, 2016, a field campaign was conducted to characterize sediment volumetric gas content in LK. To resolve the gradient of sediment properties from the littoral to the profundal zone, three freeze cores were taken at water depth of 11, 19 and 36.7 m (at station H, F and A, respectively in Fig. 1). Sediment cores (7 cm in diameter, 45-60 cm in length) were frozen while the corer was in the sediment to preserve in situ sediment volumetric gas content (Y. Dück unpubl.). The frozen cores were transported to the Baruch Padeh Medical Center in Poriya for gas content characterization using a medical X-ray computed tomography (CT) scanner (Simons AS, 120 kV). The CT images were analyzed for volumetric gas content by thresholding the 3D radiation intensity distribution (Liu et al. 2018).

A second field campaign was performed during November 27 - December 4, 2017 to collect an additional set of sediment cores for sediment CH_4 production (MP) rate measurements and chemical analyses. Duplicated cores (> 1 m in length, 6 cm in diameter) were taken using a gravity corer (Uwitec, Austria) by revisiting the station H, F and A. An additional core was taken at a site near the Jordan River inflow (station G, 20 m water depth, Fig. 1). Sediment temperature was measured at discrete depths (through taped predrilled holes) using a handheld thermistor, immediately after the cores were recovered. One set of cores was sliced at 2 cm depth intervals and sediment subsamples were transferred to 50 mL Falcon tubes. The samples were stored in darkness at 4 ºC before sending to Germany for incubation and analyses. The second set of cores was sampled immediately after recovery at defined depth intervals (2 cm in the upper 30 cm sediment layer and 4 cm below) for porewater dissolved CH_4 (DCH_4) concentration. A 3 mL plastic cutoff syringe was used to extract sediment through predrilled holes on the side wall of the corer tube. To preserve DCH_4 in sediment porewater, 3 mL wet sediment samples were immediately transferred to 20 mL glass vials that were filled with 4 mL NaOH solution (2.5%). The vials were sealed with butyl rubber stoppers and aluminum caps and kept upside down for storage. Samples were taken to Germany to measure CH_4 concentration and stable carbon isotopes ($\delta^{13}C$) in CH_4 in the head space of the vials using a gas analyzer (Picarro G2201-i Analyzer, USA). The saturation limit of porewater DCH_4 was calculated according to the formula provided by Dale et al. (2008), which was adapted from (Duan et al. 1992).

MP and CO_2 production (CP) rates were determined by incubating sediment samples anaerobically at constant temperature (19.2 ± 0.3 ºC) in darkness. Lab incubations were started within one week after sampling to avoid uncertainties caused by long-term sample storage.

Duplicated samples (3 mL) were incubated under anoxic condition in 120 mL serum bottles (Wilkinson et al. 2015). Weekly measurements were performed by taking a small sub sample (0.1 mL) from the headspace with a gas-tight syringe. The gas samples were measured with a greenhouse gas analyzer (Los Gatos Research, US) using the closed-loop operation method (Wilkinson et al. 2018). MP and CP rates were estimated from the increase of headspace CH_4 and CO_2 concentration over time. For calculating in situ sediment MP rates, corrections for in situ sediment temperature were made according to temperature dependence of MP in freshwater sediment. A temperature coefficient of 1.12 was adopted by averaging literature values reported for subtropical and temperate zones (Aben et al. 2017).

Sediment particulate organic carbon (POC) content was determined using a CHNS analyzer (Vario MicroCUBE, Germany). The remaining material was centrifuged to extract sediment porewater. Porewater electrical conductivity and pH were measured using a multi-probe sensor (WTW, Germany). After filtration using membrane filters (0.45 μm pore size), the water samples were analyzed for concentrations of sulfate and nitrate using ion chromatography (881 Compact IC pro, Metrohm, Switzerland), dissolved organic carbon (DOC) (multiNC 2100S, Analytik Jena, Germany), iron and manganese (Q-ICP-MS XSeries2, Thermo Fisher Scientific, Germany).

Hydroacoustic measurements for gas ebullition

In December 2016, the spatial distribution of gas bubbles in the water column was characterized using a split-beam scientific echo sounder (120 kHz, Simrad EY60, USA). Acoustic measurements were performed along 14 transects covering the entire lake area (for transect trajectories see Ostrovsky and Walline (2001)). The pulse width was set to 0.256 ms with a sampling rate of 5 pings s^{-1}. The lower threshold for data collection was set to -75 dB and minimum bottom-scattering strength of -35 dB for bottom detection. Data were collected in a 4-m water stratum above the lakebed. For more details of the method refer to (Ostrovsky et al. 2008).

Acoustic data were processed with Sonar 5-Pro (http://folk.uio.no/hbalk/sonar4_5/), non-bubble targets were removed using the erasing tools in the software and then the method of echo integration (Simmonds and MacLennan 2008) was applied to quantify bubble density. The volume backscattering coefficient, s_υ, was calculated in vertical bins of 4 m width and about 500 pings defining 4-9 sampling units along each transect. The volumetric concentration of bubbles in the near-bottom water, V (mL m^{-3}), was calculated using the empirical V-s_υ correlation (Ostrovsky et

al. 2008). Near-bottom gas bubble flux was quantified as volumetric bubble density multiplied by bubble rise velocity (25 cm s^{-1}). Bubble volume was corrected for in situ hydrostatic pressure to calculate the CH_4 bubble flux to the atmosphere by assuming 90% CH_4 concentration in gas bubbles at the near-bottom depth (Ostrovsky et al. 2008).

Hydroacoustic measurements for estimating sediment gas content

Additional hydroacoustic surveys were conducted in December 2016 to characterize the spatial distribution of sediment gas content. Two instruments were used in parallel: the first one was a single-beam dual-frequency linear echo sounder (EA400, Kongsberg Maritime, Norway); the second was a sub-bottom profiler (SES2000 Compact, Innomar, Germany). The EA400 (beam angle 7°×13°) emits two primary sound pulses from two transducers with frequencies of 38 and 200 kHz. SES2000 is a single-beam nonlinear (parametric) system featured with primary frequencies of 100-115 kHz and secondary frequencies of 4-15 kHz. Because of non-linearities in sound propagation at high sound pressure, both signals interfere and generate a low-frequency acoustic pulse (secondary frequency). This secondary frequency (10 kHz in our measurements) can penetrate deeper into sediment while still preserving a small footprint (Wunderlich and Müller 2003; Wunderlich et al. 2005). In the absence of free gas in the sediments, many meters of penetration can be expected. However, the echo pulse is strongly attenuated creating the so-called "acoustic turbid layer" if free gas is present (Tóth et al. 2015; Tóth et al. 2014; von Deimling et al. 2013). The parametric system was used to support sediment classification results, by the linear system with focus on free gas detection.

Stationary acoustic profiles were recorded for 30 s (> 300 pings) at the four coring stations (Fig. 1). To produce optimal results, a wide range of different pulse lengths were used (Table S1). In addition, a whole-lake acoustic survey (Fig. 1) was performed for characterizing the spatial distribution of sediment gas content.

Hydroacoustic parameters were calculated from stationary acoustic profiling at each coring station (averaged from all pings) and then correlated to sediment physical properties. The measured echo from EA400 was divided into 3 phases (Hilgert et al. 2016). Phase 1: Attack - from the moment the pulse reached the lakebed until the time when the bottom is reached by the back slope of the pulse. It has a duration of ~1 pulse length and it starts from the bottom detection point or SWI. Phase 2: Decay - starts from the end of the attack phase, a distance of one pulse length from SWI, and lasts until the time when the leading edge of the pulse reached the boundary of the ideal

beam pattern (~3 pulse lengths). Phase 3: Release - lasting until the time when the pulse completely entered the bottom. Phase 3 was not included as the calculated algebraic values can be neglected (Burczynski 1999).

Mean volume backscatter strengths (Sv in dB) were calculated separately for the first two phases of the first echo, i.e., Sv during the attack (AttackSv1); Sv during decay (DecaySv1), using the formulas provided in (Hilgert et al. 2016). The calculations were performed using the software Sonar 5-Pro. For visualization and post-processing of SES2000 data ISE2 software (Innomar, Germany) was used.

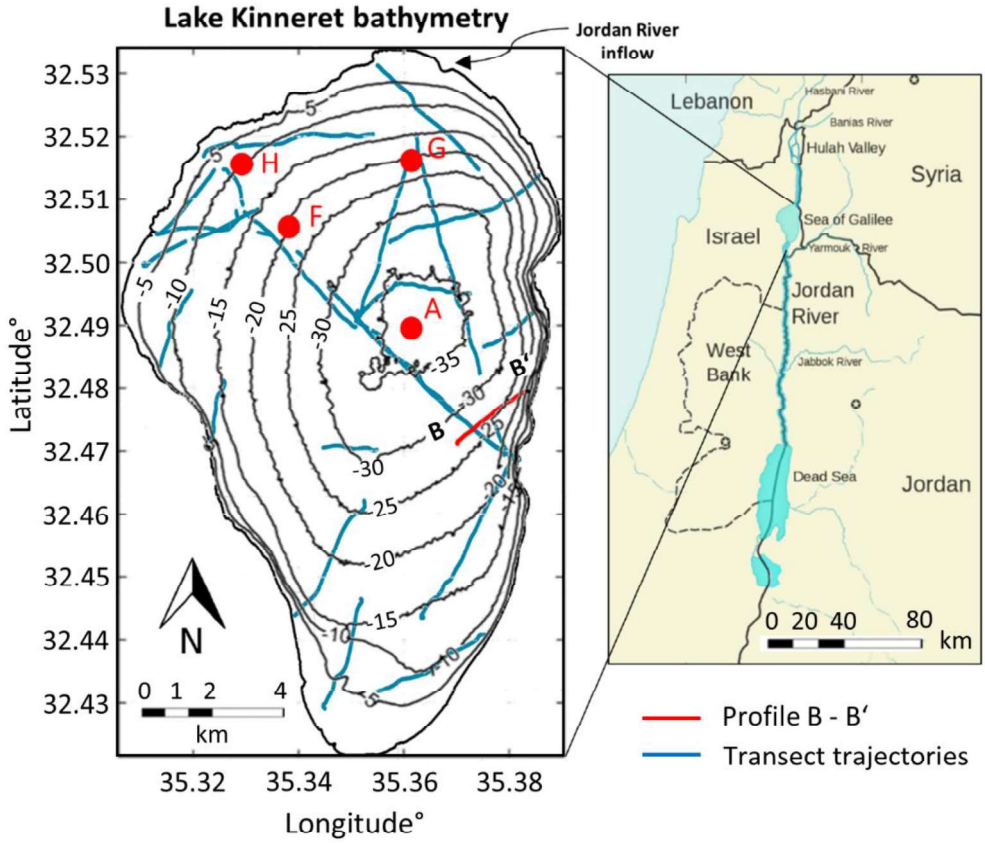

Fig. 1. Bathymetric map of Lake Kinneret. Black lines show water depth contours at water level of -213.7 m amsl. The inset map shows the geographical location of the lake at larger scale. The four coring stations are marked by red filled circles. Freeze cores were taken at station H, F and A. Gravity cores were collected at all four stations. Stationary hydroacoustic measurements were performed at all coring stations. Blue lines show trajectories of cruising hydroacoustic surveys with a transect B - B´ highlighted with a red line (see text).

Results

The control of methanogenesis on the vertical distribution sediment gas content

Oversaturation of CH_4 in sediment porewater under in situ hydrostatic pressure and sediment temperature was observed at all four sites (Fig. 2): Persistent CH_4 oversaturation starting from 25-30 cm below the SWI was observed at the deeper sampling sites (water depth > 15 m, station F, A and G). Strong spikes of in situ porewater DCH_4 concentration further suggest the presence of gas bubbles in these layers. Depth profiles of in situ sediment volumetric gas content obtained from freeze cores confirmed this finding. At station A and F, the sediment volumetric gas content tended to increase below 30 cm sediment depth and had a maximum value of 7% near the lower end of the core (~40 cm depth) at station A. At station F, even a narrow peak in volumetric gas content at ~40 cm depth coincided with a spike of DCH_4 concentration and both measures showed a minimum between depths 30-40 cm. The good agreement between depth profiles of porewater DCH_4 concentration and in situ gas content indicates that the oversaturation in DCH_4 can be a good predictor for the distribution of free gas content in sediment.

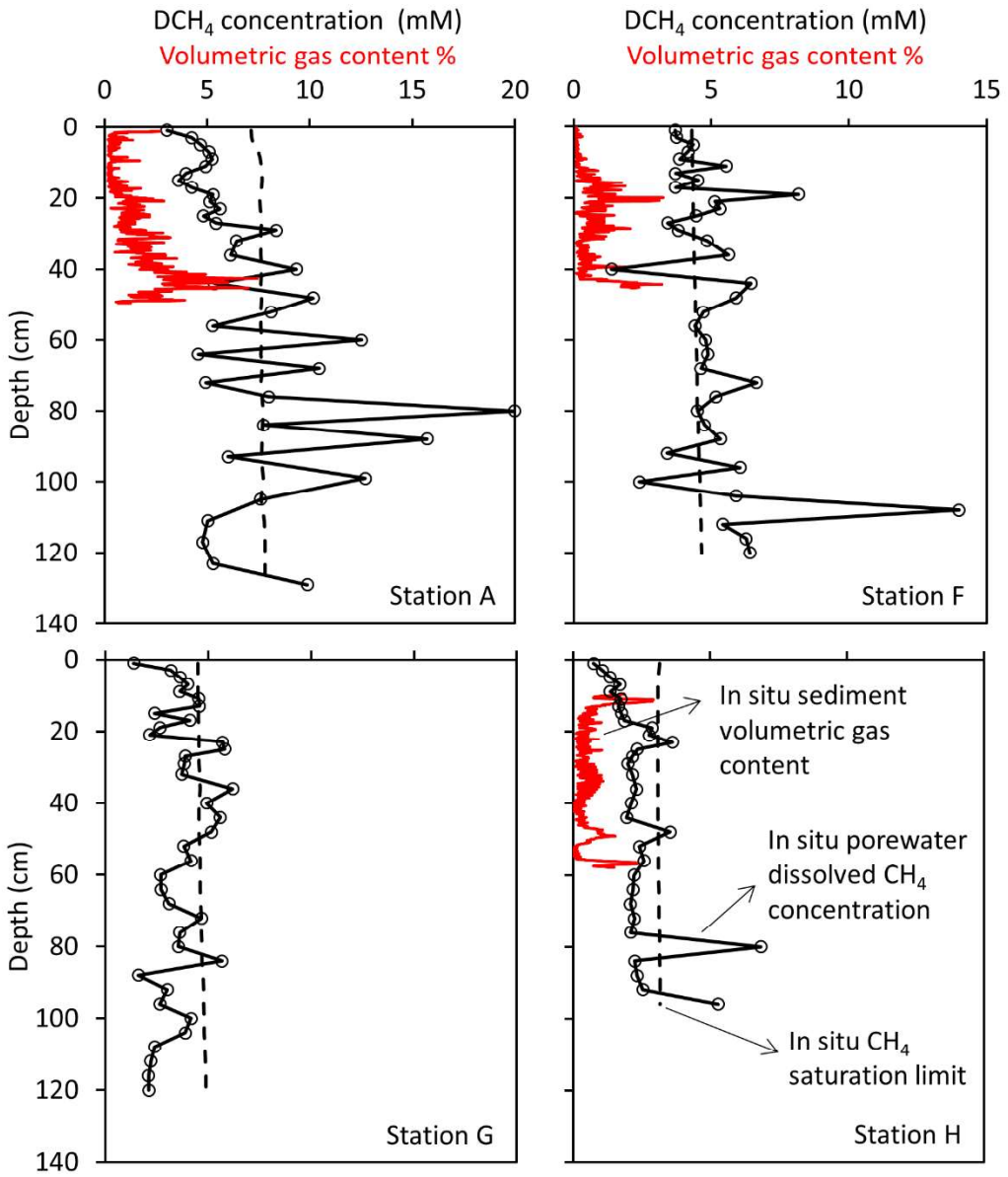

Fig. 2. Depth profiles of in situ porewater dissolved CH_4 concentration (DCH_4; solid black line with open symbols) at the four stations (sampled during November-December 2017) and volumetric gas content (red line) characterized by freeze coring at station H, F and A (collected in December 2016). Depth profiles of the CH_4 saturation limit are shown by dashed lines. Porewater DCH_4 saturation limits were calculated according to in situ hydrostatic pressure (and sediment load) and sediment temperature.

MP rates showed a sub-surface minimum at ~10-20 cm sediment depth in all four cores, though less pronounced at station F (Fig. 3a). At this depth, MP rates clearly deviated from a power-law

(MP = $a \times \text{depth}^b$; $R^2 \geq 0.83$) describing depth-dependent production rates below the minimum layer. The CH_4 production minimum in the surface layer coincided with elevated concentrations of sulfate (SO_4^{2-}), suggesting the presence of a SR zone. As for other potential CH_4 oxidizers and production inhibitors (alternative terminal electron acceptors) such as NO_3^-, Fe^{3+} and Mn^{4+}, the concentrations (data not shown) were at least one order of magnitude lower than sulfate and no correlation was found between these concentrations and MP. By fitting a power-law decay of MP over sediment depth (with the exclusion of upper 30 cm), the MP inhibition in the upper 30 cm layer of sediment was estimated by considering inhibition as the difference between predicted (extrapolation using the derived MP-depth equations below 30 cm sediment depth) and actual MP (Fig. 3b). The depth-integrated MP (corrected for in situ sediment temperature) in the surface 1 m sediment ranged 22.3-40.8 mmol m^{-2} d^{-1} at the four sites, the highest MP inhibition rate of 1.3 mmol L^{-1} d^{-1} was found at station G and the lowest (< 0.1 mmol L^{-1} d^{-1}) at station A (Table S2). In total, the MP inhibition in SR zone could account for 25-59 % of the depth-integrated potential MP (Table S2).

The in situ sediment temperature profiles (Fig. S1) showed a strong spatial gradient from the littoral zone to the profundal zone. Sediment temperature profiles at station F and G (water depth 20 m) were similar and ~4-5 °C warmer than at station A (water depth 36.7 m), while > 2 °C lower than at station H (water depth 11 m). The consistent overlying water (5 cm above the SWI) temperature at station F, G and H agrees with a well-mixed water column at water depth < 20 m at the time of sampling. Sediment temperature was affected by overlying water temperature at all sites except station H. At station H, sediment temperature was increasing with sediment depth, suggesting a strong winter cooling effect on the sediment.

CO_2 consumption (i.e., negative production) was observed at various depths and was most apparent in the upper 40-50 cm layer, except for station H (Fig. 3c). At station H, positive CP was observed over the entire sediment depth. In general, low concentrations of acetate (< 6 μM) in the SR zone (< 40-60 cm at station A and G) were observed, while the concentrations were slightly higher at the other two sites (up to 18.7 μM). Below the SR zone, significant enrichment of acetate (> 30 μM at all sites) was observed, resulting in lower pH values relative to the SR zone, while a slight increase in pH with increasing acetate concentration below 50 cm depth was observed (Fig. 3c). The relatively high POC content (up to 600 mmol g^{-1}) in the upper layer of the sediment (Fig. S2a-b) and low porewater DOC concentration (Fig. S2c) suggests that MP minima in the surface

layer is not constrained by POC source, but more by the rate of sequential utilization of labile DOC for methanogenesis. In addition, the obvious acetate enrichment at larger sediment depth (Fig. 3c) suggests that methanogenesis is not substrate limited.

Depletion of $\delta^{13}C_{CH4}$ was observed at the three sites (station A, F and G) with mean values ranging from -61.2 to -62.1 ‰. At station H, the relatively low $\delta^{13}C_{CH4}$ (mean -68.5‰) indicates the absence of strong SR and predominance of methanogenesis. At the other three sites, $\delta^{13}C_{CH4}$ showed depth gradients. A slight enrichment of $\delta^{13}C_{CH4}$ was observed at station A (from mean -62.4 to -60.3‰) and at station G (from -61.7 to -60.7‰) below 50 and 36 cm depth, respectively; while at station F, from -63‰ in the upper 10-60 cm layer to 61.7‰ below 60 cm depth with enrichment in the uppermost 10 cm layer of the sediment (mean -60.5‰).

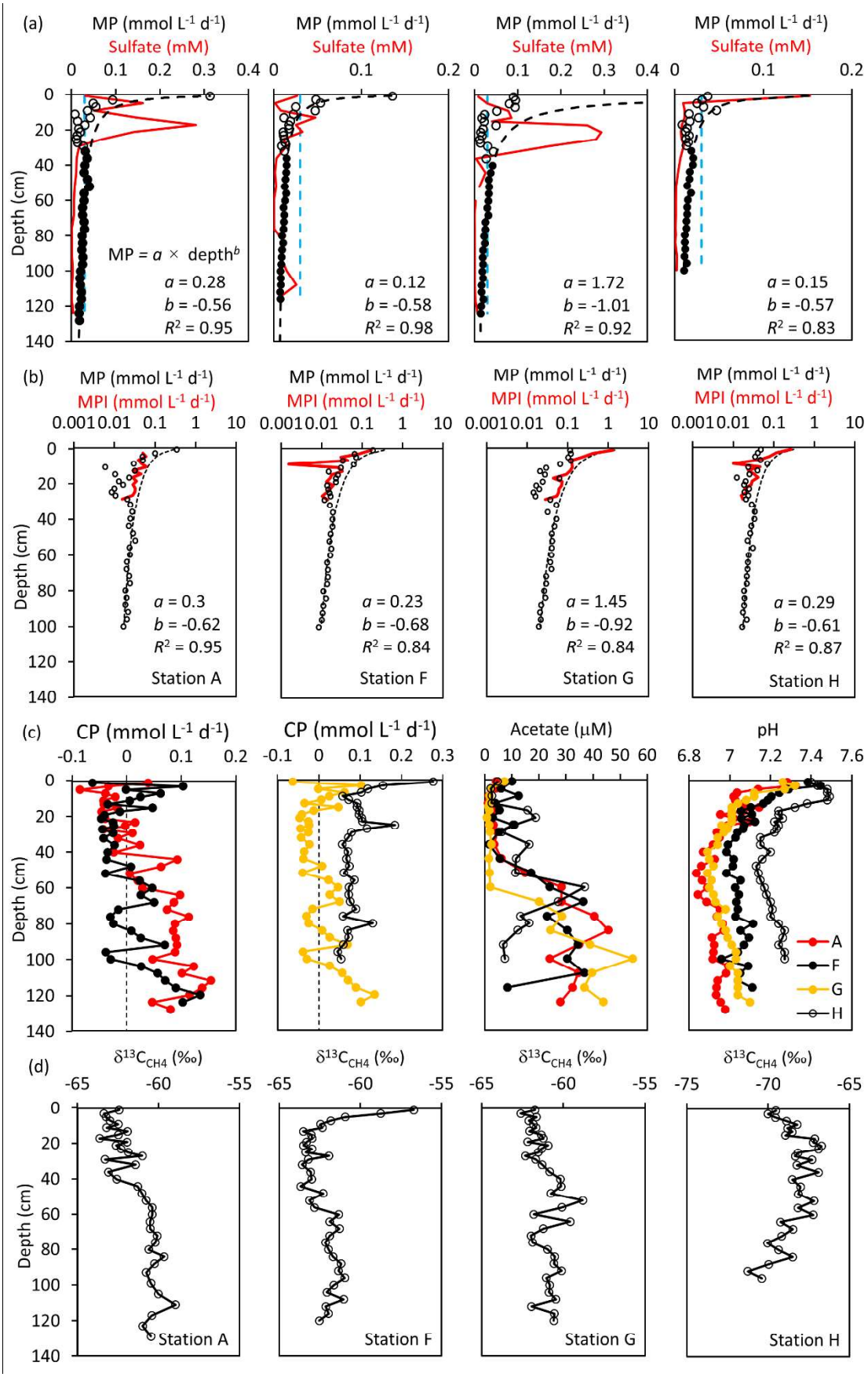
(a)
MP (mmol L-1 d-1)
Sulfate (mM)
Depth (cm)
MP = a × depthb
a = 0.28
b = -0.56
R2 = 0.95
a = 0.12
b = -0.58
R2 = 0.98
a = 1.72
b = -1.01
R2 = 0.92
a = 0.15
b = -0.57
R2 = 0.83
(b)
MP (mmol L-1 d-1)
MPI (mmol L-1 d-1)
a = 0.3
b = -0.62
R2 = 0.95
Station A
a = 0.23
b = -0.68
R2 = 0.84
Station F
a = 1.45
b = -0.92
R2 = 0.84
Station G
a = 0.29
b = -0.61
R2 = 0.87
Station H
(c)
CP (mmol L-1 d-1)
Acetate (μM)
pH
A
F
G
H
(d)
δ13CCH4 (‰)
Station A
Station F
Station G
Station H

Fig. 3. (a) Depth profiles of CH_4 production rates (MP, black symbols) and porewater sulfate concentration (red line). Dashed black lines show a power-law fit (MP = $a \times \text{depth}^b$) of MP over the lower depth range (depth > 30 cm; filled black symbols), which was extended over the sulfate-enriched layer (open black symbols). The dashed blue lines mark the threshold concentration (0.03 mM) for sulfate-reduction (Lovley and Klug 1986). (b) Depth profiles of MP and MP inhibition (MPI) rate. Open black circles are MP rates corrected for in situ sediment temperature; red thick lines are MPI rates calculated as the difference between predicted (by extrapolation according to the power-fit equations derived from depth > 30 cm) and actual MP. (c) Depth profiles of CO_2 production (CP), acetate and pH. (d) Depth profiles of $\delta^{13}C_{CH4}$ value of porewater DCH_4.

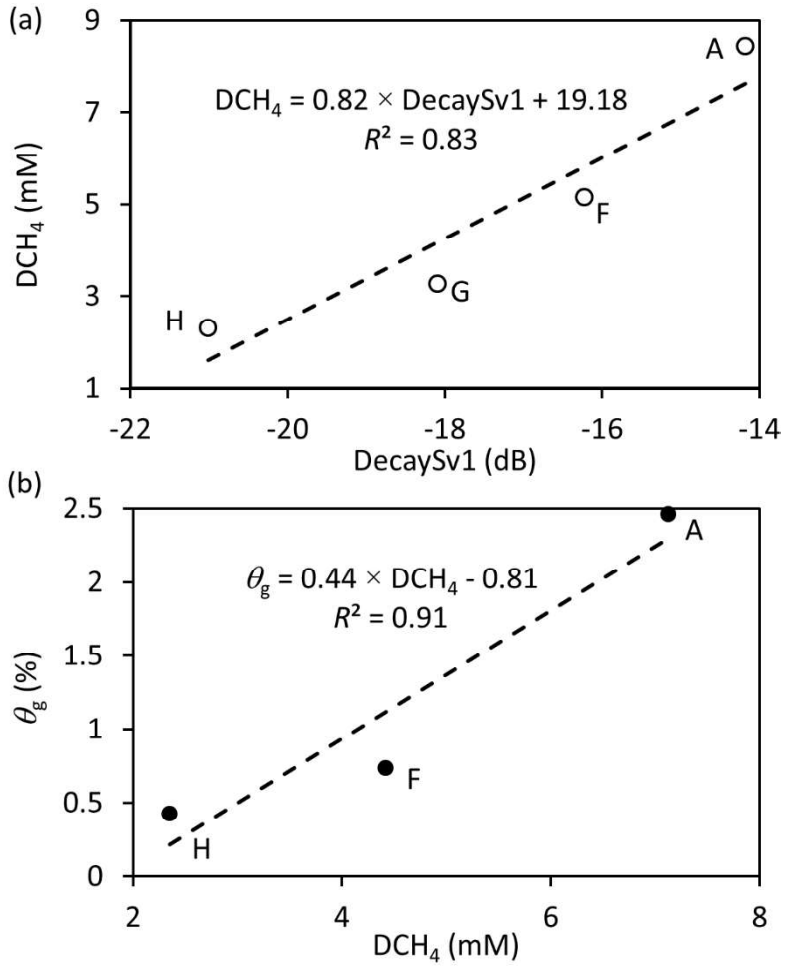

Fig. 4. (a) Linear regression between in situ porewater DCH_4 concentration (sampled during November 28-29, 2017; depth-averaged over 1 m sediment depth) and acoustic backscatter parameter DecaySv1 at the four stations. The acoustic backscatter parameter DecaySv1 was

estimated from stationary acoustic measurements at the four coring sites during December 3-5, 2016. (b) Linear regression between sediment volumetric gas content (θ_g; depth-averaged from freeze core measurements) and porewater DCH_4 concentration at the three stations (A, F and H; averaged over the corresponding length of freeze cores) where freeze cores were taken.

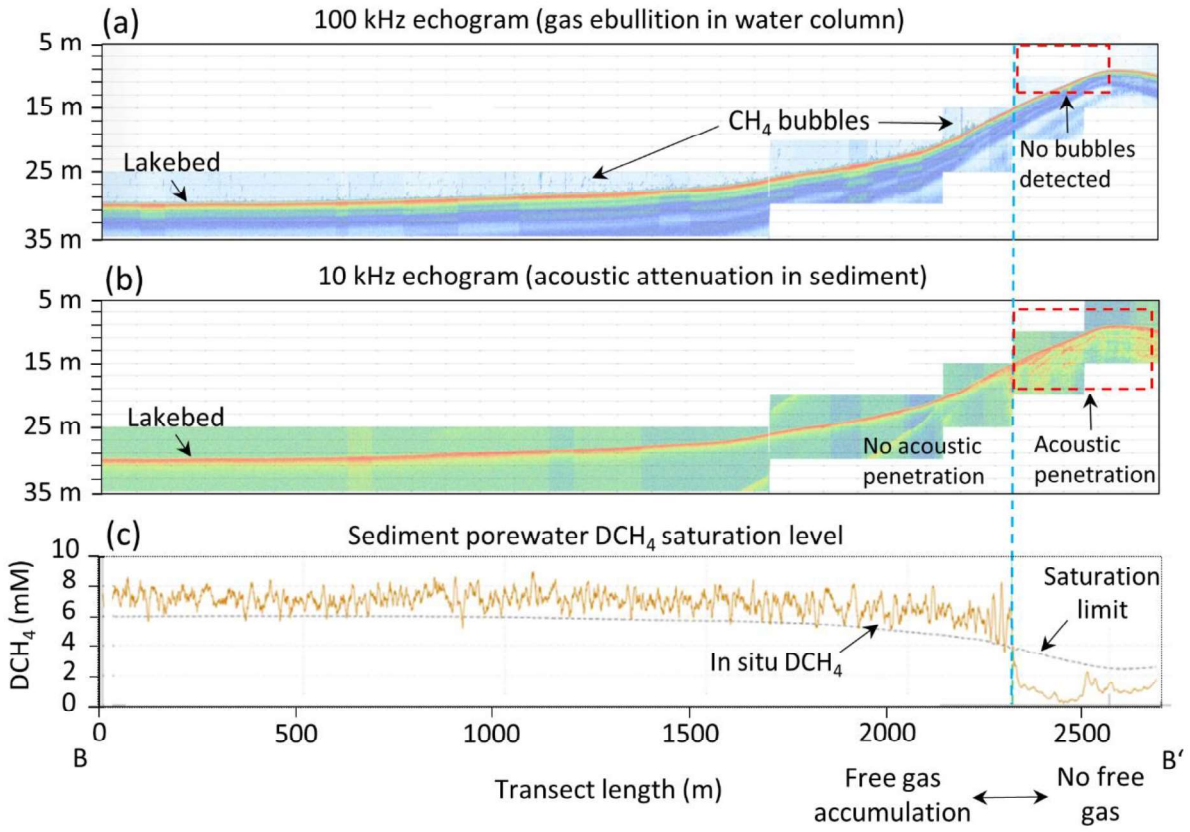

Fig. 5. Acoustic parameters along a selected transect (B - B′, Fig. 1) of the acoustic survey showing the transition of free gas accumulation in deep waters to the gas free shallow zone. (a) Echogram of the100 kHz transducer showing intense ebullition at zones where water depth > 15 m (cf. Fig. 6a for detail), while no bubbles were observed in the water column in shallow zones. (b) The 10 kHz echogram shows deep acoustic penetration into the sediment in the gas-free, shallow zone, while the penetration is blocked in the first meter of the sediment in deeper zones. (c) Computed mean porewater DCH_4 concentration (in surface 1 m sediment) estimated using the regression equation ($DCH_4 = 0.82 \times DecaySv1 + 19.18$) (Fig. 4). The saturation concentration is indicated by the dotted line. The vertical dashed line marks the transition from presence to absence of free gas in the sediment at 15 m water depth.

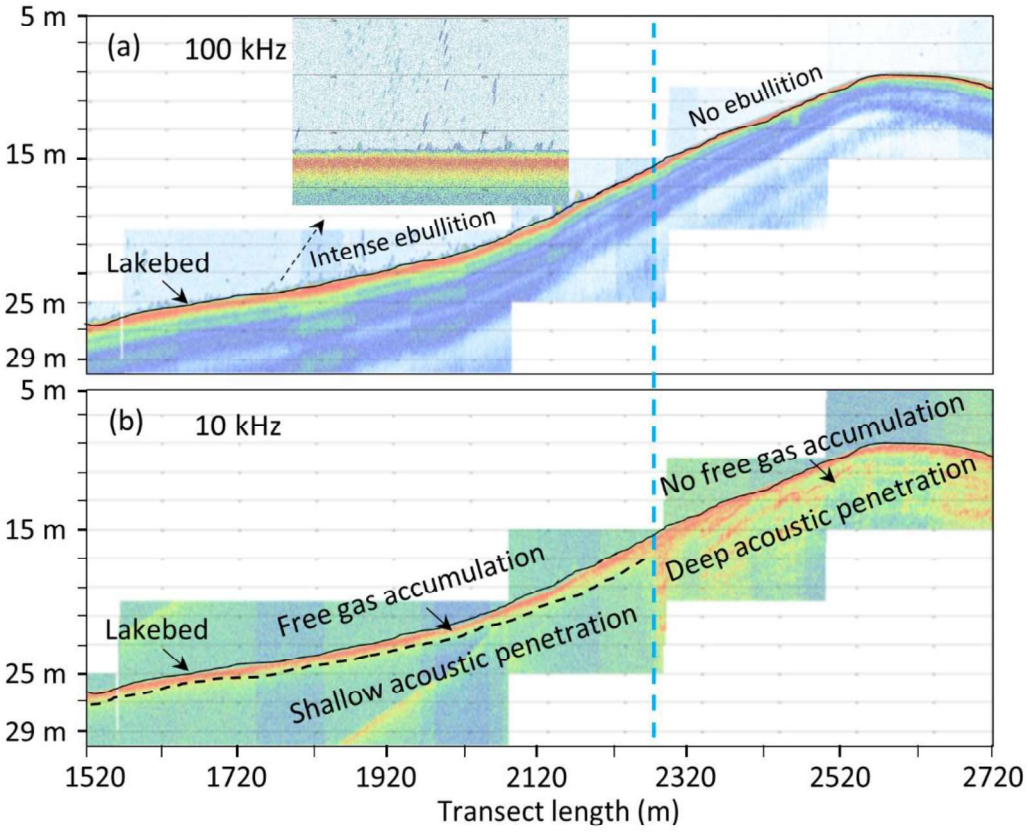

Fig. 6. Details of the transition zone of gas accumulation from Fig. 5a-b: (a) Intense ebullition near the lakebed detected with the 100 kHz echo sounder along the B - B′ transect where water depth > 17 m. Gas bubbles were clearly visible in the water column; (b) Sharp transition at 15 m water depth from gassy sediments to gas-free sediments. Shallow acoustic penetration in the deep zones (water depth > 15 m) suggests presence of free gas in the surface layer of the sediments. Deep acoustic signal penetration in the sediments indicates a gas-free zone.

Spatial (horizontal) distribution of sediment gas content

The backscatter strength during the second phase of the echo observed with the linear echo sounder (EA400) was positively correlated to porewater DCH_4 concentration (depth-averaged over 1 m sediment depth) (Fig. 4a). An equation was derived for calculating DCH_4 concentration according to acoustic parameter DecaySv1, while no correlation was found between the acoustic parameters and sediment MP rates. It is noticeable that no significant correlation was observed between sediment volumetric gas content, i.e. void fraction (from freeze core analysis) and acoustic

parameters. This could be explained by the limited length of the freeze cores that may result in inaccurate estimates of depth-averaged volumetric gas content.

The cruising acoustic measurement along a selected transect (B - B′, Fig. 1) exemplifies the good correlation between porewater DCH_4 concentration and sediment free gas accumulation and gas ebullition (Fig. 5). At water depth > 15 m, the DCH_4 concentration estimated from acoustic decay coefficients (DecaySv1) varied between 5-9 mM with a mean ~7 mM that well above the depth-dependent saturation limit (≤ 6 mM) (Fig. 5c). Following a sharp decrease at water depth of ~15 m, porewater DCH_4 concentration remained below the saturation limit in the shallower zone. A clear shift in acoustic penetration (10 kHz) was observed at the similar water depth: i.e., from strong reflection in the surface layer of the sediment at water depth > 15 m to deep acoustic penetration at shallower depths (Fig. 5b, Fig. 6b). This indicates the presence of free gas in the sediment at water depth > 15 m, in contrast to the absence of free gas content in sediment at the shallower water depths. This further suggests that porewater DCH_4 concentration can serve as a predictor of free gas accumulation in the surface sediment. The intense ebullition observed in the zone where free gas is present (Fig. 5a, Fig. 6a) suggests a potential for linking spatial variability of ebullition to the spatial pattern of sediment volumetric gas content.

Spatial patterns of ebullition and sediment free gas accumulation

We found a good linear correlation (Fig. 4b and Fig. S3) between in situ sediment volumetric gas content (void fraction) and in situ porewater DCH_4 concentration. The equation was then applied to depth-averaged (over 1 m sediment depth) porewater DCH_4 concentrations that were inferred from the acoustic decay parameter DecaySv1 (Fig. 4a). From the map of depth-averaged porewater DCH_4 concentration from DecaySv1, sediment volumetric gas content was calculated (Fig. 7). The 10 m isobath is approximately the boundary between gas-enriched sediment (sediment volumetric gas content > 1%) and gas-free sediments in the shallower areas (Fig. 7). In the eastern part of the lake, the boundary between gassy and gas free sediments occurred at water depth of 15 m (Fig. 5). Sediment volumetric gas content was low (0-1%) in the areas shallower than 10-15 m and it increased toward the profundal zone. Transient ebullition flux measured using acoustic method generally followed the spatial distribution of sediment volumetric gas content, although ebullition flux showed a rather high variability. The highest ebullition flux was detected in the northern part of the lake, close to Jordan River inflow (station G). At this site, MP and ebullition

flux were rather similar (> 40 mmol m^{-2} d^{-1}). At other sites the overall ebullition fluxes were lower than MP (by ~60-85%).

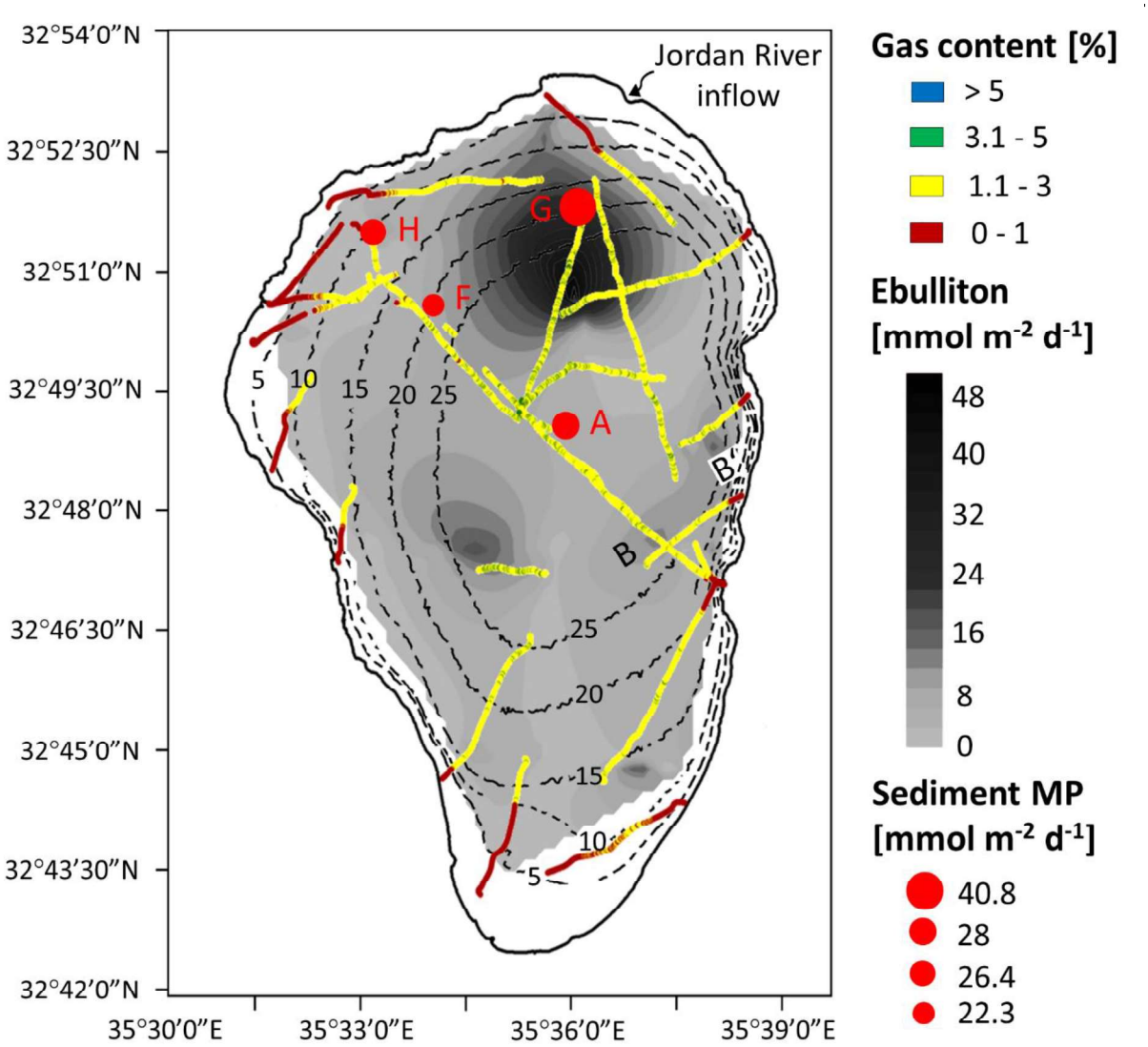

Fig. 7. Map of Lake Kinneret shows the spatial distribution of ebullition flux (grayscale) and sediment volumetric gas content (colored lines) in December 3-5, 2016. Each data point of sediment gas content was calculated by averaging 10 individual measurements. Sediment CH_4 production (MP) rate is shown by filled circles, where circle area scales with MP. The dashed lines show isobaths (m). Gas ebullition and sediment volumetric gas content were assessed using acoustic methods.

Discussion

Extended depth of sulfate-reduction zone attributable to historical anthropogenic perturbations

In LK, the upper 30 cm layer of sediment was slightly enriched with sulfate (< 0.3 mM), coinciding with reduced methanogenesis rates. In this SR zone, lower porewater DCH_4 concentrations were observed, consistent with a surface minimum of sediment free gas content (Fig. 2). The apparent linkage between SR and gas content minima in surface sediments has not been described before in freshwater lakes. The deep SR zone in LK is uncommon compared to other freshwater lakes, where methanogenesis rate often declines sharply over depth in anoxic sediments. In these systems, sulfate concentrations are typically < 30 μM, e.g. (Falz et al. 1999), and free gas accumulates near the sediment surface (Anderson and Martinez 2015).

Except for the shallow station H, sulfate concentration on the porewater of LK showed a clear maximum at ~15-30 cm depth, whereas near-surface concentrations were lower. This explains previous findings showing that sulfate-dependent AMO does not occur in the uppermost few centimeter of the sediment of LK (Adler et al. 2011; Schwarz et al. 2007). The lower concentration at the sediment-water interface appears to be contrary to the assumption that lake water is the direct source of porewater sulfate, although a comparable depth of the SR zone (25 cm) has previously been observed in sediment of a lake with higher sulfate concentrations (2 mM) (Schubert et al. 2011). Several possible mechanisms are proposed here for the depth profiles of sulfate in LK sediment. The unexpected low sulfate concentrations in the uppermost sediment could be explained by sediment-water exchange induced dilution by hypolimnion water, since lower sulfate concentrations were found in the hypolimnion during winter mixing (Hadas and Pinkas 1995). Enhanced solute flux across the SWI due to turbulent mixing was previously investigated in the shallow zones of LK (water depth < 10 m), where a reduction in porewater sulfate concentration in the uppermost 8.5 cm of the sediment was simultaneously observed (Mortimer et al. 1999). Internal wave induced convective porewater mixing is likely the reason for the enhanced sulfate exchange between sediment porewater and overlying water. The depth affected by intermittent warming and cooling due to internal waves has been found to reach 10 cm below the SWI in Lake Stechlin, Germany (Kirillin et al. 2009).

Besides seasonal variations, the sulfate concentration in lake water has been affected by historical anthropogenic perturbations. The most recent event was the construction of a pump station for taking water from LK to the National Water Carrier in 1967 (Berman et al. 2014). Onshore saline springs were diverted directly to the outlet of LK to prevent lake water from

becoming more saline. Consequently, the salinity of LK water declined consistently over the last six decades. In the center of the lake (station A), sulfate concentrations were enhanced down to 30 cm depth, where also turning points were observed in the depth profiles of wet bulk density and porewater salinity (Fig. S2d). Assuming a sedimentation rate of 4.5 mm yr^{-1}, which was determined in LK using uranium lead dating (Erel et al. 2001), this depth is equivalent to a time span of ~67 years. The turning points can thus be dated to 1950's, which is ~17 years before the diversion system was built. However, from 1951-1958 the upstream Lake Hula and surrounding swamps were drained (Berman et al. 2014) and nutrient-enriched water from these swamps was discharged into the lake. This caused dramatic changes in the biogeochemistry of lake water and sediment, e.g., sulfur content in the upper 25 cm layer of sediment at station A increased three-fold in the year 2000 (Nishri 2011).

In addition to the above-mentioned mechanisms, another possible factor could be ebullition-mediated porewater mixing. This was once reported in marine sediments where bubble release caused intense mixing of sediment porewater in the SR zone (Haeckel et al. 2007). Given the fact that increased gas content was observed below 30 cm depth in the sediment of LK, the release of gas bubbles from lower depth is likely a cause for the deepened sulfate-enriched layer. A recent modelling study based on X-ray scanned sediment pore structure also demonstrated that the formation and release of CH_4 bubbles can significantly enhance hydraulic conductivity (Mahabadi et al. 2018), which can eventually cause enhanced solute exchange across the SWI.

Sediment-water interface CH_4 flux: the importance of deep methanogenesis

Our estimates of depth-integrated MP rates (8.2 - 14.9 mol m^{-2} yr^{-1}) are in good agreement with previous long-term averaged ebullition measurements (15.4 mol m^{-2} yr^{-1}) (Schmid et al. 2017) as well as with ebullition flux measurements (10 mol m^{-2} yr^{-1}) (Ostrovsky et al. 2008). The spatial variability in sediment MP can be explained by the spatial pattern of sedimentation and in situ sediment temperature. Influenced by the Jordan River inflow, the highest sedimentation rate of 6.3 mm yr^{-1} was reported for station G, followed by the central station A (4.5 mm yr^{-1}) due to concentrated algae deposition rates (Koren and Klein 2000; Sobek et al. 2011). The low sedimentation rate (2 mm yr^{-1}) reported for the shallow water site (station H), however, did not cause a significant reduction in MP. This is due to the high sediment temperature (mean 23.6 ºC). The observed increase of sediment temperature over depth (Fig. S1) indicates the presence of

localized warm saline springs, which have been found in the littoral zone of LK (Ben-Avraham et al. 1986).

While sediment MP rates were low below the SR zone, overall they contribute 30-48% to the MP integrated over 1 m sediment depth (the sum of MP between depths 0.3 - 1 m in relation to the MP integrated over 1 m; MP below 1 m was assumed to contribute negligible to the total CH_4 flux across the SWI). In LK, ~80% CH_4 flux across SWI was found to be bubble-mediated (Schmid et al. 2017). Our measurements demonstrate a maximum sediment gas volumetric content below the SR zone, suggesting a large potential contribution of CH_4 bubbles from deep sediment to the ebullition flux across the SWI. The bubble growth and release from the deep gas-charged layer can be affected by sediment mechanical properties (Boudreau 2012; Katsman et al. 2013), and should be considered in future investigations.

While previous studies provided valuable information on sediment methanogenesis and AMO in LK, most of them were restricted to relatively shallow sediment depths (< 30 cm), i.e., the sediment below the SR zone has rarely been studied with only one recent study (Bar-Or et al. 2017) reaching 40 cm depth. By using sediment cores > 1 m long, our measurements provide new insights on some open questions about sediment methanogenesis, which have been raised in previous studies (Adler et al. 2011; Eckert and Conrad 2007; Nüsslein et al. 2003).

Our measurements suggest concurrent SR and MP in LK sediment at low sulfate concentrations (< 0.3 mM). A potential pathway of MP in the SR zone is CO_2/H-based methanogenesis coupled to sulfate-reducing process. The low acetate concentrations (< 6 μM) in the SR zone suggests an inhibition effect of acetate-based methanogenesis by sulfate-reducing bacteria that outcompete methanogens for acetate (Lovley and Klug 1986; Oremland and Polcin 1982; Winfrey and Zeikus 1977). Meanwhile, CO_2 produced by sulfate reducers can be used for methanogenesis, but its rate can be limited by the rate of sulfate reduction Nüsslein et al. (2003). This pathway is supported by the observed CO_2 consumption in the SR zone with rates that were in the same order of magnitude as MP. This syntrophic acetate CH_4 formation has been hypothesized to cause a isotopic signature of $\delta^{13}C_{CH4}$ ~-62 ‰ (Nüsslein et al. 2003), which is comparable our measurements (Fig. 3d).

Given the historic origin of porewater sulfate, which reduces MP by 25-59.1% (Table S2), CH_4 emissions from LK are likely to increase in the future as the sulfate pool depletes. Future work should integrate both processes and make a further evaluation of the effects of draining the Hula

swamps on carbon cycling in LK and other freshwater system, which are subject to anthropogenic alterations.

Linking the spatial variability of ebullition to bubble formation

Volumetric gas content in LK sediment is characterized by high spatial heterogeneity, which in general may affect the spatial variability of ebullition. The absence of free gas in the sediment and gas ebullition in littoral sediments (Fig. 7), however, is contrary to what have been observed in other natural lakes, where ebullition is often found most active in littoral zone (Natchimuthu et al. 2016; Wik et al. 2013). The active bubbling in shallow zone in lakes results from a combination of high temperature and low hydrostatic pressure. Higher water temperature is often observed in the littoral zone of deep stratified lakes, which enhances MP in the sediment. In addition, lower dissolved gas concentrations are required for reaching oversaturation and bubble formation in shallow waters. The unique pattern in LK, that the littoral zone is dominated by sandy sediments with low organic matter content, is likely related to the geological settings of the lake with warm saline springs at the lakebed of the littoral zone (Ben-Avraham et al. 1986). In addition, LK is exposed to strong wind in summer, which generates surface and internal waves that tend to focus organic materials from the littoral zone toward the profundal zone (Ostrovsky and Yacobi 1999; Ostrovsky and Yacobi 2010). Deep penetration of low-frequency sound waves was observed in these shallow zones (Fig. 5 and 6) and has also been also been reported from former acoustic surveys (Ben-Avraham et al. 1986).

It should be noticed that the spatial distribution of both ebullition and sediment gas content can be masked by the temporal variability of gas ebullition. Hydrostatic pressure changes have been demonstrated to cause strong temporal variability of ebullition (Maeck et al. 2014; Scandella et al. 2011; Varadharajan and Hemond 2012). In LK, strong dependence of the ebullition flux on water level change has been found and quantified; with the highest flux being observed in summer and fall due to the favorable conditions for bubble formation and release from sediment at decreasing water level (Ostrovsky et al. 2013; Ostrovsky and Tęgowski 2010). This explains the disagreement between sediment MP and ebullition flux we observed in winter 2016. The ebullition dynamics results from the interplay between the recharge of sediment gas voids by CH_4 formation and its dissolution, and gas release by breaking through sediment matrix (Scandella et al. 2011). Sediment can store a large amount of free gas (Anderson and Martinez 2015). The gas storage capacity of sediment is related to sediment structure and mechanical properties (Liu et al. 2018;

Liu et al. 2016). Bubble formation is a slow process that is governed primarily by sediment MP and bubble release is a fast process controlled by hydrostatic pressure changes. This means that, assuming a similar volumetric gas storage capacity, gas ebullition in the littoral zone is more sensitive to pressure changes than in the profundal zone (Ostrovsky 2003). This might explain the lower ebullition rate in the pelagic zone of the lake where higher sediment gas content was observed (Fig. 7). Thus, the short-term ebullition dynamics can be temporarily decoupled from the dynamics of sediment MP and strongly dependent on historical gas inventory in the sediment. E.g., at station A, ~5 months is required to recharge the 2.3% sediment volumetric gas content (estimated from the depth profile of porewater DCH_4 concentration according to the equation on Fig. 4b), assuming that the gas inventory is completely emptied by an extreme ebullition event.

Conclusions

By combining freeze coring, in situ porewater DCH_4 concentration profiling with hydroacoustic measurements, we successfully mapped sediment volumetric gas content in LK. This suggests a promising approach to predicting spatial patterns of ebullition by characterizing sediment gas accumulation. For the first time, we explored the linkage between ebullition and sediment gas content in a freshwater lake. Sediment volumetric gas content in LK is heterogeneous both vertically and horizontally. A large depth gradient was observed with free gas accumulated below 30 cm, above this depth gas content was notably lower. The low gas content in the upper 30 cm layer of the sediment can be explained by the sediment MP minimum there, potentially caused by sulfate reduction. The slight enrichment of sulfate (< 0.3 mM) in the upper 30 cm of sediment may be a consequence of sulfate-enriched water drained from the Hula swamps entering the lake in the 1950's. Our results suggest that SR zone is reducing depth-integrated MP in the sediment by 25-59.1%. Depth-integrated sediment MP is in close agreement with the CH_4 flux across the SWI. The high contribution (30-48%) to the total CH_4 flux coming from the gas-charged layer below the SR zone suggests that the gassy layer is an important source of gas ebullition. A large horizontal gradient of sediment volumetric gas content was identified with the hydroacoustic measurements. Free gas was absent in the littoral zone, where ebullition rates were low, and the gas content increased to > 1% towards the profundal zone. This gradient can be explained by the predominance of coarse-grained sediment with low organic matter content and the presence of underwater springs in the littoral zone.

Acknowledgements

The authors would like to acknowledge Timo Fahlenbock, Semion Kaganovsky, Oz Zabari-Dar, Moti Diamant and Beny Sulimani for their support in the field; Mr. Shimon Mendel from the Baruch Padeh Medical Center in Poriya for CT scans of the frozen sediment cores. We thank Captain Menachem Lev and his crew for their assistance onboard. Thanks to Daniel McGinnis for providing access to the instrument for stable isotope measurements and Wang Si for her help with the sediment incubation in laboratory. We also thank Werner Eckert for his critical comments to an earlier draft of the manuscript. This study was financially supported by the German Research Foundation (grant LO 1150/5) and the Ministry of National Infrastructures, Energy and Water Resources, Israel (grant 214-17-007).

References

Abegg, F., and A. L. Anderson. 1997. The acoustic turbid layer in muddy sediments of Eckernfoerde Bay, Western Baltic: methane concentration, saturation and bubble characteristics. Mar. Geol. **137:** 137-147. doi:110.1016/S0025-3227(1096)00084-00089.

Aben, R. C. and others 2017. Cross continental increase in methane ebullition under climate change. Nat. Commun. **8:** 1682. doi: 1610.1038/s41467-41017-01535-y

Adler, M., W. Eckert, and O. Sivan. 2011. Quantifying rates of methanogenesis and methanotrophy in Lake Kinneret sediments (Israel) using pore - water profiles. Limnol. Oceanogr. **56:** 1525-1535. doi: 1510.4319/lo.2011.1556.1524.1525

Anderson, A., F. Abegg, J. Hawkins, M. Duncan, and A. Lyons. 1998. Bubble populations and acoustic interaction with the gassy floor of Eckernförde Bay. Cont. Shelf Res. **18:** 1807-1838. doi:1810.1016/S0278-4343(1898)00059-00054.

Anderson, M. A., and D. Martinez. 2015. Methane gas in lake bottom sediments quantified using acoustic backscatter strength. J. Soils Sed. **15:** 1246-1255. doi: 1210.1007/s11368-11015-11099-11361.

Bar-Or, I. and others 2017. Iron-coupled anaerobic oxidation of methane performed by a mixed bacterial-archaeal community based on poorly reactive minerals. Environ. Sci. Technol. **51:** 12293-12301. doi: 12210.11021/acs.est.12297b03126.

Barnes, R., and E. Goldberg. 1976. Methane production and consumption in anoxic marine sediments. Geology **4:** 297-300. doi: 210.1130/0091-7613(1976)1134<1297:MPACIA>1132.1130.CO;1132.

Bastviken, D., J. Cole, M. Pace, and L. Tranvik. 2004. Methane emissions from lakes: Dependence of lake characteristics, two regional assessments, and a global estimate. Glob. Biogeochem. Cycles **18:** GB4009, doi: 4010.1029/2004GB002238.

Bastviken, D., J. J. Cole, M. L. Pace, and M. C. Van de Bogert. 2008. Fates of methane from different lake habitats: Connecting whole - lake budgets and CH4 emissions. J. Geophys. Res. Biogeosciences **113:** G02024, doi: 02010.01029/02007JG000608

Bastviken, D., L. J. Tranvik, J. A. Downing, P. M. Crill, and A. Enrich-Prast. 2011. Freshwater methane emissions offset the continental carbon sink. Science **331:** 50-50. doi: 10.1126/science.1196808.

Ben-Avraham, Z., G. Shaliv, and A. Nur. 1986. Acoustic reflectivity and shallow sedimentary structure in the Sea of Galilee, Jordan Valley. Mar. Geol. **70:** 175-189. doi: 110.1016/0025-3227(1086)90001-90000.

Berman, T., T. Zohary, A. Nishri, and A. Sukenik. 2014. General background, p. 1-15. *In* A. S. T. Zohary, T. Berman, and A. Nishri [ed.], Lake Kinneret - Ecology and management. Aquatic Ecology Series. Springer.

Boudreau, B. P. 2012. The physics of bubbles in surficial, soft, cohesive sediments. Mar. Pet. Geol. **38:** 1-18. doi: 10.1016/j.marpetgeo.2012.1007.1002.

Burczynski, J. 1999. Bottom classification. BioSonics Inc **Available from: www.biosonicsinc.com**.

Conrad, R. 2009. The global methane cycle: recent advances in understanding the microbial processes involved. Environ. Microbiol. Rep. **1:** 285-292. doi: 210.1111/j.1758-2229.2009.00038.x.

Dale, A. W., D. Aguilera, P. Regnier, H. Fossing, N. Knab, and B. B. Jørgensen. 2008. Seasonal dynamics of the depth and rate of anaerobic oxidation of methane in Aarhus Bay (Denmark) sediments. J. Mar. Res. **66:** 127-155. doi: 110.1357/002224008784815775.

de Mello, N. A. S. T., L. S. Brighenti, F. A. R. Barbosa, P. A. Staehr, and J. F. Bezerra Neto. 2018. Spatial variability of methane (CH4) ebullition in a tropical hypereutrophic reservoir: Silted areas as a bubble hot spot. Lake Reserv. Manage. **34:** 105-114. doi: 110.1080/10402381.10402017.11390018.

DelSontro, T., J. J. Beaulieu, and J. A. Downing. 2018. Greenhouse gas emissions from lakes and impoundments: Upscaling in the face of global change. Limnol. Oceanogr. Lett. **3:** 64-75. doi: 10.1002/lol1002.10073.

DelSontro, T., M. J. Kunz, T. Kempter, A. Wüest, B. Wehrli, and D. B. Senn. 2011. Spatial heterogeneity of methane ebullition in a large tropical reservoir. Environ. Sci. Technol. **45:** 9866-9873. doi: 9810.1021/es2005545.

Duan, Z., N. Møller, J. Greenberg, and J. H. Weare. 1992. The prediction of methane solubility in natural waters to high ionic strength from 0 to 250 C and from 0 to 1600 bar. Geochim. Cosmochim. Acta **56:** 1451-1460. doi: 1410.1016/0016-7037(1492)90215-90215.

Eckert, W., and R. Conrad. 2007. Sulfide and methane evolution in the hypolimnion of a subtropical lake: a three-year study. Biogeochemistry **82:** 67-76. doi: 10.1007/s10533-10006-19053-10533.

Erel, Y., Y. Dubowski, L. Halicz, J. Erez, and A. Kaufman. 2001. Lead concentrations and isotopic ratios in the sediments of the Sea of Galilee. Environ. Sci. Technol. **35:** 292-299. doi: 210.1021/es0013172.

Falz, K. Z. and others 1999. Vertical distribution of methanogens in the anoxic sediment of Rotsee (Switzerland). Appl. Environ. Microbiol. **65:** 2402-2408.

Flury, S. and others 2016. Controls on subsurface methane fluxes and shallow gas formation in Baltic Sea sediment (Aarhus Bay, Denmark). Geochim. Cosmochim. Acta **188:** 297-309. doi: 210.1016/j.gca.2016.1005.1037.

Hadas, O., and R. Pinkas. 1995. Sulfate reduction processes in sediments at different sites in Lake Kinneret, Israel. Microb. Ecol. **30:** 55-66. doi: 10.1007/BF00184513.

Haeckel, M., B. P. Boudreau, and K. Wallmann. 2007. Bubble-induced porewater mixing: A 3-D model for deep porewater irrigation. Geochim. Cosmochim. Acta **71:** 5135-5154. doi: 5110.1016/j.gca.2007.5108.5011.

Hilgert, S., A. Wagner, L. Kiemle, and S. Fuchs. 2016. Investigation of echo sounding parameters for the characterisation of bottom sediments in a sub-tropical reservoir. Adv. Oceanogr. Limnol. **7:** 93-105. doi: 110.4081/aiol.2016.5623.

Imberger, J., and C. L. Marti. 2014. The seasonal hydrodynamic habitat, p. 133-157. *In* A. S. T. Zohary, T. Berman, and A. Nishri [ed.], Lake Kinneret - Ecology and management. Aquatic Ecology Series. Springer.

Jones, R. I., C. E. Carter, A. Kelly, S. Ward, D. J. Kelly, and J. Grey. 2008. Widespread contribution of methane - cycle bacteria to the diets of lake profundal chironomid larvae. Ecology **89:** 857-864. doi: 810.1890/1806-2010.1891.

Katsman, R., I. Ostrovsky, and Y. Makovsky. 2013. Methane bubble growth in fine-grained muddy aquatic sediment: Insight from modeling. Earth Planet. Sci. Lett. **377:** 336-346. doi: 310.1016/j.epsl.2013.1007.1011.

Kirillin, G., C. Engelhardt, and S. Golosov. 2009. Transient convection in upper lake sediments produced by internal seiching. Geophys. Res. Lett. **36:** L18601, doi: 18610.11029/12009GL040064.

Koren, N., and M. Klein. 2000. Rate of sedimentation in Lake Kinneret, Israel: spatial and temporal variations. Earth Surf. Process. Landf. **25:** 895-904. doi: 810.1002/1096-9837(200008)200025:200008<200895::AID-ESP200109>200003.200000.CO;200002-200009.

Kuivila, K., J. Murray, A. Devol, and P. Novelli. 1989. Methane production, sulfate reduction and competition for substrates in the sediments of Lake Washington. Geochim. Cosmochim. Acta **53:** 409-416. doi: 410.1016/0016-7037(1089)90392-X.

Liu, L. and others 2018. Methane bubble growth and migration in aquatic sediments observed by X-ray μCT. Environ. Sci. Technol. **52:** 2007-2015. doi: 2010.1021/acs.est.2007b06061.

Liu, L., J. Wilkinson, K. Koca, C. Buchmann, and A. Lorke. 2016. The role of sediment structure in gas bubble storage and release. J. Geophys. Res. Biogeosciences **121:** 1992-2005. doi: 1910.1002/2016JG003456.

Lovley, D. R., and M. J. Klug. 1983. Sulfate reducers can outcompete methanogens at freshwater sulfate concentrations. Appl. Environ. Microbiol. **45:** 187-192.

---. 1986. Model for the distribution of sulfate reduction and methanogenesis in freshwater sediments. Geochim. Cosmochim. Acta **50:** 11-18. doi: 10.1016/0016-7037(1086)90043-90048.

Maeck, A. and others 2013. Sediment trapping by dams creates methane emission hot spots. Environ. Sci. Technol. **47:** 8130-8137. doi: 8110.1021/es4003907.

Maeck, A., H. Hofmann, and A. Lorke. 2014. Pumping methane out of aquatic sediments: Ebullition forcing mechanisms in an impounded river. Biogeosciences **11:** 2925-2938. doi: 2910.5194/bg-2911-2925-2014.

Mahabadi, N., X. Zheng, T. S. Yun, L. van Paassen, and J. Jang. 2018. Gas Bubble Migration and Trapping in Porous Media: Pore - Scale Simulation. J. Geophys. Res. Solid Earth **123:** 1060-1071. doi: 1010.1002/2017JB015331

Mbaka, J. G., C. Somlai, D. Köpfer, A. Maeck, A. Lorke, and R. B. Schäfer. 2014. Methane-derived carbon in the benthic food web in stream impoundments. PloS one **9:** e111392. doi: 111310.111371/journal.pone.0111392.

Mortimer, R., M. Krom, D. Boyle, and A. Nishri. 1999. Use of a high - resolution pore - water gel profiler to measure groundwater fluxes at an underwater saline seepage site in Lake Kinneret, Israel. Limnol. Oceanogr. **44:** 1802-1809. doi: 1810.4319/lo.1999.1844.1807.1802.

Natchimuthu, S. and others 2016. Spatio - temporal variability of lake CH4 fluxes and its influence on annual whole lake emission estimates. Limnol. Oceanogr. **61:** S13-S26. doi: 10.1002/lno.10222.

Nishri, A. 2011. Long-term impacts of draining a watershed wetland on a downstream lake, Lake Kinneret, Israel. Air, Soil and Water Research **4:** ASWR. S6879. doi: 6810.4137/ASWR.S6879.

Nüsslein, B., W. Eckert, and R. Conrad. 2003. Stable isotope biogeochemistry of methane formation in profundal sediments of Lake Kinneret (Israel). Limnol. Oceanogr. **48:** 1439-1446. doi: 1410.4319/lo.2003.1448.1434.1439.

Oremland, R. S., and S. Polcin. 1982. Methanogenesis and sulfate reduction: competitive and noncompetitive substrates in estuarine sediments. Appl. Environ. Microbiol. **44:** 1270-1276.

Ostrovsky, I. 2003. Methane bubbles in Lake Kinneret: Quantification and temporal and spatial heterogeneity. Limnol. Oceanogr. **48:** 1030-1036. doi: 1010.4319/lo.2003.1048.1033.1030.

Ostrovsky, I., D. F. McGinnis, L. Lapidus, and W. Eckert. 2008. Quantifying gas ebullition with echosounder: the role of methane transport by bubbles in a medium - sized lake. Limnol. Oceanogr. Methods **6:** 105-118. doi: 110.4319/lom.2008.4316.4105.

Ostrovsky, I. and others 2013. Long-term changes in the Lake Kinneret ecosystem: the effects of climate change and anthropogenic factors, p. 271-293. *In* C. R. Goldman, M. Kumagai and R. D. Robarts

[eds.], Climatic change and global warming of inland waters: Impacts and mitigation for ecosystems and societies. John Wiley & Sons.

Ostrovsky, I., and J. Tęgowski. 2010. Hydroacoustic analysis of spatial and temporal variability of bottom sediment characteristics in Lake Kinneret in relation to water level fluctuation. Geo-Mar. Lett. **30:** 261-269. doi: 210.1007/s00367-00009-00180-00364.

Ostrovsky, I., and P. Walline. 2001. Multiannual changes in the pelagic fish Acanthobrama terraesanctae in Lake Kinneret (Israel) in relation to food sources. Verh. Int. Verein. Limnol. **27:** 2097-2094. doi: 2010.1080/03680770.03681998.11901606.

Ostrovsky, I., and Y. Z. Yacobi. 1999. Organic matter and pigments in surface sediments: possible mechanisms of their horizontal distributions in a stratified lake. Can. J. Fish. Aquat. Sci. **56:** 1001-1010. doi: 1010.1139/cjfas-1056-1006-1001.

Ostrovsky, I., and Y. Z. Yacobi. 2010. Sedimentation flux in a large subtropical lake: spatiotemporal variations and relation to primary productivity. Limnol. Oceanogr. **55:** 1918-1931. doi: 1910.4319/lo.2010.1955.1915.1918.

Rimmer, A., G. Gal, T. Opher, Y. Lechinsky, and Y. Z. Yacobi. 2011. Mechanisms of long‐term variations in the thermal structure of a warm lake. Limnol. Oceanogr. **56:** 974-988. doi: 910.4319/lo.2011.4356.4313.0974

Saunois, M. and others 2016. The global methane budget 2000–2012. Earth System Science Data (Online) **8:** 697-751. doi: 610.5194/essd-5198-5697-2016.

Scandella, B. P., C. Varadharajan, H. F. Hemond, C. Ruppel, and R. Juanes. 2011. A conduit dilation model of methane venting from lake sediments. Geophys. Res. Lett. **38:** L06408, doi:06410.01029/02011GL046768.

Schmid, M., I. Ostrovsky, and D. F. McGinnis. 2017. Role of gas ebullition in the methane budget of a deep subtropical lake: what can we learn from process‐based modeling? Limnol. Oceanogr. **62:** 2674-2698. doi: 2610.1002/lno.10598.

Schubert, C. J., F. Vazquez, T. Lösekann-Behrens, K. Knittel, M. Tonolla, and A. Boetius. 2011. Evidence for anaerobic oxidation of methane in sediments of a freshwater system (Lago di Cadagno). FEMS Microbiol. Ecol. **76:** 26-38. doi: 10.1111/j.1574-6941.2010.01036.x.

Schwarz, J. I., W. Eckert, and R. Conrad. 2007. Community structure of Archaea and Bacteria in a profundal lake sediment Lake Kinneret (Israel). Syst. Appl. Microbiol. **30:** 239-254. doi: 210.1016/j.syapm.2006.1005.1004.

Sepulveda-Jauregui, A. and others 2018. Eutrophication exacerbates the impact of climate warming on lake methane emission. Sci. Total Environ. **636:** 411-419. doi: 410.1016/j.scitotenv.2018.1004.1283.

Simmonds, J., and D. N. MacLennan. 2008. Fisheries acoustics: theory and practice. John Wiley & Sons.

Sobek, S., R. Zurbrügg, and I. Ostrovsky. 2011. The burial efficiency of organic carbon in the sediments of Lake Kinneret. Aquat. Sci. **73:** 355-364. doi: 310.1007/s00027-00011-00183-x.

Tóth, Z., V. Spiess, and H. Keil. 2015. Frequency dependence in seismoacoustic imaging of shallow free gas due to gas bubble resonance. J. Geophys. Res. Solid Earth **120:** 8056-8072. doi: 8010.1002/2015JB012523.

Tóth, Z., V. Spiess, J. M. Mogollón, and J. B. Jensen. 2014. Estimating the free gas content in Baltic Sea sediments using compressional wave velocity from marine seismic data. J. Geophys. Res. Solid Earth **119:** 8577-8593. doi: 8510.1002/2014JB010989.

Tušer, M., T. Picek, Z. Sajdlová, T. Jůza, M. Muška, and J. Frouzová. 2017. Seasonal and Spatial Dynamics of Gas Ebullition in a Temperate Water - Storage Reservoir. Water Resour. Res. **53:** 8266-8276. doi: 8210.1002/2017WR020694.

Varadharajan, C., and H. F. Hemond. 2012. Time - series analysis of high - resolution ebullition fluxes from a stratified, freshwater lake. J. Geophys. Res. Biogeosciences **117:** G02004, doi: 02010.01029/02011JG001866.

von Deimling, J. S. and others 2013. A low frequency multibeam assessment: Spatial mapping of shallow gas by enhanced penetration and angular response anomaly. Mar. Pet. Geol. **44:** 217-222. doi: 210.1016/j.marpetgeo.2013.1002.1013.

Whiticar, M. J., and E. Faber. 1986. Methane oxidation in sediment and water column environments—isotope evidence. Org. Geochem. **10:** 759-768. doi: 710.1016/S0146-6380(1086)80013-80014.

Wik, M., P. M. Crill, R. K. Varner, and D. Bastviken. 2013. Multiyear measurements of ebullitive methane flux from three subarctic lakes. J. Geophys. Res. Biogeosciences **118:** 1307-1321. doi.org/1310.1002/jgrg.20103.

Wilkinson, J., C. Bors, F. Burgis, A. Lorke, and P. Bodmer. 2018. Measuring CO2 and CH4 with a portable gas analyzer: Closed-loop operation, optimization and assessment. PloS one **13:** e0193973. doi: 0193910.0191371/journal.pone.0193973.

Wilkinson, J., A. Maeck, Z. Alshboul, and A. Lorke. 2015. Continuous seasonal river ebullition measurements linked to sediment methane formation. Environ. Sci. Technol. **49:** 13121-13129. doi: 13110.11021/acs.est.13125b01525.

Winfrey, M., and J. Zeikus. 1977. Effect of sulfate on carbon and electron flow during microbial methanogenesis in freshwater sediments. Appl. Environ. Microbiol. **33:** 275-281.

Wunderlich, J., and S. Müller. 2003. High-resolution sub-bottom profiling using parametric acoustics. International Ocean Systems **7:** 6-11.

Wunderlich, J., G. Wendt, and S. Müller. 2005. High-resolution echo-sounding and detection of embedded archaeological objects with nonlinear sub-bottom profilers. Mar. Geophys. Res. **26:** 123-133. doi: 110.1007/s11001-11005-13712-y.

Supporting Information for

The control of sediment gas accumulation on spatial distribution of ebullition in Lake Kinneret

Liu Liu,[1*] Klajdi Sotiri,[2] Yannick Dück,[3] Stephan Hilgert,[2] Ilia Ostrovsky,[4] Ernst Uzhansky,[5] Regina Katsman,[5] Boris Katsnelson,[5] Revital Bookman,[5] Jeremy Wilkinson,[1] Andreas Lorke[1]

[1] Institute for Environmental Sciences, University of Koblenz-Landau, Landau, Germany

[2] Institute for Water and River Basin Management, Karlsruhe Institute of Technology, Karlsruhe, Germany

[3] Institute of Hydraulic Engineering and Water Resources Management, Cologne University of Applied Science, Cologne, Germany

[4] Yigal Allon Kinneret Limnological Laboratory, Israel Oceanographic and Limnological Research, Migdal, Israel

[5] Dr. Moses Strauss Department of Marine Geosciences, Leon H. Charney School of Marine Sciences, University of Haifa, Mount Carmel, Haifa, Israel

*Correspondence: liu@uni-landau.de

Table S1. Configurations for pulse length and corresponding echo resolution for the EA400 linear echo sounder during the stationary measurements at the coring sites.

	200 kHz			38 kHz		
Configuration	*Pulse duration [ms]*	*Pulse length [m]*	*Echo resolution [m]*	*Pulse duration [ms]*	*Pulse length [m]*	*Echo resolution [m]*
I	0.064	0.096	0.012	0.256	0.384	0.048
II	0.128	0.192	0.024	0.512	0.768	0.096
III	0.256	0.384	0.048	1.024	1.536	0.192
IV	0.512	0.768	0.096	2.048	3.072	0.384

Table S2. Depth-integrated rates of anaerobic methane production (MP) and MP inhibition in sediment. MP inhibition rate is calculated by normalizing MP inhibition with total methane production potential.

Site	MP inhibition		MP		MP inhibition rate
	mmol m^{-2} d^{-1}	mol m^{-2} yr^{-1}	mmol m^{-2} d^{-1}	mol m^{-2} yr^{-1}	%
Station A_1st	10.6	3.9	30.9	11.3	25.5
Station A_2nd	8.1	3.0	25.0	9.1	24.5
Station F	10.1	3.7	22.3	8.2	31.2
Station G	59.0	21.6	40.8	14.9	59.1
Station H	15.4	5.6	26.4	9.6	36.9

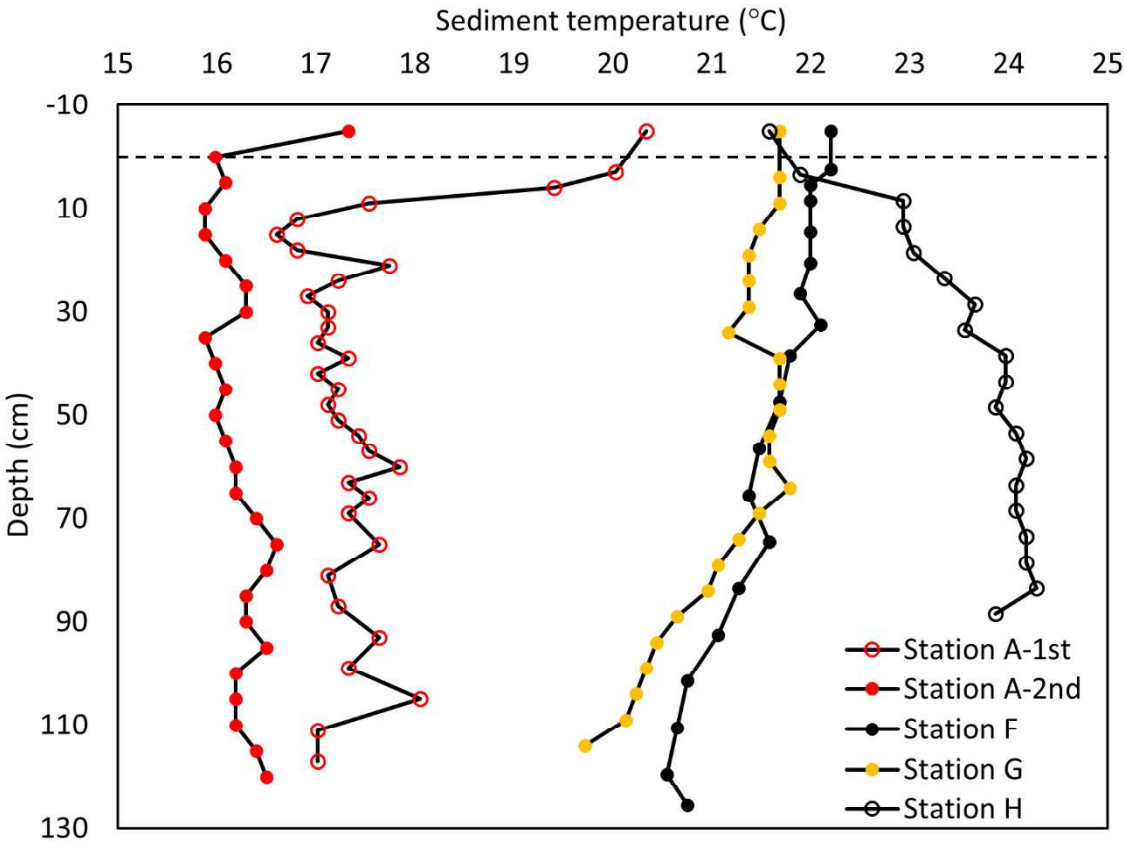

Fig. S1. Depth profiles of in situ sediment temperature (the uppermost values were measured in the overlaying water). At station A, temperature was measured in two separate cores, whereas the second core was sampled one day after the first one.

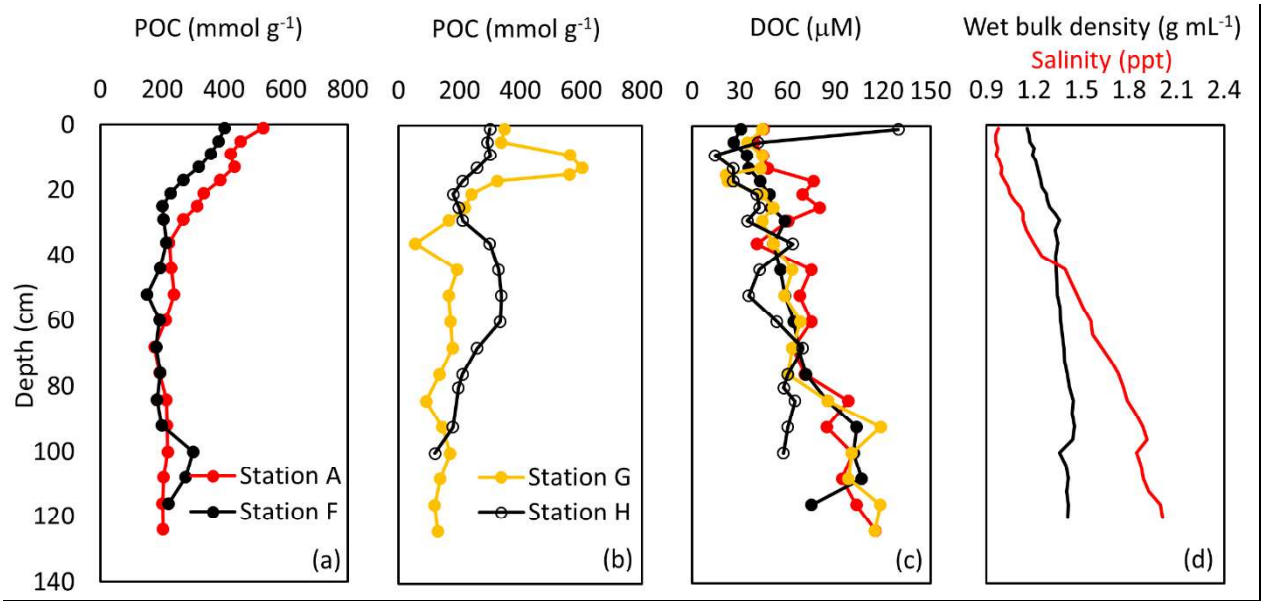

Fig. S2. (a), (b) Depth profiles of particulate organic carbon (POC). (c) Depth profiles of porewater dissolved organic carbon concentration (DOC). Line and symbol color are identical to those shown in the legend of a) and b). (d) Depth profiles of mean wet bulk density (black line) and mean salinity (red line) for the 4 cores.

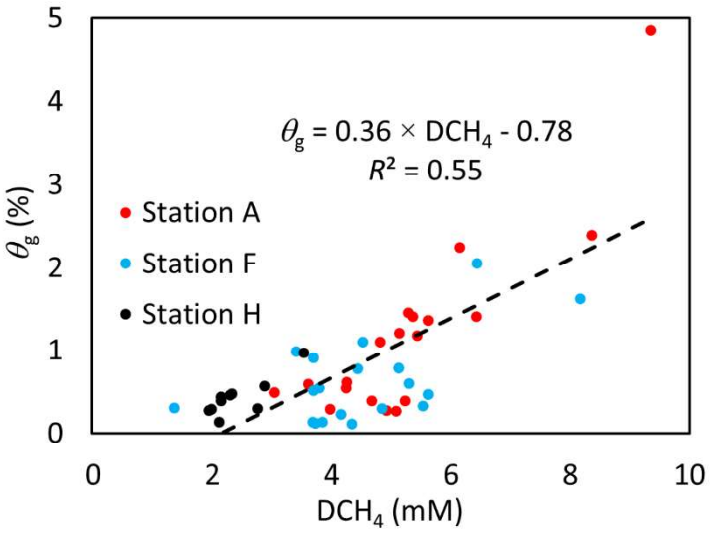

Fig. S3. Linear regression between sediment volumetric gas content (θ_g) and porewater DCH_4 concentration at different sediment depths of the three freeze-coring sites (station A, F and H). For each freeze core, data points of θ_g were extracted by averaging every 1 cm sediment depth (to reduce the noise). Data points were extracted from θ_g at different depths of freeze cores and corresponding depths of in situ porewater DCH4 concentration profiles. Red dots represent data points for station A, light blue for station F and black for station H.